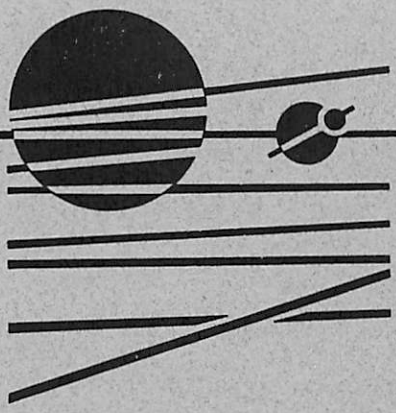

Lunar and Planetary Laboratory
Department of Planetary Sciences

Southern New Mexico

Planetary Geology Field Practicum
PTYS 594a
May 12-14, 2001

University of Arizona
on, Arizona

Editors Note

Well, its 12:30 AM on Friday...the day before we leave. Dave would have started organizing earlier, but we had to wait for one final submission: from Jay. No worries. We were able to entertain ourselves at the classy establishment that is Dirtbag's. We are always amazed at the wide variety of people that frequent that place. Now that we are starting to put this handout together, we would like to commend the large number of people who have done their handout in LaTeX, a display of the intellectual evolution that our department is undergoing. Shortly, we forsee a field-trip template being designed for everyone to use, such that the process of putting together the abstract book will be much easier. It is always exciting to read about the wide range of topics that will be discussed on our trips: from the formation of large holes, to the formation of tiny grains in dunes; from the search for ancient lakes to the search for life outside our solar system; from the launch of our first rockets to the launch of many different produce.

Dave and Fred

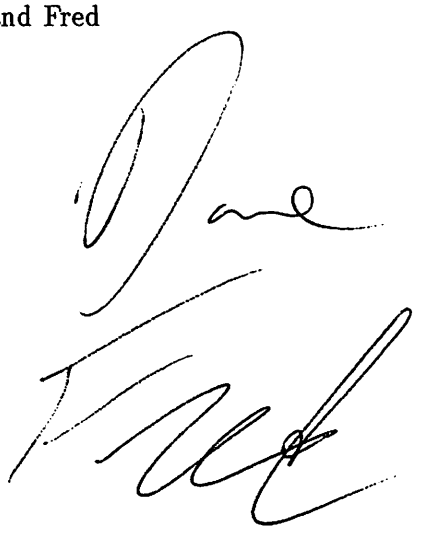

Contents

Day 3

Appendix

PTYS 594a

PLANETARY FIELD GEOLOGY PRACTICUM

Spring 2001 New Mexico Itinerary

Friday, 11 May

4:00 pm Drivers pick up vehicles in preparation for early departure on Saturday.

Saturday, 12 May

8:30 am Depart Gould/Simpson loading dock. Drive E on 2nd to Campbell, turn S and proceed East on I-10. Turn right at Exit 298, proceed to Cross Hill Quarry.

9:30 am **Andreas Eckholm** will regale us on the topic of long runout landslides and described the section exposed in the quarry face.

10:30 am Retun to I-10 and continue East. Take Exit 306 East of Benson and proceed N on Rte 76. Stop at overlook of San Pedro valley, where **Terry Hurford** will describe the Pleistocene fauna preserved in its gravels.

11:00am Return to I-10 and continue East. Stop at Texas Canyon where **Ross Beyers** will explain the prominent spheroidal weathering displayed at this famous stop.

11:30 am Continue East on I-10. Turn right at exit 331 onto Rte 191 South toward Cochise. **Paul Withers** will guide us to a stop overlooking Willcox playa, where we will make a luch stop.

1:00 pm Return to I-10 and continue East toward the New Mexico border. Exit at Lordsburg and take Rte. 70 North to Nine Mile Hill. Take a dirt ranch road SW from here and proceed 6 miles from the highway to stop at the highstand of glacial Lake Animas.

2:30 pm Return to I-10 at Lordsburg and continue East. Pass Deming and turn S onto frontage road at exit 116. Follow road B4 to intersection with A17, turn South to vicinity of Kilbourne Hole.

5:30 pm Camp at Kilbourne hole.

Sunday, 13 May

8:00 am Break camp, **Jani Radebaugh** will describe how the holes in the ground came to be formed. **Rachel Mastrapa** will describe the mantle xenoliths at Kilbourne Hole before we proceed to hike into the pit and collect our own samples of the Earth's mantle

12 noon Return to vehicles at rim, have lunch, return to I-10 via the previous day's route.

1:30 pm Continue on I-10 East to Las Cruces. Exit onto Rte-70 East to overlook in the Organ Mountains. At this commanding site **Adina Alpert** will describe the structure and tectonics of the Rio Grande Rift.

2:00 pm Continue East on Rte-70 and stop at (near) the exit for the White Sands Missile Test Center (Fort Bliss).

2:30 pm At this inspiring site **Gwen Bart** will describe the contributions of R. H. Goddard to space exploration and **Jason Barnes** will explain what happened at the first detonation of a nuclear weapon on Earth.

3:00 pm Proceed NE on Rte 70 to White Sands National Monument. Turn off into the monument road.

3:30 pm Stop at the "Heart of the Dunes" parking loop. At this bright location **Fred Ciesla** will describe the difference between these dunes and silica sand dunes. **Ralph Lorenz** will use this opportunity to show us how the dunes look from orbital radar.

5:00 pm Continue NE on Rte 70 to Alamogordo, pick up Rte 54 North and continue to Carrizozo. Turn West on Rte 380 and proceed about 7 miles to the Valley of Fire campground.

6:30 pm Camp at the Valley of the Fires. Campfire discussion may drift to the topic of Roswell, NM only a few miles to the east (where we will not go!).

Monday, 14 May

8:00 am Break camp. **Windy Jaeger** will discuss the paradoxical length of the Carrizozo lava flow before we return East to the town of Carrizozo, then turn North on Rte 54. After 10 miles turn NE onto Rte 349 where we will proceed to the ghost town of White Oak.

9:30 am **Jim Richardson** will discuss the mechanics of the laccoliths in which we will then be standing, and regale us about the history of White Oak on the CB as we approach it.

10:00 am Return to Rte 54, proceed South back to Carrizozo, then back onto Rte 380 traveling West.

11:00 am Stop at an overlook along Rte 380 looking downward into the gorge of the Rio Grande and the town of Socorro. **Joe Spitale** will describe the magma body that seethes beneath this placid-looking scene.

11:30 am Continue W on Rte 380 to join I-25. Proceed North on I-25 for 8 miles to Exit 147 at Socorro. Drive through the town and pick up Rte 60 continuing West through Magdalena and onto the site of the VLA. Exit South onto Rte 166 and drive to the administration center.

12:30 am Lunch stop. After lunch **Jonathan Fortney** will describe what all the antennas are for and discuss the SETI program.

1:30 pm Return to Rte 60 and continue West to the town of Datil.

2:00 pm In Datil **Abigail Wasserman** will treat us to a discussion of the history of Uranium mining in this area and in the Grants region farther north.

2:30 pm Proceed Southwest from Datil on Rte 12 through the Gila wilderness. We will stop at the Continental Divide for **Windy Jaeger** to regale us with the geologic story of the giant volcano that created this region.

3:30 pm Continue SW on Rte 12. Turn South at the junction of Rte 180, drive to the junction of Rte 78 and proceed to the junction of Rte 75. Turn north on Rte 75 toward Clifton.

5:00 pm Stop at the overlook to the main pit of the Morenci mine. At this site **Ingrid Daubar** will discuss the generall process of hydrothermal deposition by water in the vicinity of igneous intrusions and **David O'Brien** will enlighten us on the activities we see below.

6:00 pm Leave the Big Pit, return South on Rte 75 to its junction with historic Rte 666. Proceed through Safford and continue South until the junction with I-10. Turn West on I-10 and return to Tucson.

7:30 pm Arrive Tucson, unpack vehicles, go home. Drivers return vehicles to motor pool.

== *finis* ==

Drivers: J. Barnes, R. Beyer, F. Ciesla, I. Daubar, E. Eckholm, J. Plassmann,

Participants:

Alpert, A.
Barnes, J.
Bart, G.
Beyer, R.
Ciesla, F.
Daubar, I.
Eckholm, A.
Fortney, J.
Grier, J.
Hurford, T.
Jaeger, W.
Lorenz, R.
Mastrapa, R.
Melosh, J.
O'Brien, D.
Plassmann, J.
Radebaugh, J.
Richardson, J.
Spitale, J.
Wasserman, A.
Withers, P.

ARIZONA

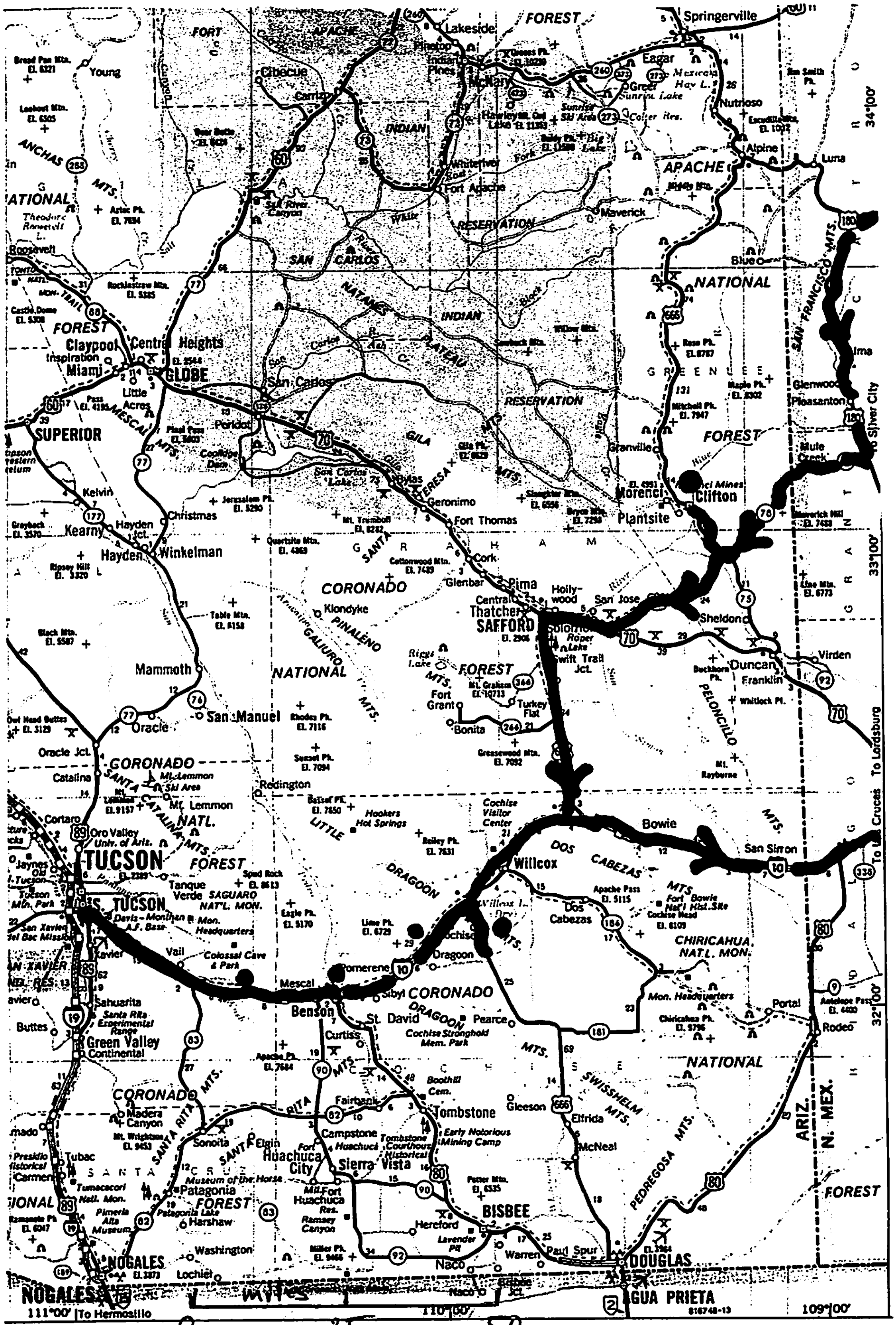

Springerville
Lakeside
FOREST
FORT
APACHE
Cibecue
McNary
Eagar
Alpine
Luna
Young
Whiteriver
Fort Apache
INDIAN
RESERVATION
APACHE
Maverick
SAN
CARLOS
NATIONAL
Blue
Roosevelt
FOREST
Claypool
Central Heights
Inspiration
Miami
GLOBE
San Carlos
Peridot
SUPERIOR
GILA
Morenci
Clifton
Plantsite
Geronimo
Fort Thomas
Kelvin
Kearny
Hayden
Winkelman
Christmas
Pima
Thatcher
SAFFORD
San Jose
Sheldon
Duncan
Franklin
Virden
CORONADO
Klondyke
NATIONAL
FOREST
Mammoth
San Manuel
Oracle
Oracle Jct.
Bonita
Redington
Mt. Lemmon
Cortaro
Oro Valley
TUCSON
S. TUCSON
Vail
Bowie
San Simon
Willcox
Dos Cabezas
Pomerene
Mescal
Benson
St. David
Dragoon
Pearce
CHIRICAHUA NAT'L. MON.
Portal
Rodeo
Sahuarita
Green Valley
Continental
Tombstone
Gleeson
Elfrida
McNeal
Sonoita
Elgin
Huachuca City
Sierra Vista
Patagonia
Hereford
BISBEE
Naco
DOUGLAS
AGUA PRIETA
NOGALES
Lochiel
Washington
Tubac
ARIZ.
N. MEX.
To Silver City
To Lordsburg
To Las Cruces
To Hermosillo
111°00'
110°00'
109°00'
34°00'
33°00'
32°00'
MILES
0
25
50

NEW MEXICO

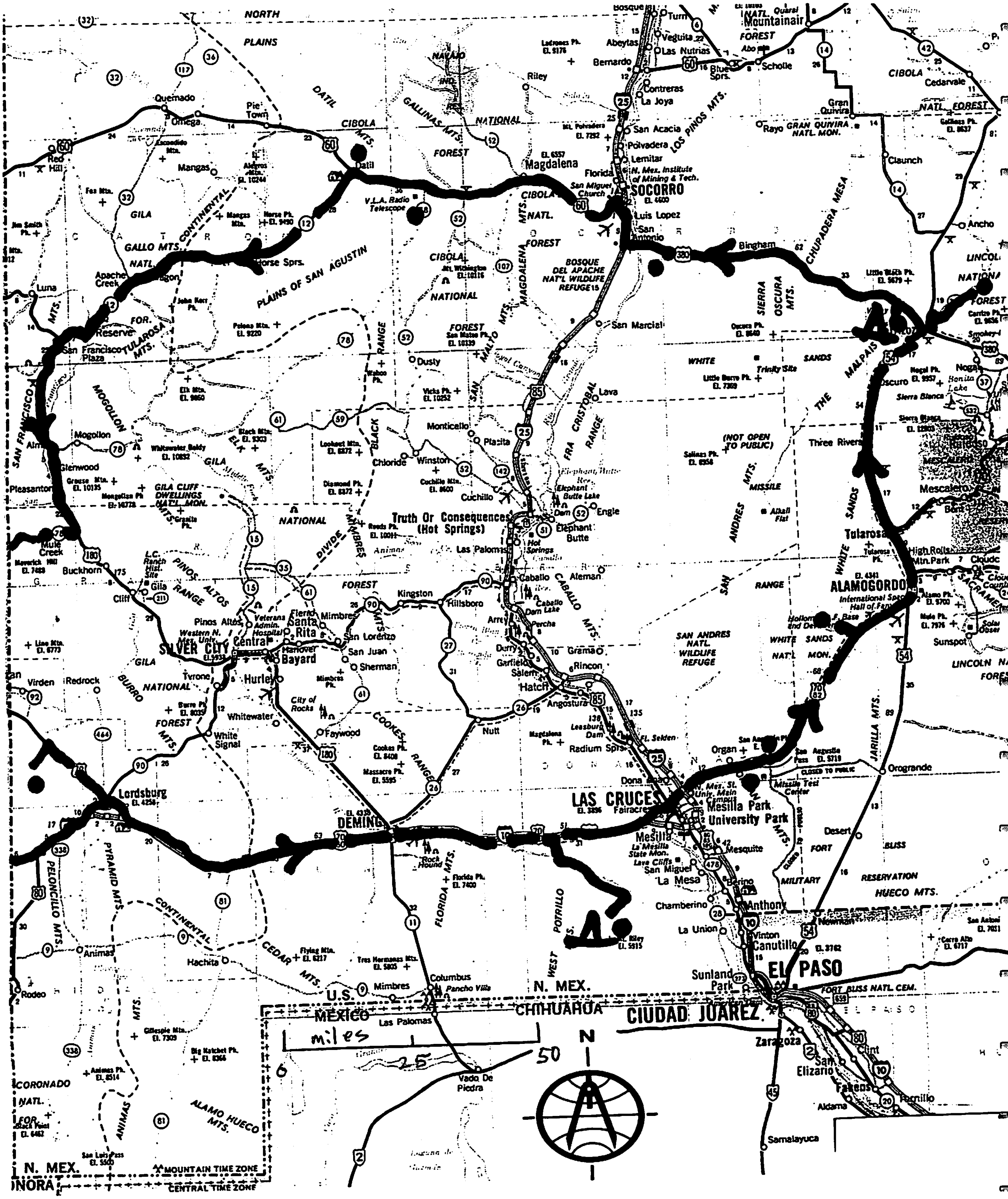

0 25 50
miles

Generalized Geologic Map of New Mexico

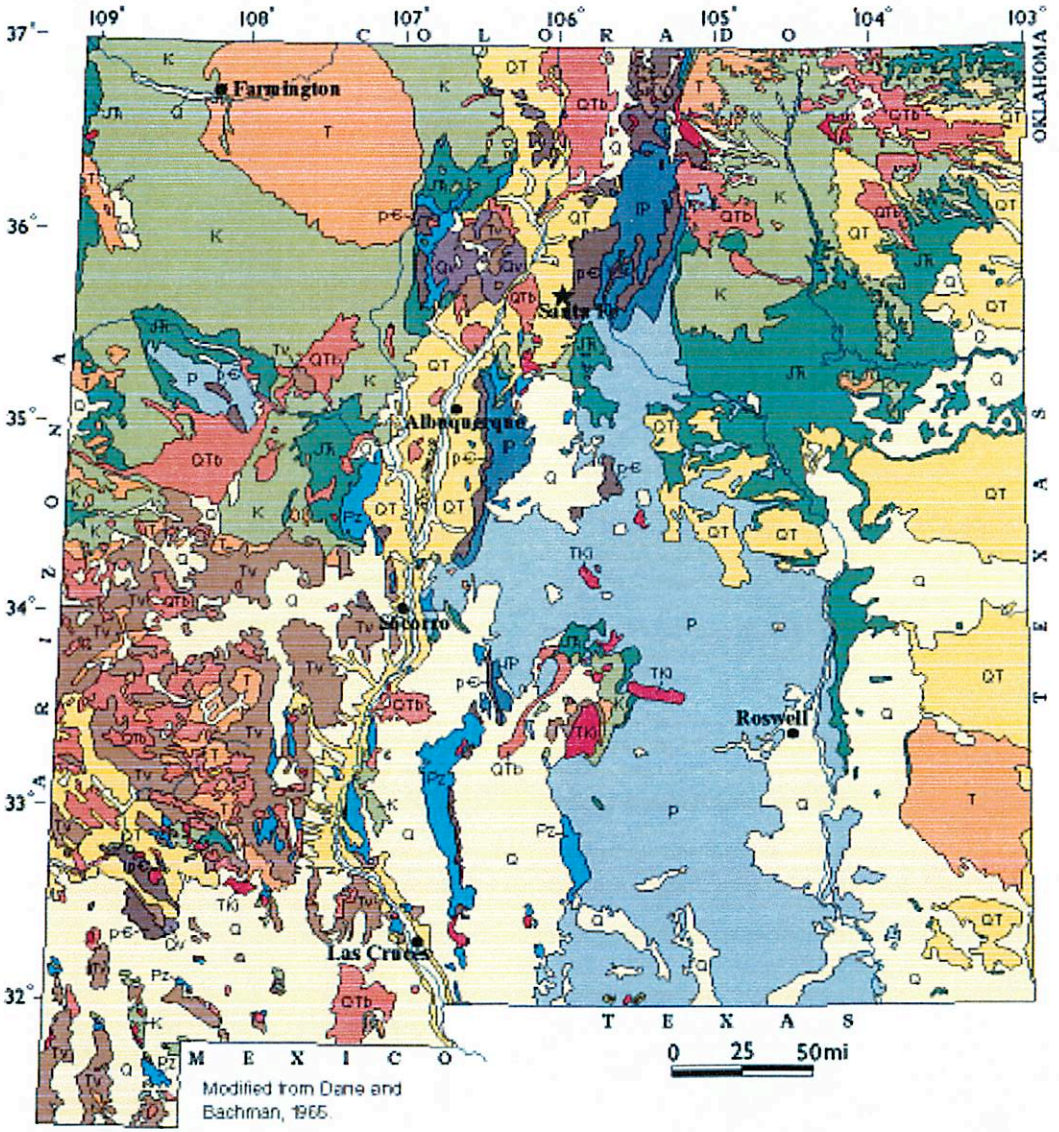

EXPLANATION

ERA	PERIOD	SEDIMENTARY	IGNEOUS
CENOZOIC 65 m.y.-present	QUATERNARY	Q, QT	Qv, QTb
	TERTIARY	T, QT	Tv, QTb, TKi
MESOZOIC 245 m.y.-65 m.y.	CRETACEOUS	K	
	JURASSIC	JR	
	TRIASSIC	JR	
PALEOZOIC 544 m.y.-245 m.y.	PERMIAN	P, Pz	
	PENNSYLVANIAN	IP, Pz	
	MISSISSIPPIAN	Pz	
	DEVONIAN	Pz	
	SILURIAN	Pz	
	ORDOVICIAN	Pz	
	CAMBRIAN	Pz	
PRECAMBRIAN 4.5 b.y.-544 m.y.		p€	

- Q — Quaternary sediments
- QT — Quaternary-Tertiary sediments
- Qv — Quaternary rhyolites and tuffs
- QTb — Quaternary-Tertiary basalts and andesites
- T — Tertiary sediments
- Tv — Tertiary volcanics
- TKi — Tertiary-Cretaceous intrusives
- K — Cretaceous sediments
- JR — Jurassic-Triassic
- P — Permian
- IP — Pennsylvanian
- Pz — Paleozoic undifferentiated
- p€ — Precambrian

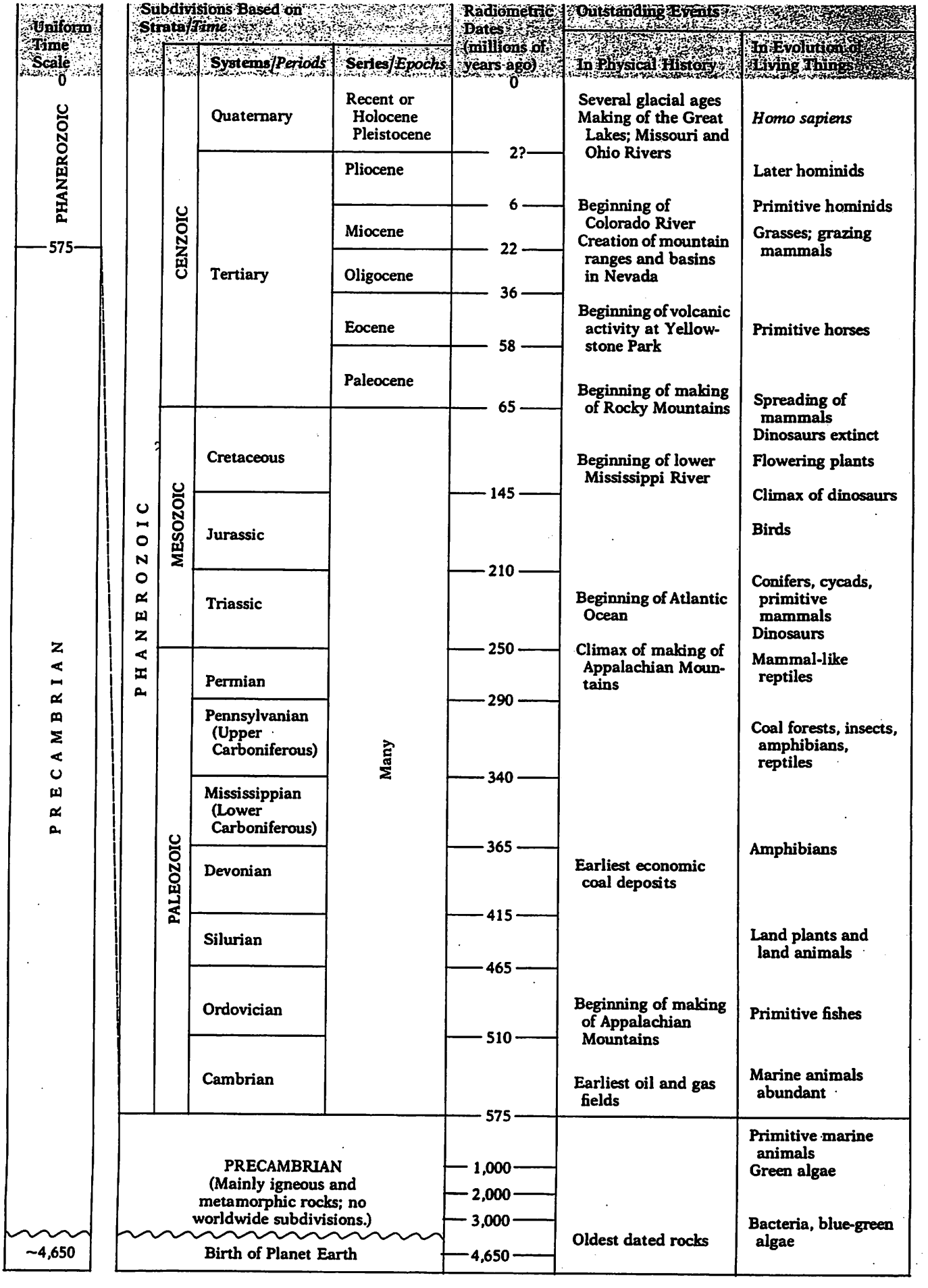

Flint & Skinner, "Physical Geology" 2 ed (1977)

MINERAL NAMES

Mineral	Formula	Mineral	Formula
Åkermanite	$Ca_2MgSi_2O_7$	Hematite	Se_2O_3
Alabandite	(Mn,Fe)S	Hercynite	$(Fe,Mg)Al_2O_4$
Albite	$NaAlSi_3O_8$	Hibonite	$CaAl_{12}O_{19}$
Andradite	$Ca_3Fe_2Si_3O_{12}$	Ilmenite	$FeTiO_3$
Anorthite	$CaAl_2Si_2O_8$	Kaersutite	$Ca_2(Na,K)(Mg,Fe)_4TiSi_6$-$Al_2O_{22}F_2$
Apatite	$Ca_3(PO_4)_2$		
Aragonite	$CaCO_3$	Kamacite	α-(Fe,Ni)
Armalcolite	$FeMgTi_2O_5$	Krinovite	$NaMg_2CrSi_3O_{10}$
Augite	$Mg(Fe,Ca)Si_2O_6$	Lawrencite	$(Fe,Ni)Cl_2$
Awaruite	Ni_3Fe	Lonsdaleite	C
Baddeleyite	ZrO_2	Mackinawite	FeS_{1-x}
Barringerite	$(Fe,Ni)_2P$	Maghemite	Se_2O_3
Bassanite	$CaSO_4 \cdot 1/2H_2O$	Magnesiochromite	$MgCr_2O_4$
Bloedite	$Na_2Mg(SO_4)_2 \cdot 4H_20$	Magnesite	$(Mg,Fe)CO_3$
Brezinaite	Cr_3S_4	Magnetite	Fe_3O_4
Brianite	$CaNa_2Mg(PO_2)$	Majorite	$Mg_3(MgSi)Si_3O_{12}$
Buchwaldite	$NaCaPO_4$	Marcasite	FeS_2
Calcite	$CaCO_3$	Melilite solid solution	
Carlsbergite	CrN	åkermanite (Ak)	$Ca_2MgSi_2O_7$
Caswellsilverite	$NaCrS_2$	gehlenite (Ge)	$Ca_2Al_2SiO_7$
Chalcopyrite	$CuFeS_2$	Merrihueite	$(K,Na)_2Fe_5Si_{12}O_{30}$
Chamosite	$Fe_6Mg_3[(Si_4O_{10})(OH)_8]_2$	Merrillite	$Ca_9MgH(PO_4)_7$
Chaoite	C	Mica	$(K,Na,Ca)_2Al_4[Si_6Al_2O_{70}]$-$(OH,F)_4$
Clinopyroxene	$(Ca,Mg,Fe)SiO_3$		
Chlorapatite	$Ca_5(PO_4)_3Cl$	Molybdenite	MoS_2
Chromite	$FeCr_2O_4$	Monticellite	$Ca(Mg,Fe)SiO_4$
Cohenite	$(Fe,Ni)_3C$	Montmorillonite	$Al_4(Si,Al)_8O_{20}(OH)_4Mg_6$-$(Si,Al)_8O_{20}(OH)_4$
Copper	Cu		
Cordierite	$Mg_2Al_4Si_5O_{18}$	Nepheline	$NaAlSiO_4$
Corundum	Al_2O_3	Niningerite	(Mg,Fe)S
Cristobalite	SiO_2	Oldhamite	CaS
Cronstedtite	$(Mg,Fe)_2Al_3Si_5AlO_{18}$	Olivine	$(Mg,Fe)_2SiO_4$
Cubanite	$CuFe_2S_3$	Olivine solid solution	
Daubreelite	$FeCr_2S_4$	fayalite (Fa)	Fe_2SiO_4
Diamond	C	forsterite (Fo)	Mg_2SiO_4
Diopside	$CaMgSi_2O_6$	Orthoclase	$KAlSi_3O_8$
Djerfisherite	$K_3CuFe_{12}S_{14}$	Orthopyroxene	$(Mg,Fe)SiO_3$
Dolomite	$CaMg(CO_3)_2$	Osbornite	TiN
Enstatite	$MgSiO_3$	Panethite	$(Ca,Na)_2(Mg,Fe)_2(PO_4)_2$
Epsomite	$MgSO_4 \cdot 7H_2O$	Pentlandite	$(Fe,Ni)_9S_8$
Farringtonite	$Mg_3(PO_4)_2$	Perovskite	$CaTiO_3$
Fassaite	$Ca(Mg,Ti,Al)(Al,Si)_2O_6$	Perryite	$(Ni,Fe)_5(Si,P)_2$
Fayalite	Fa_2SiO_4	Pigeonite	$(Fe,Mg,Ca)SiO_3$
Feldspar solid solution		Plagioclase	
albite (Ab)	$NaAlSi_3O_8$	albite	$NaAlSi_3O_8$
anorthite (An)	$CaAl_2Si_2O_8$	anorthite	$CaAl_2Si_2O_8$
orthoclase (Or)	$KAlSi_3O_8$	Portlandite	$Ca(OH)_2$
Ferrosilite	$FeSiO_3$	Potash feldspar	$(K,Na)AlSi_3O_8$
Forsterite	Mg_2SiO_4	Pyrite	FeS_2
Gehlenite	$Ca_2Al_2SiO_7$	Pyrope	$Mg_3Al_2(SiO_4)_3$
Gentnerite	$Cu_8Fe_3Cr_{11}S_{18}$	Pyroxene solid solution	
Graftonite	$(Fe,Mn)_3(PO_4)_2$	enstatite (En)	$MgSiO_3$
Graphite	C	ferrosilite (Fs)	$FeSiO_3$
Greigite	Fe_3S_4	wollastonite (Wo)	$CaSiO_3$
Grossular	$Ca_3Al_2Si_3O_{12}$	Pyrrhotite	$Fe_{1-x}S$
Gypsum	$CaSO_4 \cdot 2H_2O$	Quartz	SiO_2
Haxonite	$Fe_{23}C_6$	Rhönite	$Ca_4(Mg,Al,Ti)_{12}(Si,Al)_{12}O_{40}$
Heazlewoodite	Ni_3S_2	Richterite	$Na_2CaMg_5Si_8O_{22}F_2$
Hedenbergite	$CaFeSi_2O_6$	Ringwoodite	$(Mg,Fe)_2SiO_4$
Heideite	$(Fe,Cr)_{1+x}(Ti,Fe)_2S_4$	Roaldite	$(Fe,Ni)_4N$

MINERAL NAMES *continued*

Mineral	Formula	Mineral	Formula
Roedderite	$(K,Na)_2Mg_5Si_{12}O_{30}$	Stanfieldite	$Ca_4(Mg,Fe)_5(PO_4)_6$
Rutile	TiO_2	Suessite	Fe_3Si
Sanidine	$KAlSi_3O_8$	Sulfur	S
Sarcopside	$(Fe,Mn)_3(PO_4)_2$	Taenite	γ-(Fe,Ni)
Scheelite	$CaWO_4$	Tetrataenite	FeNi
Schöllhornite	$Na_{0.3}(H_2O)$ $[CrS_2]$	Thorianite	ThO_2
Schreibersite	$(Fe,Ni)_3P$	Tridymite	SiO_2
Serpentine (or chlorite)	$(Mg,Fe)_6Si_4O_{10}(OH)_8$	Troilite	FeS
Sinoite	Si_2N_2O	Ureyite	$NaCrSi_2O_6$
Smythite	Fe_9S_{11}	V-rich magnetite	$(Fe,Mg)(Al,V)_2O_4$
Sodalite	$Na_8Al_6Si_6O_{24}Cl_2$	Valleriite	$CuFeS_2$
Sphalerite	(Zn,Fe)S	Vaterite	$CaCO_3$
Spinel	$MgAl_2O_4$	Whewellite	$CaC_2O_4 \cdot H_2O$
Spinel Solid Solution		Wollastonite	$CaSiO_3$
spinel	$MgAl_2O_4$	Yagiite	$(K,Na)_2(Mg,Al)_5(Si,Al)_{12}O_{30}$
hercynite	$FeAl_2O_4$	Zircon	$ZrSiO_4$
chromite	$FeCr_2O_4$		
magnesiochromite	$MgCr_2O_4$		
V-rich magnetite	$(Fe,Mg)(Al,V)_2O_4$		

"Meteorites & The Early Solar System" Kerridge & Matthews, ed. U of A Press (1988).

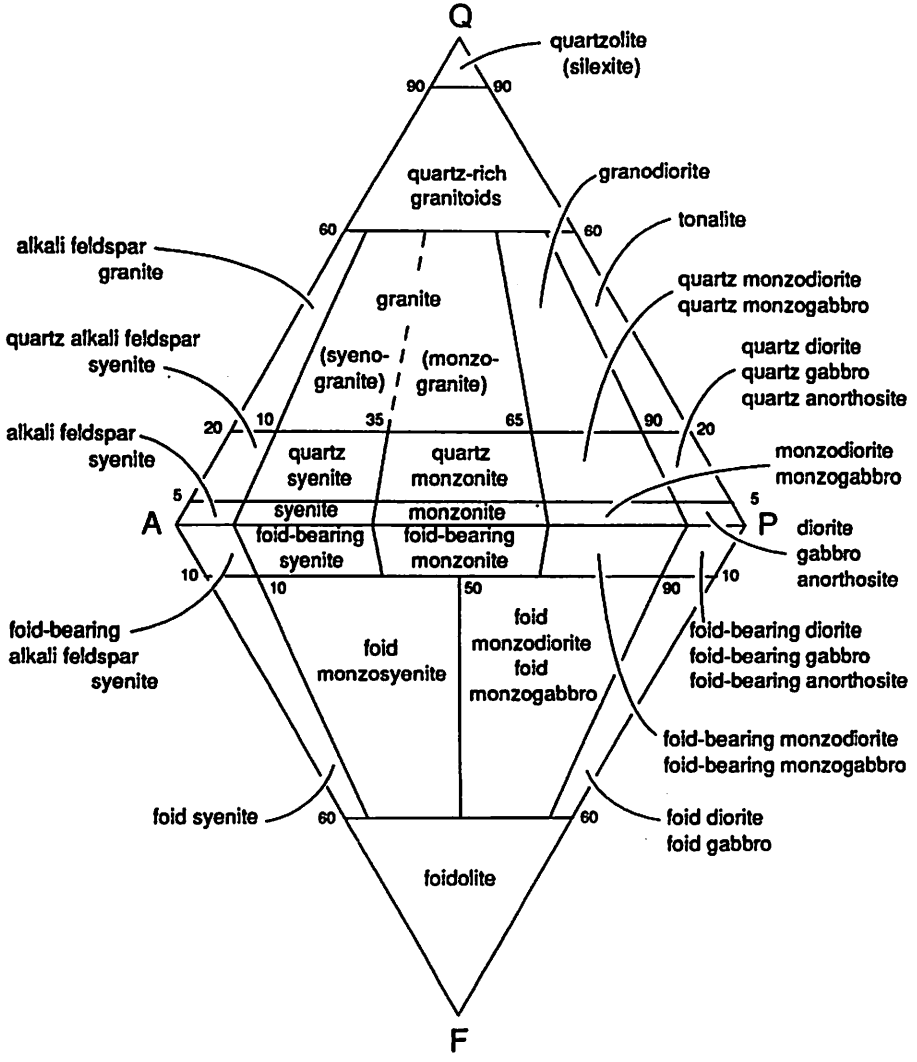

Fig. B.4. Classification and nomenclature of plutonic rocks according to their modal mineral contents using the QAPF diagram (based on Streckeisen, 1976, Fig. 1a). The corners of the double triangle are Q = quartz, A = alkali feldspar, P = plagioclase and F = feldspathoid. However, for more detailed definitions refer to section B.2. This diagram must not be used for rocks in which the mafic mineral content, M, is greater than 90%.

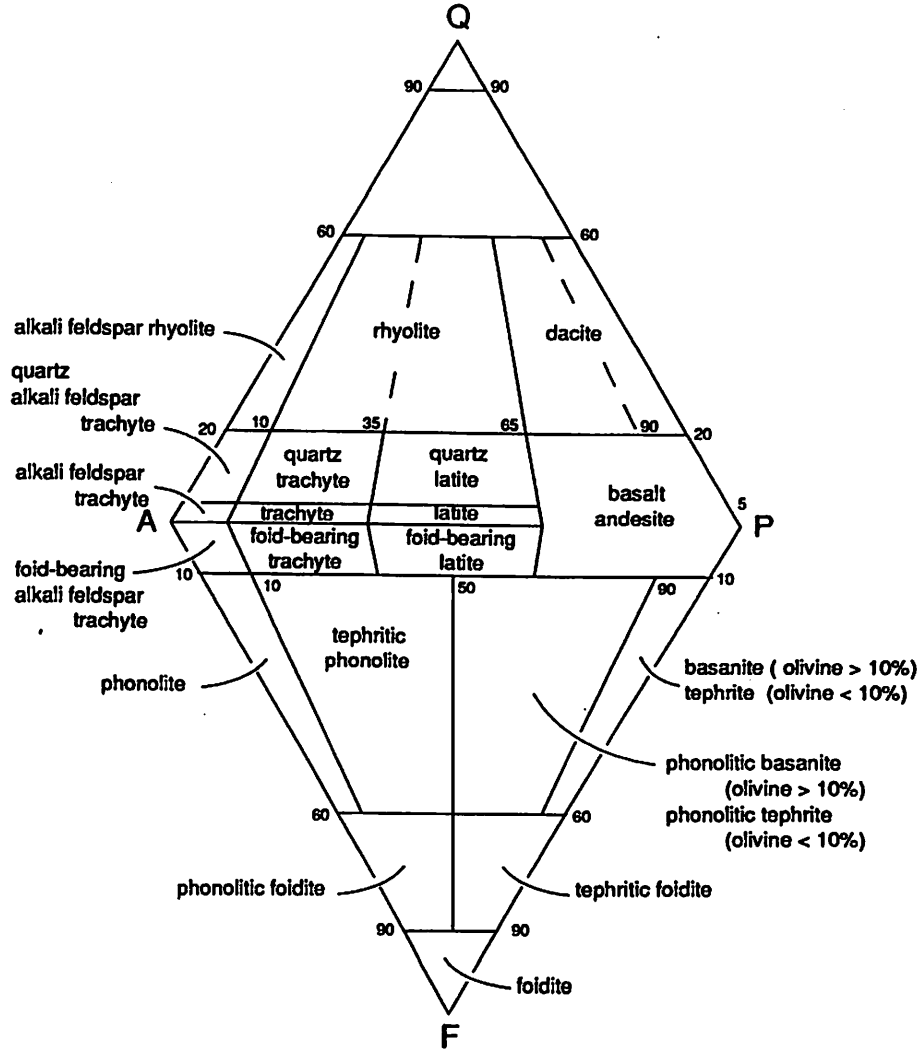

Fig. B.10. Classification and nomenclature of volcanic rocks according to their modal mineral contents using the QAPF diagram (based on Streckeisen, 1978, Fig. 1). The corners of the double triangle are Q = quartz, A = alkali feldspar, P = plagioclase and F = feldspathoid. However, for more detailed definitions refer to section B.2.

"Classification of Igneous Rocks and Glossary of Terms" Le Maitre, ed. Blackwell Scientific Publications (1989)

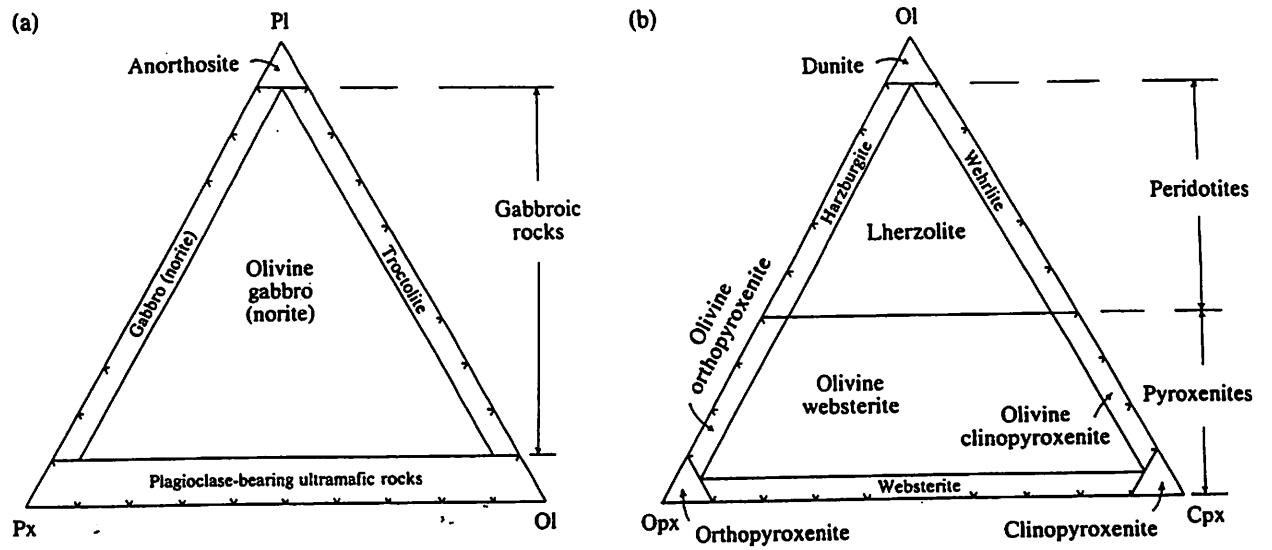

Figure 5-26 Classification of phaneritic rocks comprised of some combination of plagioclase, olivine, and pyroxene. (a) Rocks with major amounts of plagioclase (usually labradorite–bytownite). The field of gabbro is large and modifying prefixes are helpful, such as feldspathic gabbro, leuco-gabbro, olivine-rich gabbro, and so on. Gabbro in which the pyroxene is principally orthopyroxene can be called norite. (b) Classification of ultramafic phaneritic rocks comprised of olivine and pyroxenes. [After A. Streckeisen, 1979, Classification and nomenclature of volcanic rocks, lamprophyres, carbonatites, and melilitic rocks: Recommendations and suggestions of the IUGS Subcommission on the Systematics of Igneous Rocks, *Geology* 7.]

Best, "Igneous & Metamorphic Petrology"

FIG. 13.47. *(a)* Pyroxene compositions in the system $CaSiO_3$-$MgSiO_3$-$FeSiO_3$. General compositional fields are outlined. Representative tielines across the miscibility gap between augite and more Mg-Fe-rich pyroxenes are shown. The "augite" field is labeled with quotation marks because all augite compositions contain considerable Al which is not considered in this triangular composition diagram.

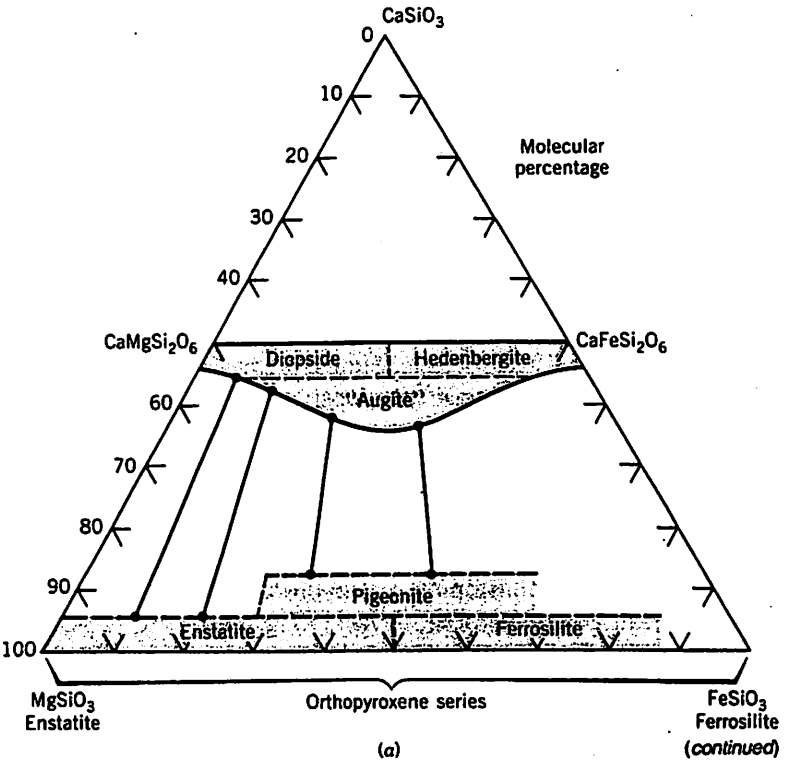

Klein & Hurlbut, "Manual of Mineralogy"

(continued)

The Cross Hill Landslide

Andreas Ekholm

Landslides

A landslide can be of one of three main types: a fall, a slide, or a flow. Falls involve free-falling material, slides are characterized by the moving mass displacing along one or more narrow shear zones, and flows move in a manner resembling that of a viscous fluid. All three types can occur in different materials and topographic settings; often, more than one type occur in a single event. Landslides are relatively common in the Basin-and-Range province, as it is/has been a tectonically active region.

The Cross Hill landslide is of the flow type; more specifically, it is (or rather, was) a *rock avalanche*. It is a relatively large landslide — the associated breccia deposit crops out over an area of more than 6 km^2, and its total volume is estimated at over 2×10^7 m^3. Large rock avalanches (volume greater than ~10^7 m^3) are anomalous in the sense that they flow out horizontally for a much longer distance than one would expect based on the energy of the flow and the coefficient of friction of the constituent material. Small rock masses travel horizontally about one or two times the vertical fall. Large rock avalanches, however, can travel horizontal distances tens of times larger than the total vertical drop.

There are a number of suggestions in the literature for how this can happen (e.g. air lubrication/cushioning and melt-layer sliding); the currently favored model (at least by Jay!) is acoustic fluidization. In the acoustic fluidization model, the effective viscosity of the flow is reduced by the action of elastic waves (i.e. sound) within the material; even though the average pressure at any given point in the flow is equal to the overburden pressure, the low-pressure "troughs" of passing elastic waves temporarily lower the pressure enough to let the individual rock fragments slide past one another.

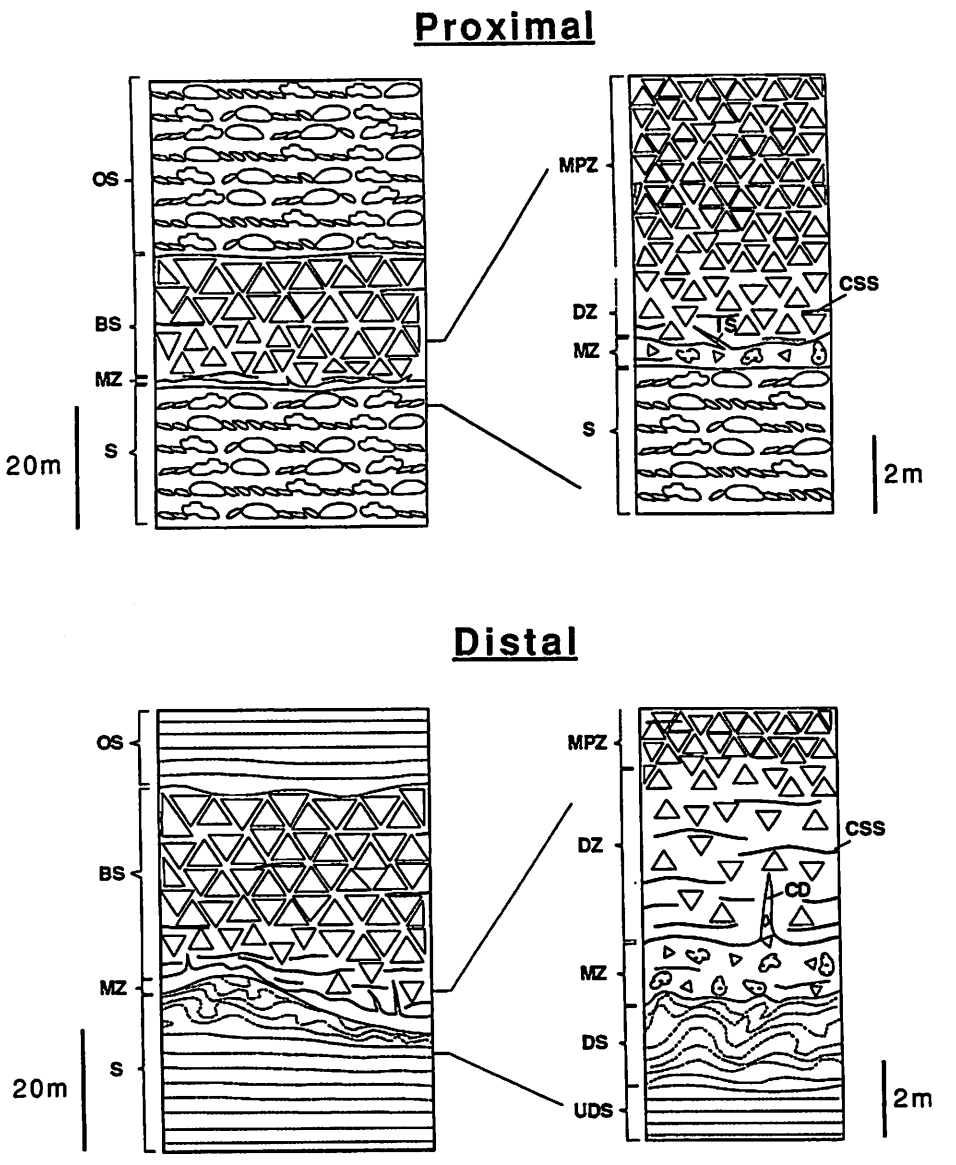

Figure 15. Characteristic features within proximal and distal portions of large rock-avalanche deposits investigated, showing: substrate (S); undisturbed substrate (UDS); disturbed substrate (DS); mixed zone of entrained substrate and comminuted breccia (MZ); disturbed zone (DZ) of the breccia sheet (BS) that displays comminuted slip surfaces (CSS), and is intruded by clastic dikes (CD) and intrusive stringers (IS; load structures and poorly-developed clastic dikes) derived from the mixed zone; matrix-poor zone (MPZ) of the breccia sheet; and overlying sediments (OS). In places, a discontinuous megabreccia cap occurs along the top of the breccia sheet.

Characteristics of Large Rock Avalanche Deposits

Substrate. In a dry climate region, the substrate sediments are usually coarser under the proximal portion of a rock avalanche deposit than under the distal portion. The reason for this is that the proximal portion is located farther up the basin side, where the underlying alluvial fan sediments are coarser than closer to the basin floor (where very fine-grained lacustrine sediments may also be present). The upper surface of the substrate may be scoured to depths of 5–10 m or more, and the bedding in sediments immediately below

the basal contact may be folded or contorted. Substrate deformation is more severe underneath the distal portion of the avalanche deposit and usually dies out over an interval of 1–15 m below the avalanche-substrate contact.

Mixed zone. The mixed zone is a region of substrate/avalanche mixing at the base of the avalanche deposit. It is composed of a silty to sandy conglomerate, and generally thickens distally (as does the entire avalanche deposit). Particle sizes are significantly smaller than in the overlying breccia sheet, and large breccia blocks are rare to absent.

Clastic dikes. Clastic dikes of mixed-zone material often extend up into the overlying breccia sheet, especially in the distal portion of the avalanche. They range from a few centimeters to one meter in thickness, and are generally 2–3 m in length.

Breccia sheet. The breccia sheet consists of a disrupted zone near its base and an overlying matrix-poor zone. It also locally contains well-developed comminuted slip surfaces. The disrupted zone is up to 10 m thick and composed of a matrix-rich breccia, whose clasts usually range from a few centimeters to several meters in size. The matrix material typically consists of silty sandstone that is predominantly derived from adjacent clasts, although minor admixture of substrate fines also occurs. The matrix-poor zone is dominated by jigsaw and crackle-breccia facies.* Avalanche blocks contained within this zone, most of which are internally brecciated, can range from a few meters to many tens of meters in size.

The Cross Hill Landslide

Cross Hill is located in the Cienega Gap south of the Rincon Mountains, about a mile north of I-10 and roughly 30 miles southeast of downtown Tucson. The hill is the site of a quarry where the high-alumina clays of the upper Pantano Formation are being mined for brick production by the Arizona Portland Cement Company. The quarry provides an excellent exposure of the base of the distal portion of the Cross Hill landslide.

The Cross Hill landslide occurred in the late Oligocene to early Miocene (about 20–25 My ago), and originated from the north or northeast during tectonic denudation of the Santa Catalina-Rincon metamorphic core complex. The landslide breccia crops out over an area greater than 6 km^2, is more than 4.5 km long, and ranges in thickness from 0 to 50 m (thinning southward). At Cross Hill, it is deposited mostly on top of (but also disrupts) the clay layer of the upper Pantano Formation. It is composed of debris derived from four different rock types: middle Proterozoic Rincon Valley Granodiorite, Cambrian Bolsa Quartzite, the shale and limestone of the Cambrian Abrigo Formation, and the Devonian Martin Formation limestone.

The proximal part of the deposit a few km north of Cross Hill is about 30 m thick and dominated by jigsaw and crackle breccia facies derived from the Abrigo and Martin Formations. Yarnold and Lombard describe the distal part exposed at Cross Hill as follows:

---

* Jigsaw breccia: A breccia facies in which the internal fragments are separated from one another by thin bands of matrix material, but are not significantly rotated with respect to one another; the pieces can be put back together as in a jigsaw puzzle.
Crackle breccia: A zone or transported block of pervasively shattered rock, in which the internal fragments show little to no separation and rotation relative to one another.

"The distal portion of the rock-avalanche lobe is well exposed at Cross Hill Quarry, where it overlies gently-dipping gypsiferous claystone. Its base is broadly undulatory with up to 20 m of relief, and the underlying claystone displays folding and imbrication over an interval of about 4 m immediately below the avalanche-substrate contact (Figure 12).

The rock-avalanche debris displays a basal layer up to 75 cm thick of thoroughly comminuted limestone that is overlain by a thick interval of matrix-rich to crackle breccia facies segregated into nearly monolithologic zones derived from Abrigo Formation, Bolsa Quartzite, and Rincon Valley Granodiorite. The entire thickness of the deposit at Cross Hill Quarry is approximately 30 m."

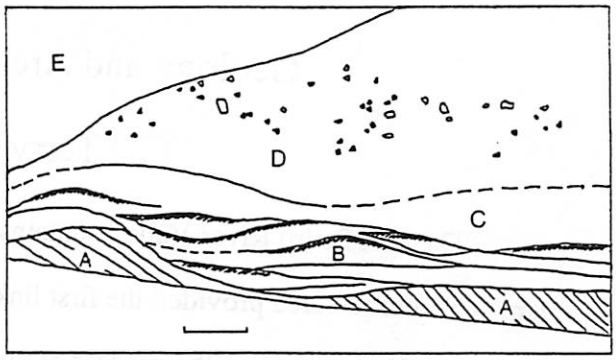

Figure 12. Basal contact of the Cross Hill breccia deposit at Cross Hill clay quarry, showing (A) east-dipping undeformed substrate sediments, (B) imbricated slices of sandstone and mudstone substrate sediments (marker bed shaded), (C) interval of thoroughly comminuted limestone, (D) matrix-rich breccia with cobbles, and (E) matrix-poor breccia. Scale bar is 1 m.

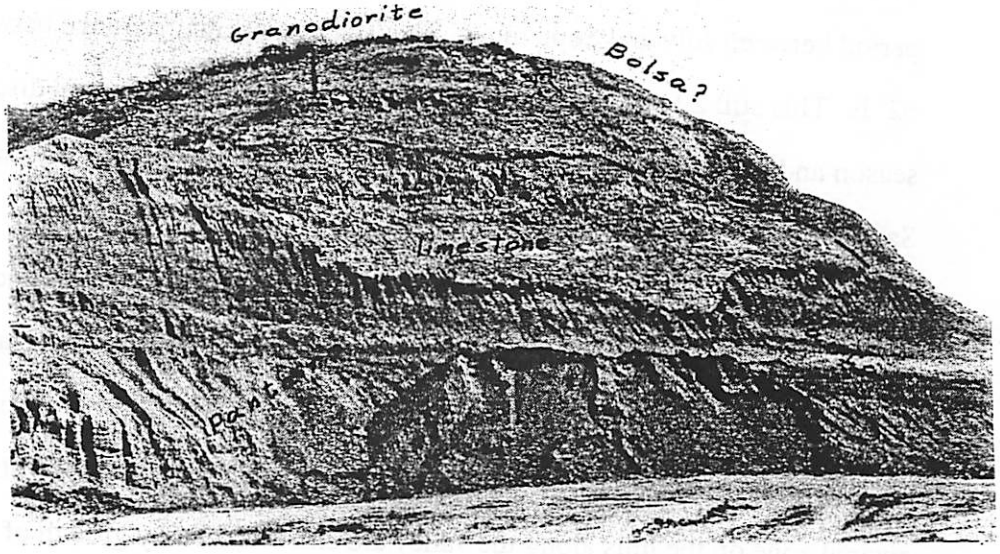

Bibliography

Arnold, L. C., 1971, Structural geology along the southeastern margin of the Tucson basin, Pima County, Arizona; M. S. Thesis, University of Arizona, Tucson.

Drewes, H., 1988, Southeast Arizona tectonics, in *Geological Society of America field trip guidebook, 1988*; Centennial Meeting, Denver, Colorado.

Houser, B. B. (ed.), 1992, Industrial minerals of the Tucson area and San Pedro Valley, southeastern Arizona; Arizona Geological Society, Tucson, Arizona.

Melosh, H. J., 1986, The physics of very large landslides, *Acta Mechanica* **64**, 89–99.

Yarnold, J. C., and Lombard, J. P., 1989, A facies model for large rock-avalanche deposits formed in dry climates, in Colburn, I. P., Abbott, P. L., and Minch, J. (eds.), *Conglomerates in basin analysis: A symposium dedicated to A. O. Woodford*, Pacific Section of the Society of Economic Paleontologists and Mineralogists **62**, 9–31.

San Pedro River Valley:

Geology and Archeology of the Area

Terry Hurford

The San Pedro River Valley contains important clues to the lifeways of prehistoric man. This unique area provided the first links between man and now extinct animals in the southwest. Understanding the process of change in Southern Arizona sheds light on its history and geological background.

Present Climate:

Present climate of the San Pedro Valley is described as semi-arid and mesothermal. The area receives about 13 inches of rain a year, the majority of it falling during the rainy period between July and September. The yearly temperatures range between 44 ° F and 62° F. This still allows the San Pedro to be perennial, with minimal discharge in the dry season and many stretches of subsurface flow. There never exists a water surplus in the San Pedro during any season.

The San Pedro provides for three life zones; arid grasslands, encinal, and montane. The valley floor is characterized by the arid grassland. A plethora of grass species exist and are encroached upon by mesquite trees and other small shrubs. Relict islands of cottonwoods , willows and oak remain confined to the channel of the stream itself. The encinal zone on the hills along the valley are characterized by growth of oaks. Here too mesquites are quite common. Finally the montane area of pine and spruce rim the valley area.

Resent Climate:

Within the last century noticeable changes can be seen to have taken place in the San Pedro Valley. The current entrenchment of the stream began in 1883 and moved 125 miles in ten years. This entrenchment began at the mouth and moved headward as the arroyo eroded the river channel. The entrenchment excavated the stream. One example comes

from Hereford, Az. where in 1910 a narrow channel of 3 feet in depth flowed. Prior to that in 1890 the stream was a series of grassy swells.

Before the 1800's accounts by Spanish explorers and Father Kino tell of a valley with a river running through it that could support native fish and beavers. These early Spanish settlers introduced cattle and horses to the valley, finding it a suitable place for grazing.

Prehistoric Climate:

At the end of the last ice age Southern Arizona had a much wetter, cooler climate. Since that time the area has been growing more arid. Now extinct animals like the Mammoth used to thrive in this area having migrated into the New World through a land bridge between Alaska and Asia. The water level used to be much higher too. Ancient prehistoric lakes and swamps have been identified in the San Pedro valley.

San Pedro Sediments and Artifacts:

The San Pedro is know for its rich archeological record. In 1952 at Naco and 1955 at Lehner ranch Mammoth remains were found with human spear points associated with them. These spear points showed that man was present and organized enough to hunt the large creatures around 10,000 yrs ago. The remains of the Mammoth were found after an arroyo had eroded into sediments that had been deposited since the kill. The kill itself was found in association with a prehistoric perennial stream. They were then covered by deposits of material identified as a swamp. This rich material was covered by gravels and river deposits. The lowering of the water table accelerated by livestock and human inhabitancy allowed the stream to erode quickly to the kill site.

The site itself is higher then other sediments from that time period 10,000 yrs. ago. Thermal upwelling in the San Pedro area has lifted the level of the site. This allowed the river to cut down to its level and recently expose the kill site.

CENOZOIC

STRATIGRAPHIC COLUMN
SAN PEDRO RIVER VALLEY
STUDY AREA

Formation Name	Yrs x 10^6	Description
Unnamed gravels	≤ 2	Pleistocene and Recent: river gravels and alluvial fan deposits (possibly the informal Tres Alamos Fm of Montgomery, 1963).
Quiburus Fm	4-7	Pliocene: fine-grained lacustrine deposits with some fluvial deposits in places overlain by unnamed Pleistocene gravels and alluvial fans. The main sedimentary unit exposed in the river valley in the area of study.
Galiuro volcanic	22-29	Oligocene and Miocene: rhyolite to andesite lava flows and ash flow tuffs.
"Teran" beds	≥ 27	Oligocene: fanglomerates, sandstone, shale and mudstone with a centrally situated andesite

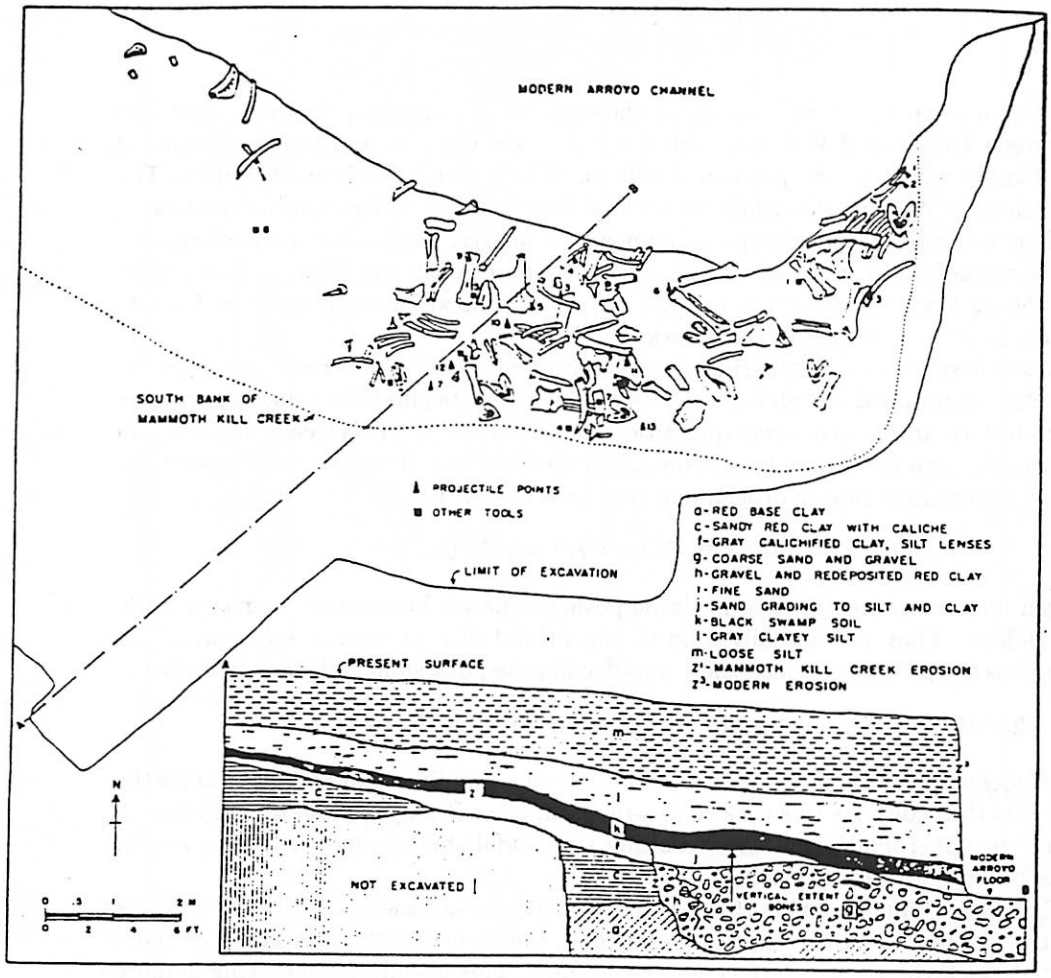

Figure 8.4. Geological profile of area of bone and artifact concentration. Main bone elements only are shown. Deposits b. d. e. n. o and erosion Z^2 do not appear in this profile but are shown in Figure 8.9. Bones occurred in deposits g–j.

The uncovering of the bones began at the eastern edge of the ex-

By the time th
ments of eight m
Bones of bison, r
three teeth and va
of the bone bed.
between two ribs
jectile points, eig
and eight miscell
sent refuse from
the projectile poi
of charcoal becam
upstream, and o
for radiocarbon d
only after the sec
ruary, 1956.

Spheroidal Weathering in Texas Canyon, AZ

Ross A. Beyer

Texas Canyon is an excellent example of the spheroidal weathering process. The I-10 highway between Tucson and Wilcox travels through Texas Canyon, and the large rounded boulders and knobs which are the product of spheroidal weathering are difficult to miss. The Roadside Geology of Arizona describes the rock of Texas canyon to be a quartz monzonite porphyry. It is basically an igneous rock composed of quartz, plagioclase, orthoclase, and other stuff, essentially a granite with large crystals. These rocks are dated as being from the Eocene (50-52 Ma). However, it's not just the rocks that we are interested in, but the processes that have been acting on these rocks.

That process is spheroidal weathering, a combination of chemical and mechanical weathering that produces rounded morphologies. The whole process begins with rain, as rainwater travels to the surface, it dissolves small quantities of carbon dioxide. This weak carbonic acid then percolates through the soil and dissolves more carbon dioxide from decaying vegetation. This carbonic acid ionizes into hydrogen ions and bicarbonate ions:

$$H_2O + CO_2 \rightarrow H_2CO_3 \rightarrow H^+ + (HCO_3)^-$$

The hydrogen ions are quite effective in decomposing minerals because of their extremely small ionic radius. They are actually able to slip in and disrupt crystal structures. An example of this is the process in which these ions decompose potassium feldspar (orthoclase):

$$2KAlSi_3O_8 + 2H^+ + H_2O \rightarrow 2K^+ + Al_2Si_2O_5\,(OH)_4 + 4SiO_2$$

So the orthoclase gets decomposed into Potassium ions, Kaolinite, and Silica. This is the chemical process that converts this rock to less-resistant clay. It may explain the weathering part, but not the spheroidal part. The resulting spheroidal shape comes from the way in which the carbonic acid attacks the rock.

This carbonic acid can only affect the rock surfaces that it can reach, so it attacks surfaces and joints. If we were to have a rock that was a cube, the corners and edges would be more susceptible to attack than a flat surface (see diagrams). This chemical weathering is more efficient on portions of the rock that have more surface area (corners and edges), ideally it would act to turn our cubical rock into a sphere. This decomposition is accompanied by a slight increase in volume of the weathered material, which sets up small forces that cause it to separate from the main body of the rock.

Spheroidal weathering exploits joint sets and small cracks. We often see long rows of weathered boulders still lined up along planes defined by the joints in the original rock mass.

What's the planetary connection? Good question. The process of spheroidal weathering essentially requires two things: an erosional agent, and a fractured rock mass susceptible to that erosional agent. This makes spheroidal weathering difficult on airless bodies. Of course, the most effective way to achieve spheroidal weathering is for that erosional agent to be water-born, and to continually whet the rocks, an unlikely scenario on planets other than the Earth.

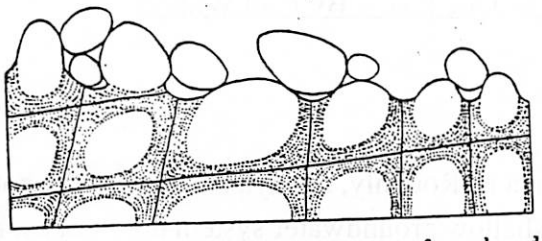

Stages in the development of egg-shaped boulders from rectangular joint blocks. (After W. M. Davis.)

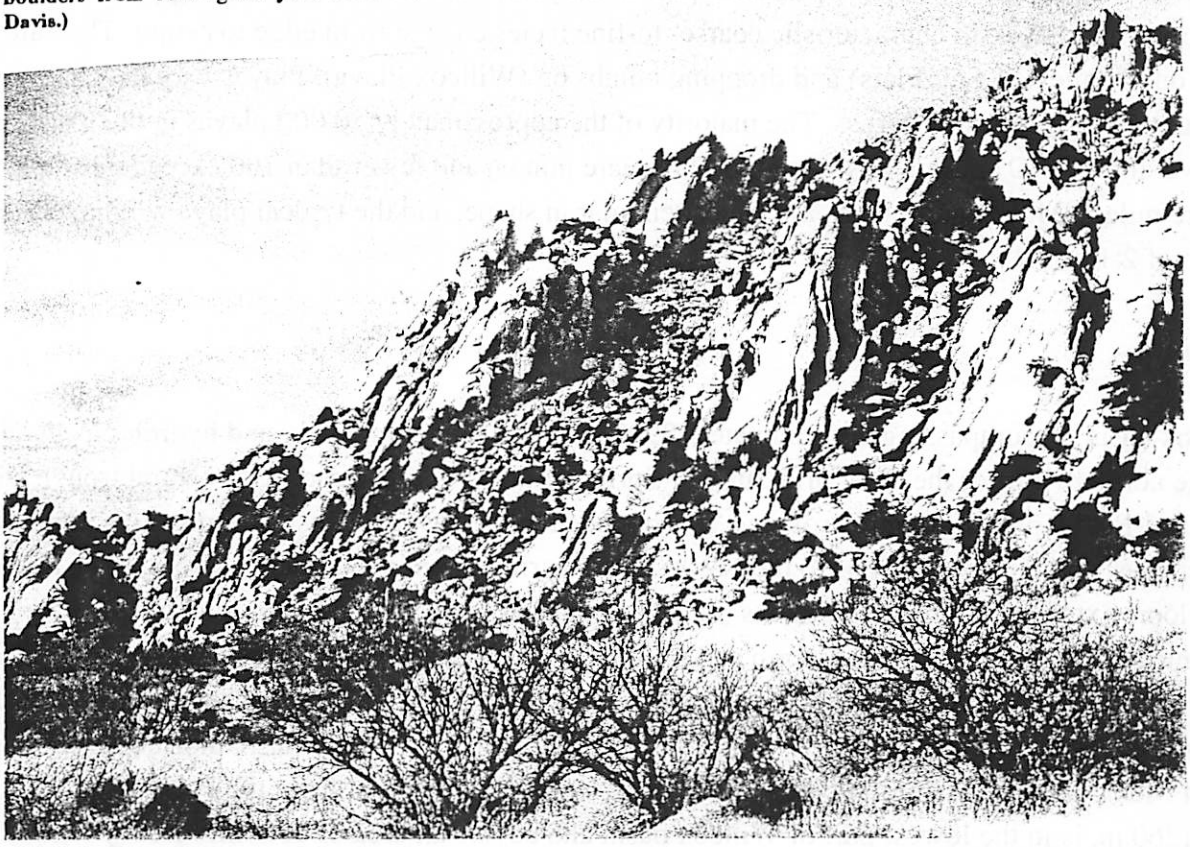

Texas Canyon stock, an Eocene 2-mica granitic rock that weathers to spectacular knobs and boulders, near the Dragoon exit of I-10, Arizona. Photo by Jack Rathbone.

Geometry of spheroidal weathering.

A. Solutions that occupy joints separating nearly cubic blocks of rock attack corners, edges, and sides at rates that decline in that order, because the numbers of corresponding surfaces are 3, 2, and 1. Corners become rounded; eventually the blocks are reduced to spheres.

B. Energy of attack has now become distributed uniformly over the whole surface, so that no further change of form can occur.

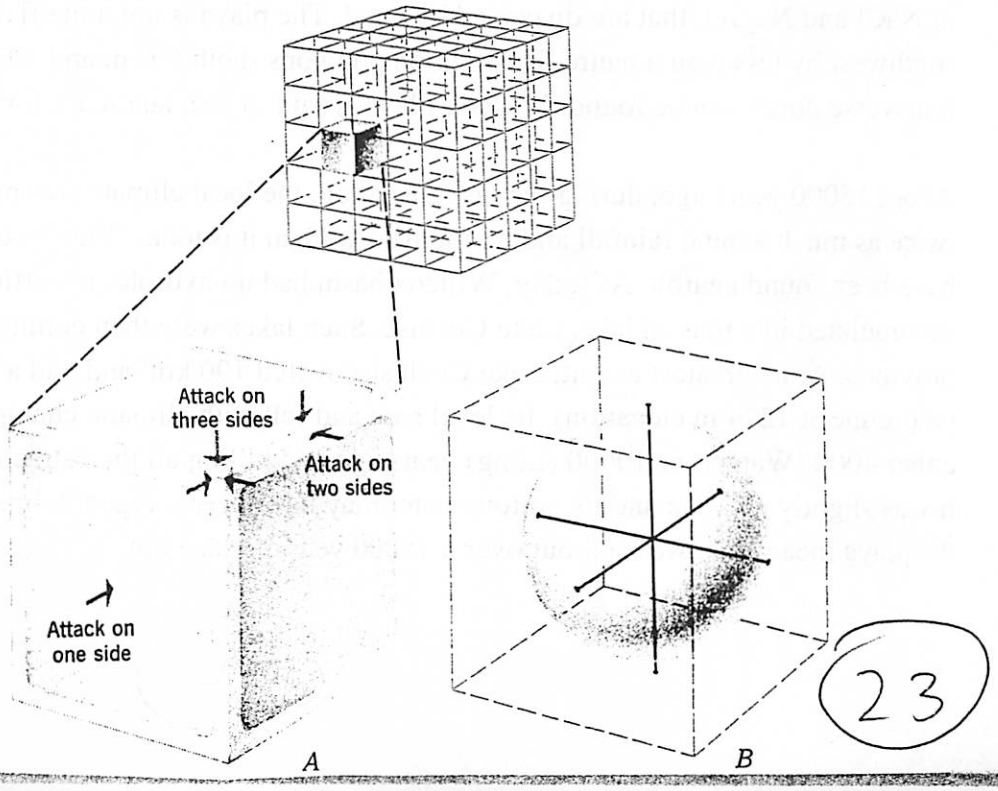

Playas and Pleistocene Lakes – Buy One, Get One Free – By Paul Withers

Playas

As is typical in geology, there is no agreement on what a playa is. Roughly, a playa is what's at the bottom of an internal drainage system in arid regions. The regional shallow groundwater system does not connect with an ocean and the surface is dry for at least part of the year. Near-surface strata are typically sedimentary evaporites with characteristic coarse- to-fine facies change from edge to centre. They are good for racing on (Bonneville Salt Flats) and dropping bombs on (Willcox Playa). Playas vary in size from tens of metres to tens of kilometres across. The majority of the approximately 50,000 playas in the world are small. Fewer than 1,000 exceed 65 square km (25 square miles), and fewer than 100 exceed 520 square km (200 square miles). Most small playas are almost circular in shape, and the typical playa will have a length-width ratio of 2:1 or 3:1.

Willcox Playa

The Willcox basin, encompassing approximately 3900 km^2, is a topographically and hydrologically closed basin in the northern part of the semi-arid Sulphur Springs Valley, a NW-trending structural trough within the Basin-and-Range physiographic province. It is bounded to the east and west by mountains (Dragoons and Chiricahuas, and their extensions to the NW) formed during the mid-Tertiary that rise 1 - 2 km above the basin floor. Extensive alluvial pediments (bajadas) emanate from the mountains and circumscribe the basin, forming drainage divides to the north and south. The basin probably contains about 1 km of alluvial fill, though drills have only reached 300 m. Local annual rainfall is 30 cm, over half of which falls in July and August during the summer monsoons, which are caused by the arrival of warm, moist tropical air from the Gulf of Mexico. Winter rainfall comes from frontal storms moving east from the Pacific. Willcox Playa, elevation 1260 m, is in the lowest part of Willcox basin and covers an area of 130 km^2. Heavy rainfall creates a shallow (< 30 cm deep) lake in Willcox Playa that evaporates within a week, leaving white patches of NaCl and Na_2SO_4 that are dispersed by wind. The playa is not quite flat, it slopes down to the west-southwest by less than a metre. Dessication polygons (both 10 cm and 10 m across) and 10 cm-high transverse dunes can be found. Willcox Playa is said to be a landmark for astronauts.

About 15000 years ago, during the last glaciation, the local climate was much cooler and wetter (maybe twice as much annual rainfall and no monsoons) than it is today. Pleistocene mammoth and camel bones have been found nearby. As today, Willcox basin had no hydrologic outflow, and so the extra rainfall accumulated in a pluvial lake, Lake Cochise. Such lakes were then common in the Basin-and-Range province. At its greatest extent, Lake Cochise covered 190 km^2 and had a maximum depth of 11 m (shoreline at 1274 m elevation). Its level rose and fell with climatic changes, finally drying up completely either 4000 (Waters) or 10000 (Long) years ago and killing all the ostracods that had been thriving within it. It was slightly alkaline and its bottom water may have been oxygen deficient. Present day aeolian erosion of the playa means that we look out over a 15000 year old lake bottom.

Palaeoshorelines at Willcox Playa

Beach ridges border the playa on the east and west sides and are the major preserved shore features of Pleistocene Lake Cochise. The ridges stand out when viewed both from the ground and from the air because they support a good growth of mesquite trees and yucca. Of the 80 km of shoreline, only about 50 km are defined by this shoreline feature. At the north and south ends of the playa it does not appear that the ridges were ever built because these were the sites of the influx of fluvial sediments during the late Pleistocene. The ridges are a few metres high and as much as 100 m wide. The fore slope is about 3 times steeper than the backslope. Prior to actual beach ridge formation, beach sands and gravels were supplied by the streams entering Lake Cochise. Longshore drift and waves were responsible for sediment transport and mixing. Periodically storm waves built up the beach level more rapidly. Formation of a beach ridge is indicative of a gently sloping lake bottom. Hence, waves break far from the shore, building up a subaqueous bar which then grows by longshore drift. When the ridge pokes above the lake surface, further growth proceeds by the addition of wave-tossed sediments. Lagoons, which formed behind the bar, appear today as broad, flat areas behind the beach ridges. The uppermost portion of the beach ridge sediments, deposited subaqueously, are unstratified and unconsolidated, in contrast to the underlying bedded, calcium carbonate-cemented sediments, which were deposited subaerially. The beach ridge sediments range in composition from relatively mud-free gravelly sands to slightly gravelly sandy muds. For most of its length the beach ridge surface is gravelly because the fines have been washed away. Roller and disc shapes dominate the pebbles.

Lake Animas and Alkali Flats

Just like Willcox, only in a different state. This is a little more complicated, with four sub-basins to the 6300 km^2 Aminas basin. The eastern boundary of this basin is the Continental Divide. Two Pleistocene lakes were present in this basin, Lake Cloverdale, to the south straddling the current border, and Lake Animas, to the north straddling the current I-10. Lake Animas had an area of 388 km^2, a depth of 20 m, and its highstand was at an elevation of 1280 m. The lake grew and shrank with Quaternary climate changes, probably in a similar fashion to Lake Cochise, giving it palaeoshorelines at several elevations. Like Lake Cochise, it also has beach ridge shoreline features. Two playas, North and South Alkali Flats, currently lie at the bottom of Lake Animas.

Martian Oceans

Were the northern plains of Mars covered by a late-Hesperian ocean? The northern plains are exceedingly flat and smooth, consistent with formation by subaqueous sedimentation. Outflow channels descending from the southern highlands tend to terminate at the same elevation, consistent with entry into an ocean. Tim Parker mapped two contacts between geological units at the southern boundary of the northern plains and suggested that they marked two separate highstands of an ocean. The outflow channels and "Contact 2" all lie close to the -3760 m equipotential. However, spectroscopy (TES) has failed to reveal any minerals

indicative of aqueous alteration and proposed shoreline candidates do not look like oceanic landforms in either MOC imaging or MOLA topography.

References

Fleischhauer HL and Stone WJ (1982) Quaternary geology of Lake Animas, Hidalgo County, New Mexico, *New Mexico Bureau of Mines and Mineral Resources*, Circular 174.

Hawley JW *et al.* (2000) Trans-international boundary aquifers in southwestern New Mexico, prepared by the New Mexico Water Resources Research Institute for the Environmental Protection Agency.

Head JW *et al.* (1999) Possible ancient oceans on Mars: Evidence from Mars Orbiter Laser Altimeter data, *Science,* **286,** 2134 – 2137.

Kennedy JF *et al.* (2000) The hydrogeologic framework of basin-fill aquifers and associated ground-water-flow systems in southwestern New Mexico – an overview, in *Southwest Passage – A trip through the Phanerozoic*, the 51st field conference guidebook of the New Mexico Geological Society, 235 – 244.

Krider PR (1998) Paleoclimatic significance of late Quaternary lacustrine and alluvial stratigraphy, Animas Valley, New Mexico, *Quaternary Res.,* **50,** 283 - 289.

Long A (1966) Late Pleistocene and recent chronologies of playa lakes in Arizona and New Mexico, PhD Thesis, University of Arizona.

Malin M and Edgett K (1999) Oceans or seas in the Martian northern lowlands: High-resolution imaging tests of proposed coastlines, *GRL,* **26,** 3049 – 3052.

Parker TJ *et al.* (1989) Transitional morphology in west Deuteronilus Mensae, Mars - Implications for modification of the lowland/upland boundary, *Icarus,* **82,** 111 – 145.

Parker TJ *et al.* (1993) Coastal geomorphology of the Martian northern plains, *JGR,* **98,** 11061 - 11078.

Robinson RC (1965) Sedimentology of beach ridge and nearshore deposits, pluvial Lake Cochise, southeastern Arizona, MS Thesis, University of Arizona.

Rosen MR (1994) The importance of groundwater in playas: A review of playa classifications and the sedimentology and hydrology of playas, in *Paleoclimate and basin evolution of playa systems,* GSA Special Paper 289, 1 – 18.

Schreiber JF (1978) Geology of Willcox Playa, Cochise County, Arizona, in *Land of Cochise – Southeastern Arizona*, the 29th field conference guidebook of the New Mexico Geological Society, 277 – 282.

Schreiber JF *et al.* (1972) Sedimentologic Studies in the Willcox Playa area, Cochise County, Arizona, in *Playa Lake Symposium*, pub. International Center for Arid and Semi-Arid Land Studies, Texas Tech, 133 – 184.

Waters MR (1989) Late Quaternary lacustrine history and paleoclimatic significance of pluvial Lake Cochise, southeastern Arizona, *Quaternary Res.,* **32,** 1 – 11.

Waters MR and Woosley AI (1990) The geoarchaeology and preceramic prehistory of the Willcox Basin, SE Arizona, *J. Field Archaeology*, **17,** 163 – 176.

Withers P and Neumann GA (2001) Enigmatic northern plains of Mars, *Nature,* **410,** 651.

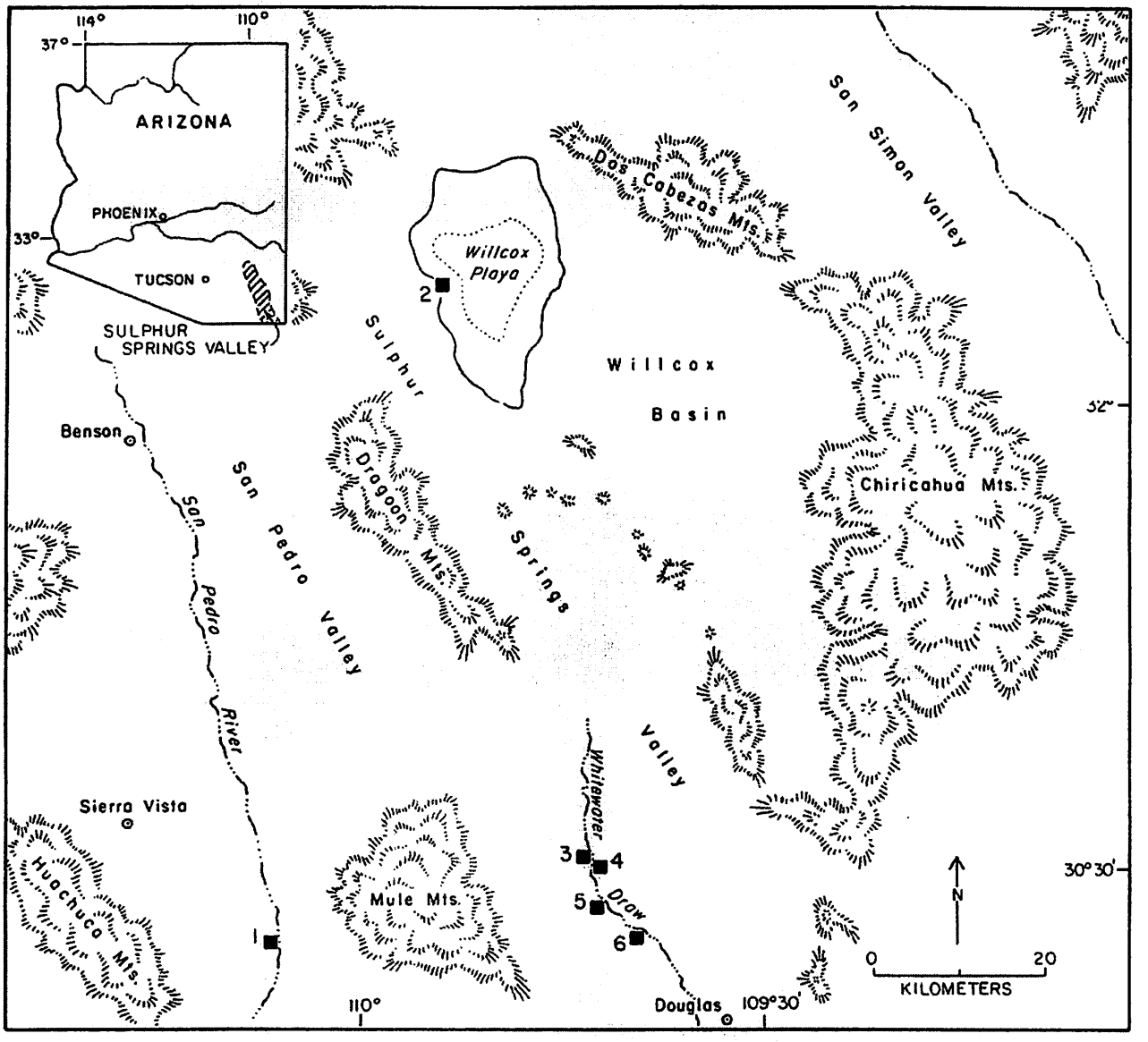

Figure 1. The Willcox basin, with towns, geological and archaeological sites, and physiographic features mentioned in the text. The Willcox Playa (dotted line) and the 1274 m shorelines of Pleistocene Lake Cochise (solid line) are indicated. 1: Lehner Clovis site; 2: Sites AZ CC:13:3, AZ CC:13:5, AZ CC:13:66, and gravel pits along Lake Cochise shoreline; 3: Sulphur Spring site AZ FF:6:9; 4: Sulphur Spring site AZ FF:6:8, 5: Sulphur Spring site AZ FF:10:1 (Double Adobe); 6: Sulphur Spring site AZ FF:10:14. Hatched area on the inset indicates position of the Sulphur Springs Valley in SE Arizona.

The topographically lowest portion of the basin is now occupied by the Willcox Playa, a barren depression covering approximately 130 sq km (FIG. 2; Meinzer and Kelton 1913; Schreiber 1978; Schreiber et al. 1972). The Willcox Playa is dry for most of the year but will fill with water after heavy rainfall, when runoff from the mountains and surrounding alluvial piedmont collects in the playa. This water creates a shallow lake that, if not recharged, disappears via evaporation within a few days to a week.

The Willcox Playa is also the former bed of a much

Index	Basin System
1	Mimbres basin
2	Hachita-Moscos basin
3	Playas basin
4	Animas basin
5	Gila River basin
6	San Bernardino basin
7	San Basilio basin
8	Rio Casas Grandes basin

Figure 1a. Basin system index map

Figure 1b. Hydrologic subbasins

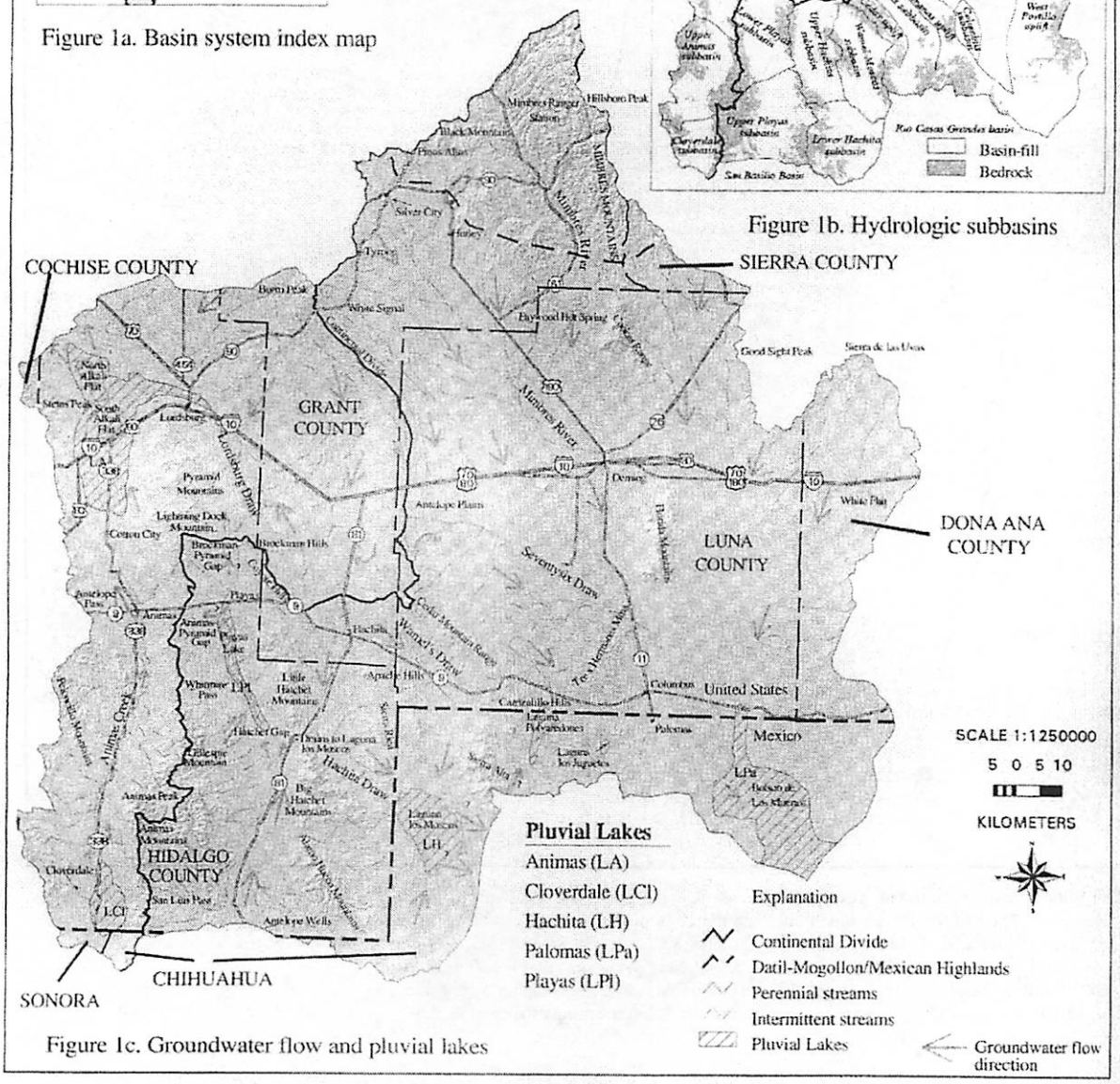

Figure 1c. Groundwater flow and pluvial lakes

FIGURE 1. Location of the study area in southwestern New Mexico. The locations of the following basin systems are shown on Figure 1a: (1) Mimbres, (2) Hachita-Moscos, (3) Playas, (4) Animas, (5) Gila River, (6) San Bernardino, (7) San Basilio, and (8) Rio Cases Grandes. Each basin system is comprised of numerous subbasin units (Fig. 1b). The following pluvial lakes are listed on Figure 1c: Animas (LA), Cloverdale (LCl), Hachita (LH), Palomas (LPa), and Playas (LPl).

28

Kilbourne Hole Maar Crater
Structure and Origin

Jani Radebaugh

Kilbourne Hole, and its neighbor directly to the south, Hunts Hole, are odd features in southern New Mexico. Both have margins that rise up gently about 100 feet above the surrounding flat plains, and center depressions about 300 feet below most of the local terrain. At first glance, they may appear to be shallow impact craters, yet their origin is vastly different.

Both features are **Maar Craters**, created by the outward explosion and dispersal of material when hot magma encountered the water table. This magma rose upward in the form of a **diatreme**, or a pipe of gas rich igneous material that blasted its way through sediments.

Four separate units can be seen in the craters: (1) Santa Fe Group sediments, (2) olivine basalt (Afton basalt), (3) bedded hydroclastic tuffs (base surge and air fall) and vent breccia, and (4) Holocene wind-blown sand.

Themis image of Kilburn and Hunt maars

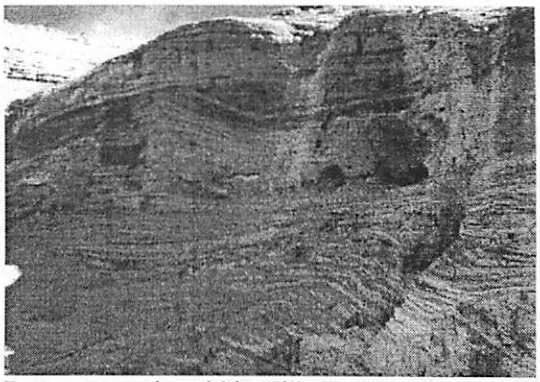

Base surge units within Kilbourne Hole

The first two units predated the maar formation, and the third was a rapidly-moving surge unit that erupted from the diatreme.

The maars lie on the north-south trending Fitzgerald fault line, which is on the west edge of the Rio Grande rift. This rifting led to the formation of the **Potrillo alkali basalt volcanic field**, and subsequent formation in the Pleistocene of Kilbourne and Hunt maar craters, plus Potrillo, Malpais, and Riley maar craters.

The rifting of the crust in this region led to heating of the lower crust and magmatism, because fractures acted as new pathways for magma to the surface. One of the most interesting aspects of Kilbourne Hole maar is that the diatreme was so deep that it brought up mantle xenoliths of lherzolite (~60% olivine, plus ortho- and clino-pyroxene—Rachel will talk more about this).

Wood and Kienle, 1990, Volcanoes of North America: United States and Canada: Cambridge University Press, 354p., Contribution by Jerry Hoffer (Kilbourne, Potrillo)

Scherer, E. E., et al., 1997, Lu-Hf geochronology applied to dating Cenozoic events affecting lower crustal xenoliths from Kilbourne Hole, New Mexico, Chem. Geol. 142, 63-78.

http://www.topowest.com/New_Mexico
http://paces.geo.utep.edu/elpjuarez/Kilbourne.html
http://vulcan.wr.usgs.gov/Volcanoes/NewMexico/description_new_mexico_volcanics.html

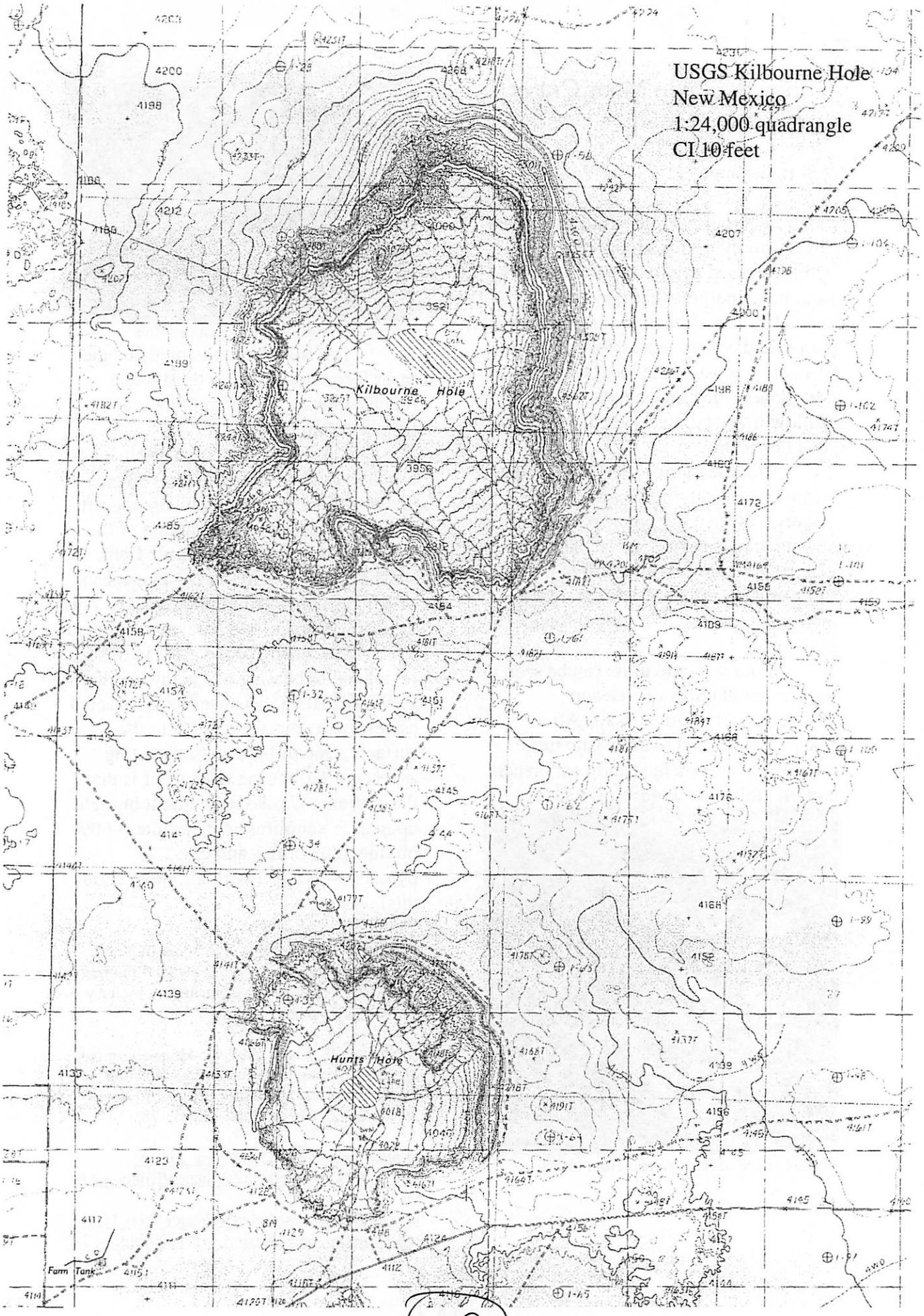
USGS Kilbourne Hole
New Mexico
1:24,000 quadrangle
CI 10 feet
Kilbourne Hole
Hunts Hole
Farm Tank

Kilbourne Hole Xenoliths

brought to you by ®

Xenolith - A piece of foreign (compositionally different) rock ocurring as an inclusion within a plutonic or volcanic rock mass.

Autholith - rock genetically (compositionally) similar to rock mass i.e. something that solidified from the same melt and was later moved by the flow of that melt..

Xenoliths

Xenoliths are useful for figuring out where the source of magma for an igneous rock was. The magma itself can be contaminated by melting of the rock it passes through as it makes its way to the surface. The magma can also fractionate while in an intrusion. Therefore, an un-melted chunk of rock brought up with the magma is a better indicator of where the magma came from.

Xenoliths are one of the lines of evidence that magma comes from the mantle. Geologists determined this by looking at the P-T stability ranges of the minerals in xenoliths. The table below is an example of the stability ranges of different xenoliths. Figure 1 is a plot of the stability of different rock types with depth.

Rock Type	**Stability Depth**
Igneous Rocks	
Gabbro	crust
Spinel Peridotite	~25 km, upper mantle
Garnet Peridotite	~35-120 km
Kimberlites (diamonds)	~150 km
Metamorphic Rocks	
Amphibolite and Granulite	crust
Eclogite	~25 km, upper mantle

Rare Earth Elements (REE's)

Rb & Sr

Rubidium and Strontium are REE's that substitute for Potassium and Calcium, respectively. Since Rb can substitute into K, Rb is concentrated in alkali rocks (K-feldspar). ^{87}Rb decays into ^{87}Sr so the abundance of ^{87}Sr in relation to its stable isotope ^{86}Sr can give you information amount of alkali minerals, so long as you scale the value based on the age of the rock. The mantle is poor in K bearing minerals (except phlogopite) and therefore has a $^{87}Sr/^{86}Sr$ value of less than 0.704. The crust has more K bearing minerals and so the Sr ratio is higher than 0.710.

Sm & Nd

Samarium and Neodymium are fractionated during magmatic processes and can give similar information about the sources of magma. ^{147}Sm decays into ^{143}Nd. The bulk Earth value is $^{143}Nd/^{144}Nd = 0.51264$. Mantle rocks have a higher value and crustal rocks have a lower value.

Sr and Nd together can give a good description of the distribution of magma sources. Figure 2 show Nd vs. Sr plots for different igneous rocks on Earth.

Kilbourne Hole

Kilbourne Hole was formed in the late Pleistocene out of alkali basalts (for details see Jani's talk). These eruptions also brought many mantle and crustal xenoliths to the surface. Some of the mantle xenoliths include spinel lherzolites (upper mantles). Measurements of Sr and Nd from the clinopyroxenes (cpx) in the lherzolites plot at the extreme end of the MORB field, see Figure 3. Some of the cpx's, do not plot with the others and are interpreted to be "enriched." This means that they the magmas that they formed from were depleted at least once, if not multiple times. This tells us that the upper mantle in this area may be heterogeneous in composition.

The heterogenous mantle theory is supported by other evidence such as the Oxygen isotopic abundances. The $^{18}O/^{16}O$ values of xenoliths from the lower crust below Kilbourne Hole also show a range of values. The range of values are believed to represent the different source areas for the xenoliths. The upper mantle beneath Kilbourne Hole must be very dry to prevent the equilibration of Oxygen isotopes at such high temperatures.

These sort of measurements are made to determine the thermal history of the lower crust and upper mantle in the area. The main models considered are 1) a solid state mixing model, where tiny bits of the mantle are melted and mixed recently, and 2) discrete mixing, where two distinct melt events occurred, separated by a Ga. As always the data seems to say that it is a mix of both.

References

James, D. E., et al. (1980) Geophysical Research Letters, 7 (5), 321-324.

Raymond, L. (1995) Petrology: The Study of Ingneous, Sedimentary, and Metamorphic Rocks, W. C. Brown Publishers, Dubuque, IA.

Roden, M. F., et. al. (1988) Geochimica et Cosmochimica Acta, 52, 461-473.

Wilson, M. (1996) Igneous Petrogenesis: A Global Tectonic Approach, Chapman & Hall, London, England.

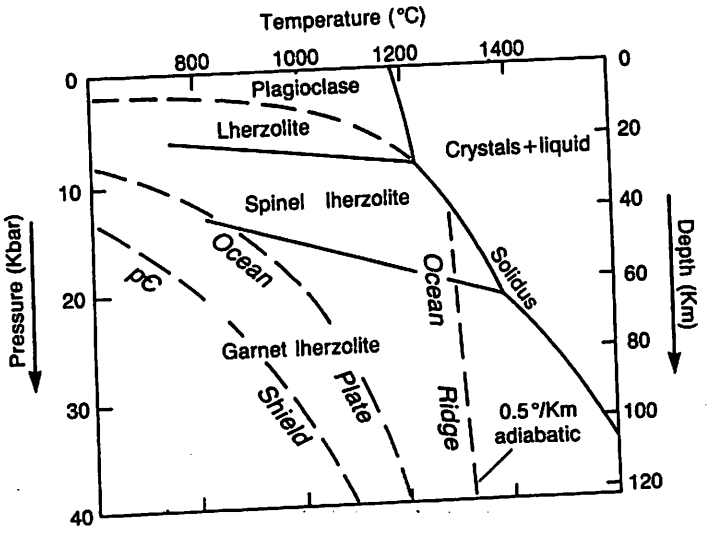
Temperature (°C)
800
1000
1200
1400
0
10
20
30
40
Pressure (Kbar)
Depth (Km)
0
20
40
60
80
100
120
Plagioclase
Lherzolite
Crystals + liquid
Spinel lherzolite
Ocean
pC
Ocean
Solidus
Garnet lherzolite
Shield
Plate
Ridge
0.5°/Km
adiabatic

I

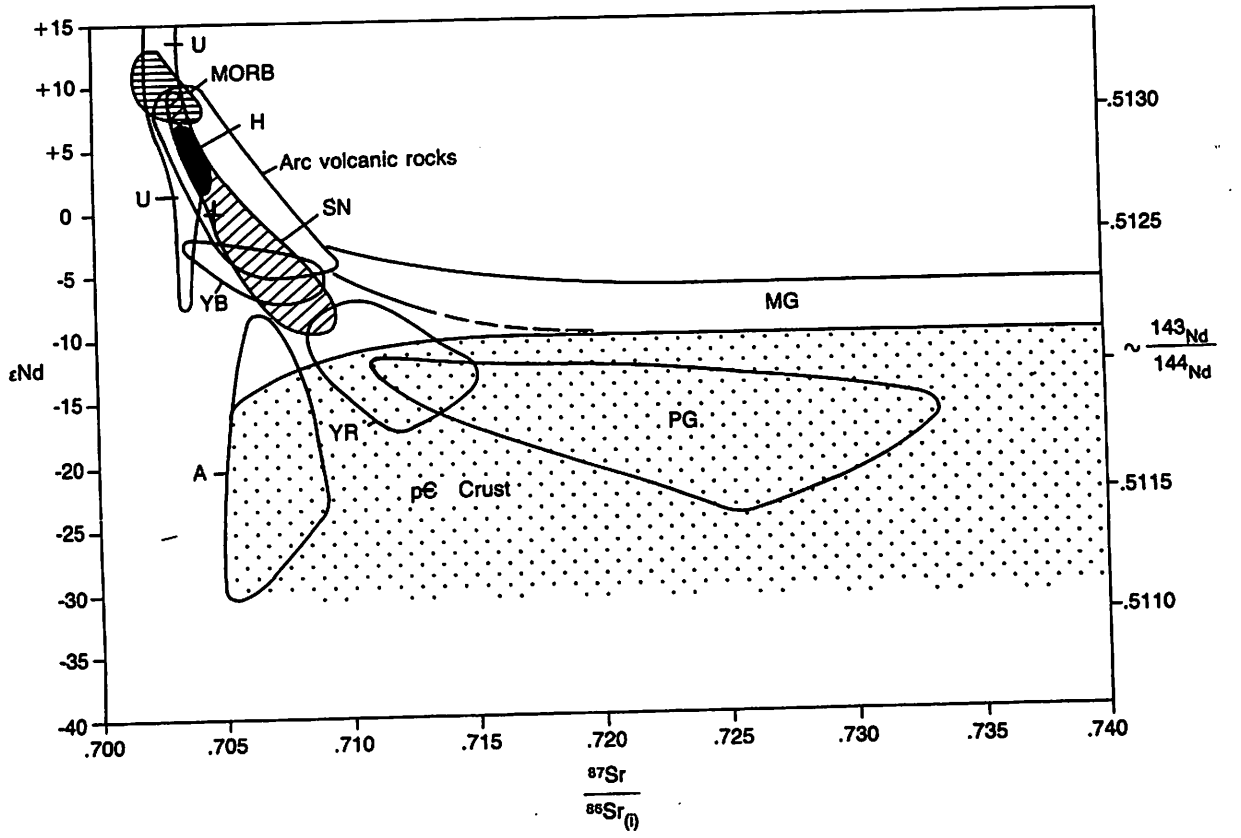
+15
+10
+5
0
-5
-10
-15
-20
-25
-30
-35
-40
εNd
U
MORB
H
Arc volcanic rocks
U
SN
YB
MG
YR
PG.
A
pC Crust
.700
.705
.710
.715
.720
.725
.730
.735
.740
87Sr / 86Sr(i)
.5130
.5125
.5115
.5110
~ 143Nd / 144Nd

33

IIa.

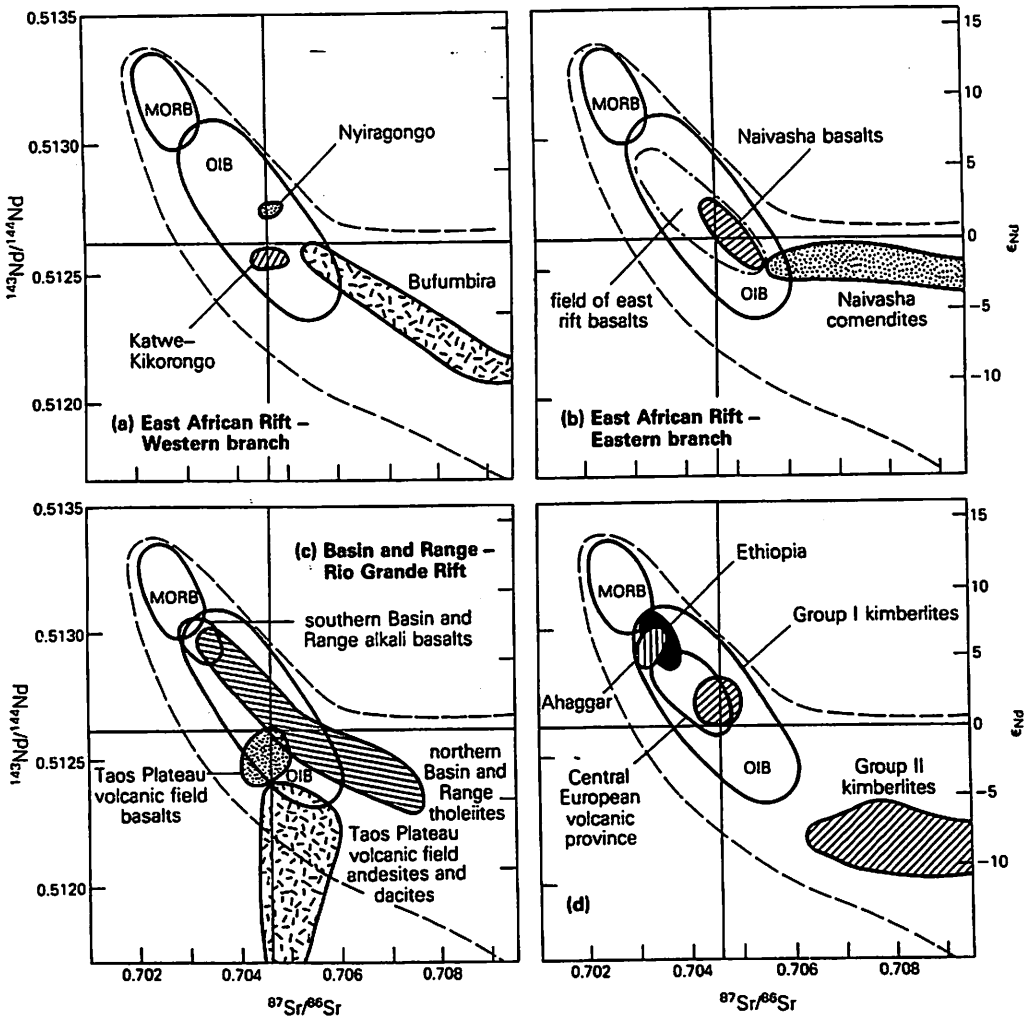
MORB
OIB
Nyiragongo
Bufumbira
Katwe–
Kikorongo
(a) East African Rift –
Western branch
Naivasha basalts
field of east
rift basalts
Naivasha
comendites
(b) East African Rift –
Eastern branch
(c) Basin and Range –
Rio Grande Rift
southern Basin and
Range alkali basalts
Taos Plateau
volcanic field
basalts
northern
Basin and
Range
tholeiites
Taos Plateau
volcanic field
andesites and
dacites
Ethiopia
Group I kimberlites
Ahaggar
Central
European
volcanic
province
Group II
kimberlites
(d)
0.5135
0.5130
0.5125
0.5120
0.702
0.704
0.706
0.708
15
10
5
0
−5
−10
$^{143}Nd/^{144}Nd$
$^{87}Sr/^{86}Sr$
ϵ_{Nd}

II b

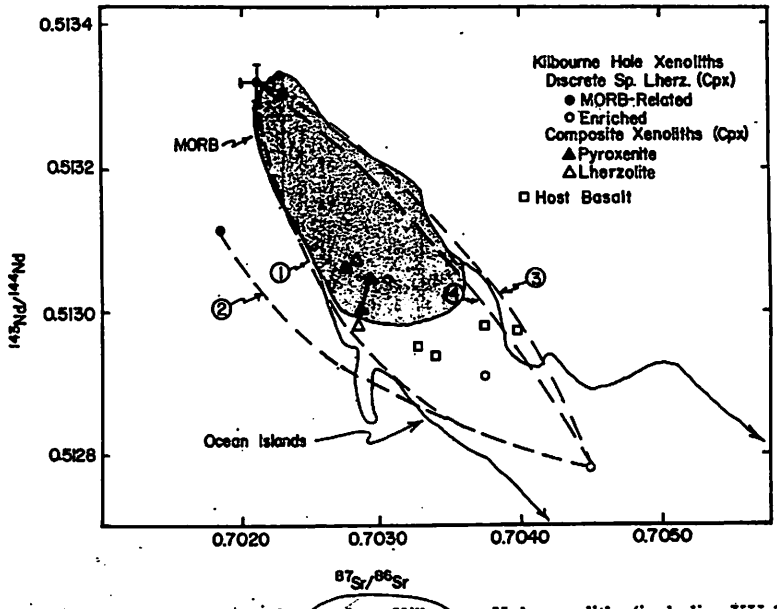
Kilbourne Hole Xenoliths
Discrete Sp. Lherz. (Cpx)
● MORB-Related
○ Enriched
Composite Xenoliths (Cpx)
▲ Pyroxenite
△ Lherzolite
□ Host Basalt
MORB
Ocean Islands
①
②
③
④
0.5134
0.5132
0.5130
0.5128
0.7020
0.7030
0.7040
0.7050
$^{143}Nd/^{144}Nd$
$^{87}Sr/^{86}Sr$

III

The Rio Grande Rift

Adina Alpert

Introduction

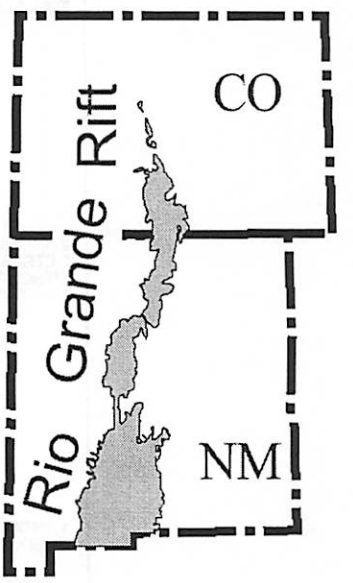

The Rio Grande Rift is part of the Basin and Range extensional province of the western United States. The geology of central New Mexico is dominated by this rift. The rift starts in central Colorado's Rocky Mountains and runs southward through Colorado and New Mexico into the Mexican State of Chihuahua. The rift is comprised of a series of connected basins in which lava, volcanic ash, and sediments have accumulated. The rift widens to the south where it is physiographically indistinguishable from the adjacent Basin and Range to the west. The rift formed where a section of the Earth's crust arched, weakened, and spread apart due to heat from basaltic magma welling up from the mantle 29 million years ago. The stretched and brittle crust in the rift thinned and fractured. West of the rift the crust of the Colorado Plateau is approximately 45 kilometers thick; east of the rift the crust beneath the Great Plains is 50 kilometers thick; beneath the rift zone the crust is only 35 kilometers thick (Chapin and Cather, 1994). As it is a topographic low, the Rio Grande River naturally found its course within the rift.

Tectonic Model for Rift Formation

Phase 1: Normal Subduction - Continental arc volcanism

Phase 2: Early slab retreat, Lithospheric Magmatism, and Basin Formation

- Widespread crustal melting, emplacement of silicic magmas into large chambers
- Voluminous outflow sheets from large calderas
- Eruption of mafic to intermediate lavas formed by partial melting of lithosphere

Phase 3: Rapid Basin Subsidence and Asthenospheric Magmatism

- Continued foundering of slab,
  - emptied space filled by asthenosphere, establishes convection cell
- Decompression melting of asthenosphere when cell sufficiently large
  - asthenospheric magmatism supplants lithospheric magmatism

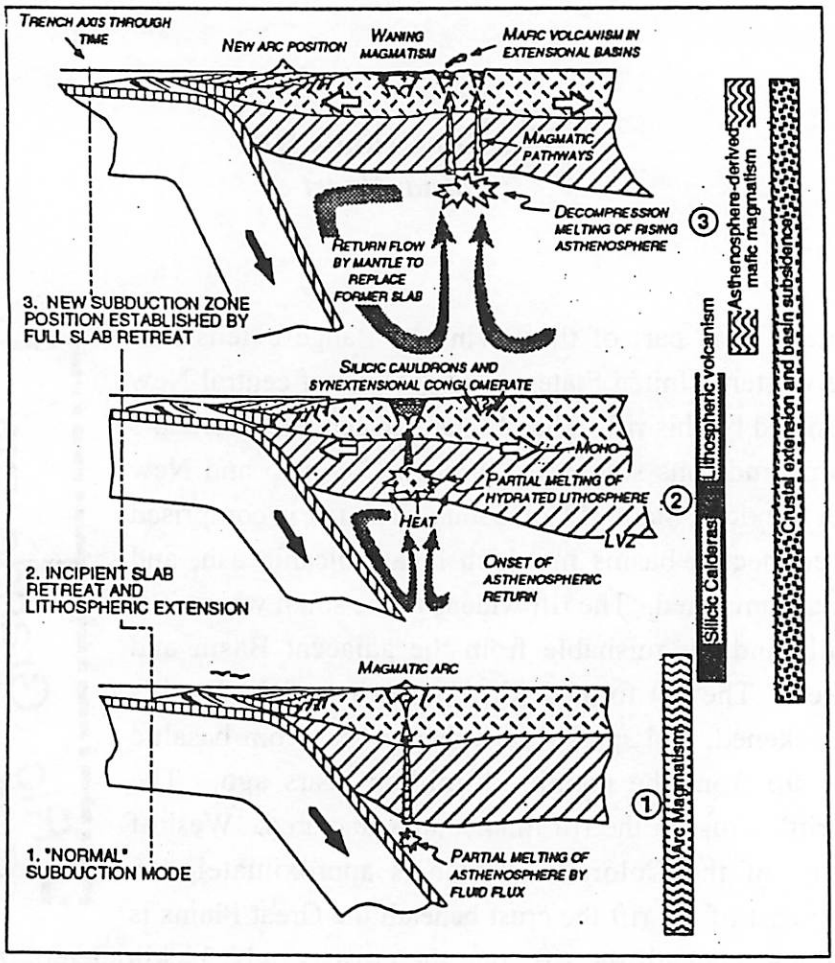

Tectonic and Volcanic History

Formation of the rift began first in the northernmost sections about 29 Ma (late Oligocene), in the first of two major extension episodes. This episode lasted 10-12 Ma and ended in the early Miocene. The faults active during this episode were low angle normal faults. Strain rates were less during this early phase of rifting, except where volcanism and high heat flow caused local concentration of extensional strain. The second episode of extension, the mid-Miocene to Quaternary phase, began about 17 million years ago and continues today. It involves normal faults of both high and low angles. The most rapid phase of regional extension was during this period, from middle to late Miocene time. Evidence of continuing rifting includes young fault scarps, seismicity, high heat flow, and ongoing uplift as established by geodetic measurements, particularly in the Socorro area.

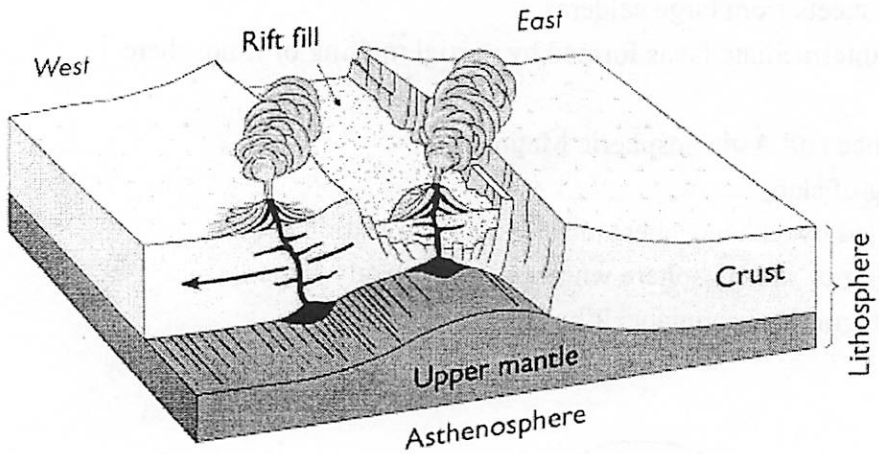

The rift formed along previously existing zones of weakness left over from the Ancestral Rockies and Laramide orogenies. The onset of rifting coincided with a period of intense volcanism associated with the early rift basins – as is common in other rift valleys of the world. As extensional forces continued and the crust beneath the widening rift zone was thinned, magma surged to the surface. Most of the volcanism was concentrated on the western side of the Rio Grande rift, where immense eruptions spewed ash over the region. In some areas magma flowed onto the surface and created vast lava fields. Some lavas flowed quietly from vents, forming broad flows that accumulated in layers to from expansive, gently sloping shield volcanoes. In other areas thick lava flows eventually built up to from major mountains. Huge calderas were created when the volcanoes collapsed into vacated magma chambers beneath the volcanoes. Much of the lava is basaltic, evidence that the faults along the rift reach down to the mantle, the source of most basaltic magma (Lipman and Mehnert 1975).

Smaller volcanic eruptions, some of them within the last few thousand years, have added cinder cones, flows of dark basalt, squeeze-ups, and lava tunnels to the area. These volcanic episodes may have been witnessed by some of North America's early human inhabitants Clovis and Folsom Man. It is thought that early humans may have witnessed the eruption that formed the Capulin cinder cone at what is now the Capulin Mountain National Monument in northern New Mexico. Capulin Mountain is near the center of the Raton-Clayton volcanic field, which is related to the Rio Grande rift (Stormer, 1987).

The intense volcanic activity along the Rio Grande rift fractured the nearby rocks and permitted the movement of superheated, mineral-rich solutions that formed hydrothermal deposits. These deposits brought in a later group of human inhabitants – the prospectors and miners. Most of New Mexico's mining districts with their deposits of gold, silver, lead, copper, zinc, molybdenum, fluorite, and barite are concentrated along this mineralized trend near the edges of the Rio Grande rift .

Basins

The Rio Grande rift first developed as a chain of closed basins or half graben, which gradually filled with lava, ash flows, and sediments that washed in from nearby mountain ranges. Large amounts of sand, gravel, lava, and volcanic ash fill the rift basins to a depth as great as 7.3 kilometers. Sedimentation began in most rift basins in late Oligocene to early Miocene time; however, the basin fill deposits of middle to late Miocene age are dominant in volume. The sedimentary and volcanic deposits of the Rio Grande rift are collectively known as the Santa Fe Group. The Santa Fe Group includes fine to coarse-grained sandstone interbedded with siltstone, conglomerate, and volcanic material. The sediments are generally soft and easily eroded.

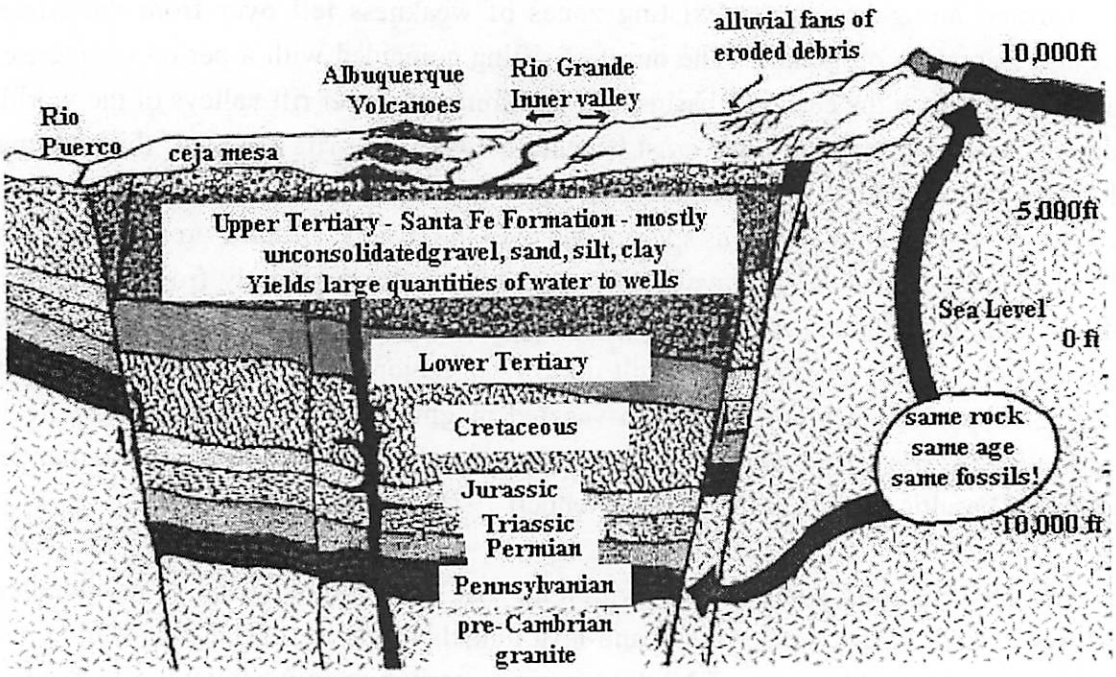

Today, starting near Leadville, Colorado and southward to Soccorro, New Mexico, a distance of 550 kilometers, the north-trending rift consists of a series of four en echelon basins that join. These basins range from 80 to 240 kilometers in length and from 5 to 95 kilometers in width. The average basin width is 50 kilometers (Chapin and Cather, 1994). From north to south these basins are the Upper Arkansas, San Luis, Española, and Albuquerque Basins.

South of the Albuquerque Basin the rift branches out and widens into a pattern of tilted ranges and parallel basins that resembles the Basin and Range province. Some researchers consider the rift south of the Albuquerque Basin to be part of the Basin and Range province. Others feel the Rio Grande rift should be distinguished from the adjacent Basin and Range province on the basis of its high heat flow, more frequent Pliocene and Quaternary faulting, deep basins, and late Quaternary volcanism (Chapin and Cather, 1994).

References:

Chapin, Charles E., and Cather, Steven M., 1994, Tectonic setting of the axial basins of the northern and central Rio Grande rift, Geological Society of America Special Paper 291, p.5-21.

Lipman, P.W., and Mehnert, H.H., 1975, Late Cenozoic basaltic volcanism and development of the Rio Grande depression in the southern Rocky Mountains, Geological Society of America, Mem.144, p.119-154.

Stormer, John C. Jr., 1987, Capulin Mountain volcano and the Raton-Clayton volcanic field, northeastern New Mexico: Geological Society of America Field Guide - Rocky Mountain Section, p.421-424.

ROCKETS
by
Gwen Bart

"How many more years I shall be able to work on the problem, I do not know; I hope, as long as I live. There can be no thought of finishing, for 'aiming at the stars,' both figuratively and literally, is a problem to occupy generations, so that no matter how much progress one makes, there is always the thrill of just beginning."
– Goddard to H. G. Wells

Robert Goddard (1882-1945)

The story of Robert Goddard is really a different story from the story of modern rocketry. One of the main things that characterized his research was secrecy, almost to the point of paranoia. He would almost never share his work with anyone, so everyone else had to redo on their own what he had already done.

For his first attempt at a rocket, he had some crazy idea that ignored the law of conservation of momentum. He ignored everyone who said it wouldn't work and tried it anyway. At the end of his experimentation, he decided that there might be something to Newton's laws after all, and he determined to study physics and math. He earned his Ph.D. in 1911 from Clark University.

In 1914, Goddard patented his ideas for rockets, including the fundamental features of rockets and the basic principle of rocket propulsion. Solid fuel rockets burning black powder had been known since the Middle Ages. But these rockets burned their fuel in a few seconds and could only travel hundreds of feet. Ultimately, Goddard's unique contribution was to combine liquid fuels with multiple stages and the sustained feeding of fuel into the combustion chamber. These modifications are what allow us to leave Earth's atmosphere entirely.

After many years of failures, Goddard gave up trying to find a mechanism to feed cartridges of fuel into the combustion chamber. In 1921 he switched to using liquid fuel, which generated far more energy per pound than the smokeless powder he had been using. The world's first liquid fueled rocket reached a height of 41 feet and a distance of 184 feet on its voyage in 1926. The rocket weighed 6 pounds empty and 10½ pounds full. This flight remained a secret until 1936.

In 1929, while testing yet another rocket in his friend's field, it crashed, and police, ambulances, and news reporters were summoned by the neighbors. When the police realize what was happening, they told Goddard to find another place to fly his rockets. He moved to Camp Devens, a military installation near Worcester, but due to regulations there, he was unable to get much work

done. Soon after he got a call from Charles Lindbergh. Goddard surprisingly agreed to meet with him. As Lindbergh was impressed with Goddard's work, he was able to get him a 4 year, $100,000 grant from Daniel Guggenheim, a copper tycoon and philanthropist. With this money, Goddard no longer had to stay in the Worcester area, and moved to Roswell, NM. By the end of 1930, Goddard had launched a new rocket that reached an altitude of 2,000 feet, 20 times higher than any of his previous attempts. At Roswell, he launched rockets that broke the sound barrier and reached altitudes of more than 1½ miles.

Until 1936, Goddard was ahead of the world in building rockets. But during the war, the US government had no interest in developing long range missiles, and refused funding to Goddard, instead moved him to doing jet propulsion research. Goddard's health declined during the war, and he died on August 10, 1945.

In addition to Robert Goddard, Knostantin Tsiolkovsky, a Russian, and Hermann Oberth, a German scientist, also contributed to the theory and design of rockets. While they did a lot of work on the theory of rocketry, Goddard first put it into practice and his designs and models led to the development of much larger rockets.

Wernher von Braun led the Germans in perfecting the V-2 rocket during the war. After the war, the components of the rocket and the rocket development team were brought to White Sands Missile Range to continue their work, this time for the US government.

White Sands Missile Range

White Sands Missile Range (WSMR) in New Mexico was set up in 1945 by the US government as a place where they could test rocket technology and missile weapons. Since 1960, WSMR has designated call up areas along its north and west border from which it can occasionally evacuate residents to nearly double the size of the range. In addition, there are several launching sites in New Mexico, Utah, and Idaho from which they can launch rockets to WSMR for long range testing. The rockets tested at WSMR use mostly solid fuels. This allows the rockets to be smaller and always ready to fire, which is a clear benefit for the military. Rockets today also usually have some kind of guidance system to get them to their target and a payload, which can be anything from an astronaut to a bomb.

The planetary connection is clear. Without rockets we would still be restricted to observing space from the surface of the Earth. Our knowledge of the Solar System has improved dramatically because of our ability to send people and equipment beyond our atmosphere. Not only do rockets allow us to get off our own planet, but they allow us to go to other planets, even very specific locations on other planets, to land in a controlled manner on the planet, to take off again, and to get back to Earth in one piece. Both the pioneers of rocketry and the people who continue to improve rockets allow planetary science to exist as it does today.

"The Rocket Man" by Curt Wohleber.

Invention and Technology, Summer 1996, p. 36-45.

http://www.wsmr.army.mil/paopage/PAO.htm

Earth's First Nuclear Explosion

Jason W. Barnes

May 9, 2001

In 1944 the Manhattan Project was progressing to the point where a the question of whether or not to test the bomb was decided. Eventually it was determined that the Fat Man (spherical, implosion plutonium) bomb should be tested, but that the Thin Man (linear, bullet-type uranium) bomb was foolproof enough to not require it.

The bomb test required that the location be close to and easily accessible from Los Alamos, sufficiently remote so as not to pose a threat to people, mostly free from vegetation, and fair-weathered. After extensive aerial surveys, the site in the Jornada del Muerto (Journey of Death) valley in central New Mexico was decided upon (see figure). The Jornada del Muerto is a broad, high plain between El Paso and Socorro which was used by the Spanish on the route to Santa Fe when they controlled the area. The blast site was named Trinity. Trinity is located 30 miles southeast of Socorro, and some 50 miles Northwest of Alamogordo at $33^o\ 40'N\ 106^o31'W$.

The first test executed at the Trinity site was a 100 ton test – literally. A wooden tower was built onto which 100 tons of TNT were loaded and exploded in order to calibrate measurements and instruments that would be used in the atomic test.

Initial production of Plutonium and Uranium at the Hanford and Oak Ridge facilities was slow and very difficult, thus General Groves (military administrator for the project) feared a fizzle where the 12 precious pounds of plutonium were blasted into an aerosol and not able to be recovered for another attempt. Thus it was decided to attempt to contain the bomb (!) in case the 1000 pounds of high explosive went off but the fission failed. Jumbo was born. The Jumbo containment vessel was a 215 ton cylinder with 15" steel walls, and was built and transported to Trinity at enormous expense. In the end however, higher confidence in the success of the test and desire to not disrupt the measurements with the container made its use unnecessary.

The date of the first nuclear test was set by political considerations to be July 16, 1945 while Truman was in Potsdam. The project weather forecaster objected to this date as unsuitable, which turned out to be not far from the mark. An ideal day would have been one with no blowing dust, visibility 45, no rain within 12 hours before or after the scheduled test time, winds blowing from the southwest such that the cloud wouldn't be blown over any populated areas. However, on the morning of the test a rather intense thunderstorm blew through the Trinity test site at 2:00AM. General Groves wanted to cancel the test, but the forecaster insisted that, in fact, after the storm had blown through the weather would turn clearer and that the winds would be acceptible for the test. In the end the weather forecaster was right again, and the test, postponed from 4:00AM, went as scheduled at 5:30AM.

Scientists and other observers were housed in bunkers of concrete covered by dirt with small windows of welding glass to look through. All were told not to look directly at the blast initially, but that after a few seconds it would be safe to look through the portals at the effects. All followed this advice except Richard Feynman, who went temporarily blind in one eye becoming the first man to directly observe a nuclear explosion. The Trinity bomb released an energy equivalent to 20,000 tons of TNT, a total of 18% efficiency, higher than all of the bets in the pool but one. The resulting mushroom cloud rose to 30,000 feet over the next 10 minutes and proceeded northeastward where it dropped fallout over most of central New Mexico.

41

Central New Mexico. Gray lines show early measurements of fallout pattern (in Roentgens). Data from LA 1027-DEL.

This document consists of 1 Page(s)
No 4 of 4 Copies, Series A

My Observations During the Explosion at Trinity on July 16, 1945 — E. Fermi

On the morning of the 16th of July, I was stationed at the Base Camp at Trinity in a position about ten miles from the site of the explosion.

The explosion took place at about 5:30 A.M. I had my face protected by a large board in which a piece of dark welding glass had been inserted. My first impression of the explosion was the very intense flash of light, and a sensation of heat on the parts of my body that were exposed. Although I did not look directly towards the object, I had the impression that suddenly the countryside became brighter than in full daylight. I subsequently looked in the direction of the explosion through the dark glass and could see something that looked like a conglomeration of flames that promptly started rising. After a few seconds the rising flames lost their brightness and appeared as a huge pillar of smoke with an expanded head like a gigantic mushroom that rose rapidly beyond the clouds probably to a height of the order of 30,000 feet. After reaching its full height, the smoke stayed stationary for a while before the wind started dispersing it.

About 40 seconds after the explosion the air blast reached me. I tried to estimate its strength by dropping from about six feet small pieces of paper before, during and after the passage of the blast wave. Since at the time, there was no wind I could observe very distinctly and actually measure the displacement of the pieces of paper that were in the process of falling while the blast was passing. The shift was about 2½ meters, which, at the time, I estimated to correspond to the blast that would be produced by ten thousand tons of T.N.T.

Enrico Fermi's observations on the Trinity blast.

43

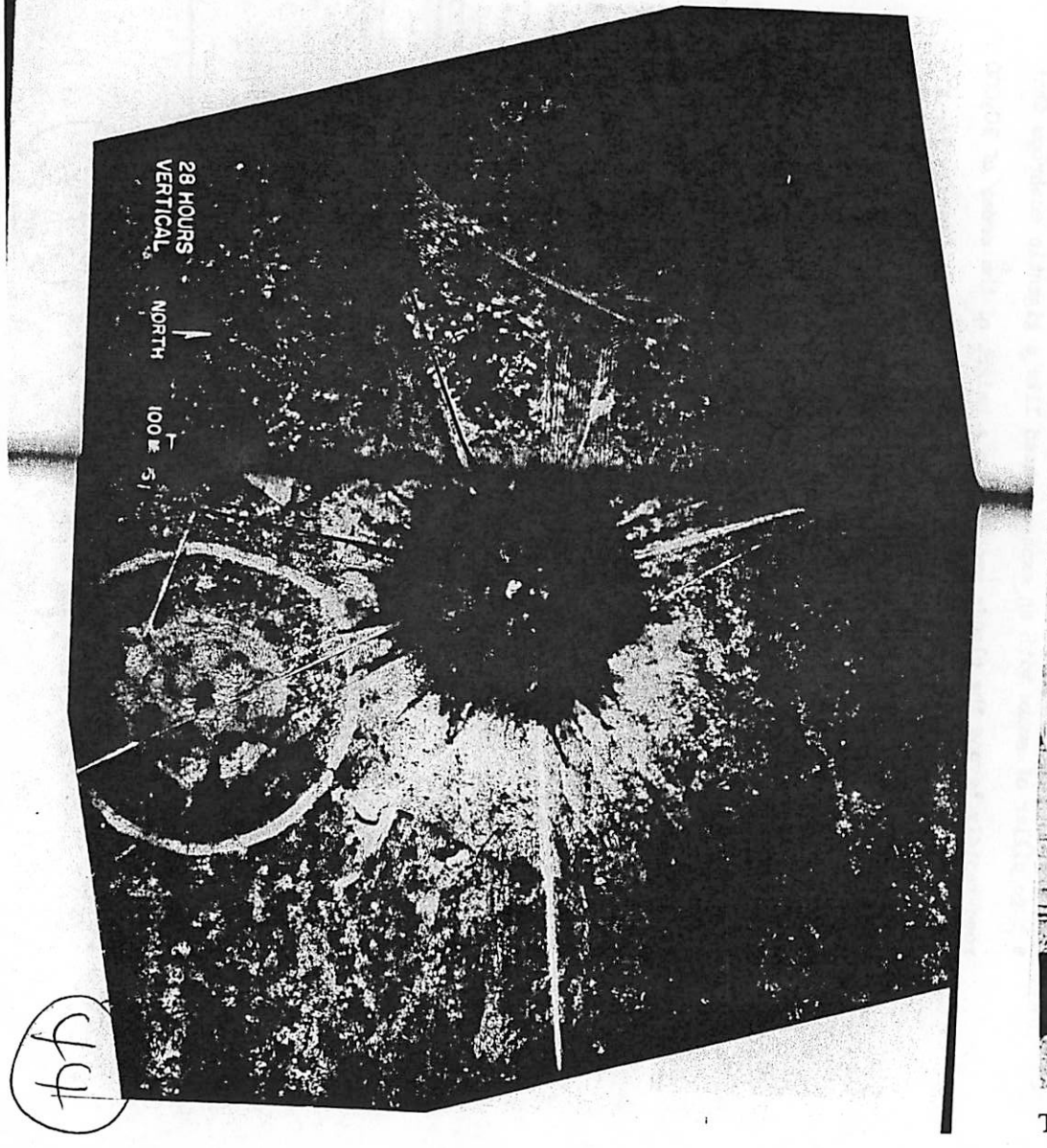

Ground Zero two days after the explosion. (Courtesy of LANL and the National Atomic Museum.)

The monument at Ground Zero.

REFERENCES:

LAMONT, LANSING. DAY OF TRINITY. ATHENEUM PUBLISHING, NEW YORK 1965.
SZASZ, FERENC. THE DAY THE SUN ROSE TWICE. UNIVERSITY OF NEW MEXICO PRESS, ALBUQUERQUE, 1985.

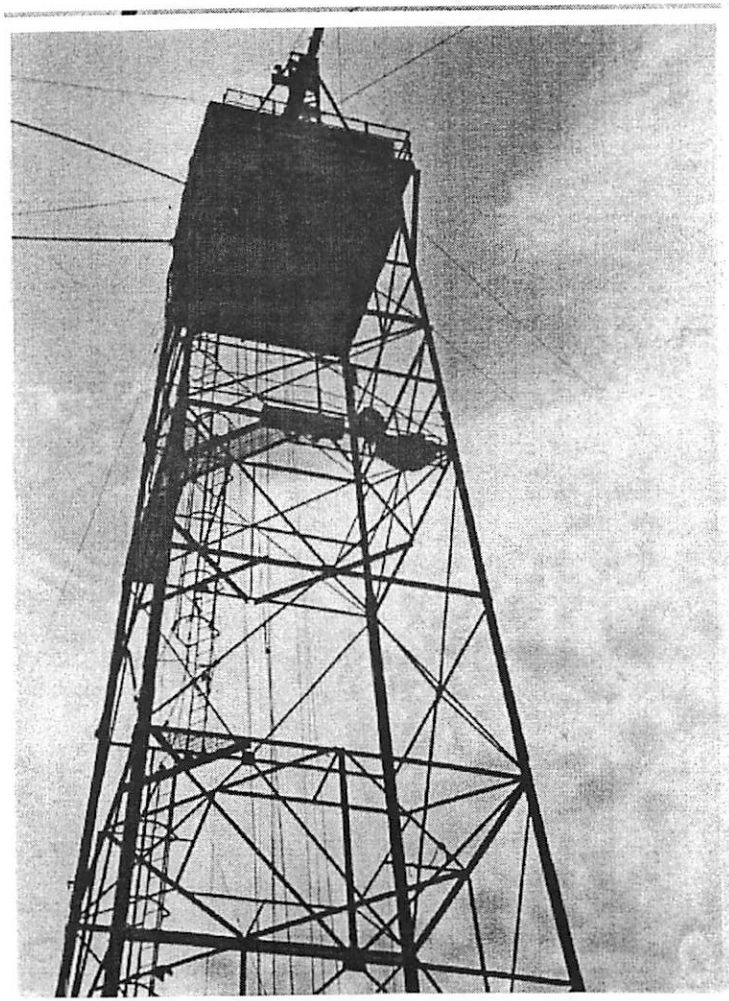

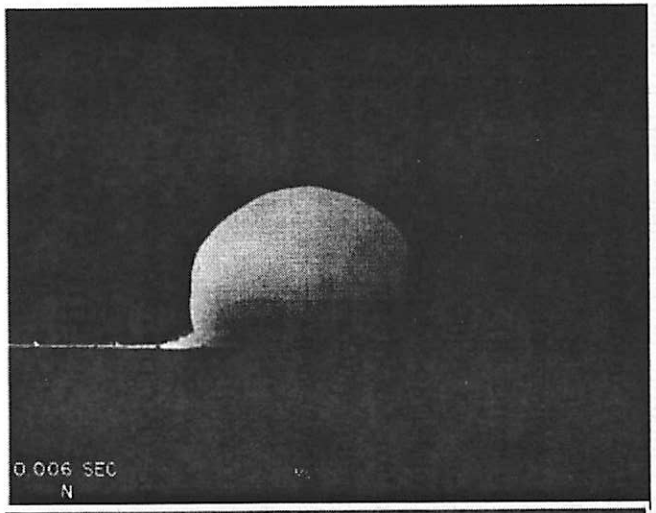

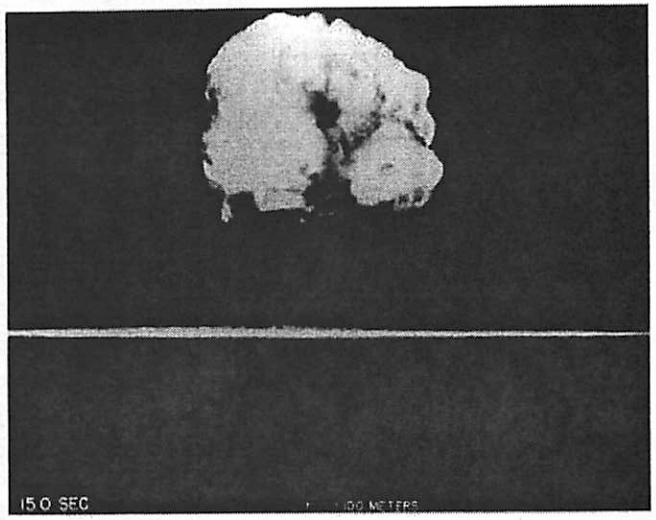

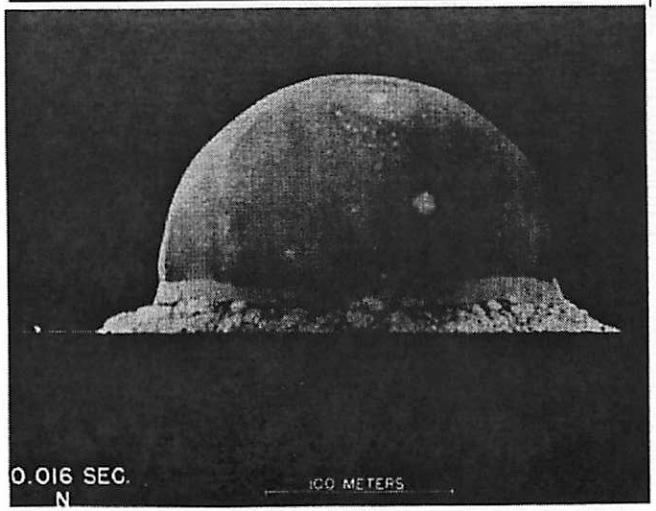

Colorful (A)Eolian Processes: White Sands and the Red Planet

Fred Ciesla

May 2, 2001

1 Why all the white stuff?

Gypsum is a hydrous form of clacium sulfate ($CaSO_4 \cdot 2H_2O$), and is soluble in water. It is very soft, and, as we're going to see, very reflective (it can be). It tends to form small, clay like particles. So notice the texture of these grains as opposed to other quartz type dunes that we've seen on other trips.

The gypsum here was originally depositted as marine sediments some 250 million years ago. This region was uplifted around 70 million years ago during the formation of the Rocky Mountains, and the gypsum bearing rock formed a dome. About 10 million years ago, the center of the dome collapsed to form the Tularosa Basin. When Rain and snow fall in the surrounding mountains, it dissolves the gypsum from the rocks in the surrounding mountains and carries it, where it accumulates (there is no drainage). The water then sinks into the ground, evaporates, or pools up in areas, leaving behind the gypsum.

What gets left behind is a crystalline form of gypsum called selenite. It is the breaking down of this selenite that provides the ammunition for (a)eolian transport (it is easy to understand how the finer stuff not in crystal form can get blown away). The selenite is broken down (weathered) in a few ways: freezing/thawing of water in cleavage planes (huh-huh, I wrote cleavage), water preferentially dissolving crystals along the cleavage (huh, I did it again) planes, or just the temperature differences between day and night stressing the mineral.

46

2 C'mon, why do WE care? Earth isn't a planet...

Dunes were first seen on Mars back in the days of the Mariner missions. One of the issues to come out of those observations is: what are the dunes made out of? It hasn't been an easy question to answer, as theoretical calculations of what particle sizes can transport easily haven't exactly matched up with calculations of dune particle sized based on scattering and reflectance. Also, we don't expetct quartz on Mars, because we don't expect to find any granite (why do you think?) that would produce the quartz.

Most of the dunes found on Mars were dark which lead to the belief that the source of particles forming dunes was basalt. The basalt could form particles appropriate for dune formation by being crushed and processed through impacts, or in the polar regions by frost-thaw processing ($C0_2$ maybe?).

But what about all this gypsum then? Well, there have been observations made of some very bright dunes (albedo around 0.32 in visible wavelenghts). In a 1999 *Nature* paper, Thomas *et al.* observed and characterized these bright dunes, and speculated that they were composed of gypsum or some other sulphate. Because Mars was wetter in its history, we should not be surprised by the presence of evaporite minerals. Those dunes may have a similar history to what we see in New Mexico.

3 For more information...

Check out the MSSS web pages for some pretty MOC images. For info on the physics of dunes, check out: The Physics of Blown Sand and Desert Dunes by R.A. Bagnold. Also check out Wind as a Geological Process by Greeley and Iversen if you're scared by things with the word *Physics* in them. The paper on gypsum dunes on Mars was in *Nature*, v.397 p.592-594.

47

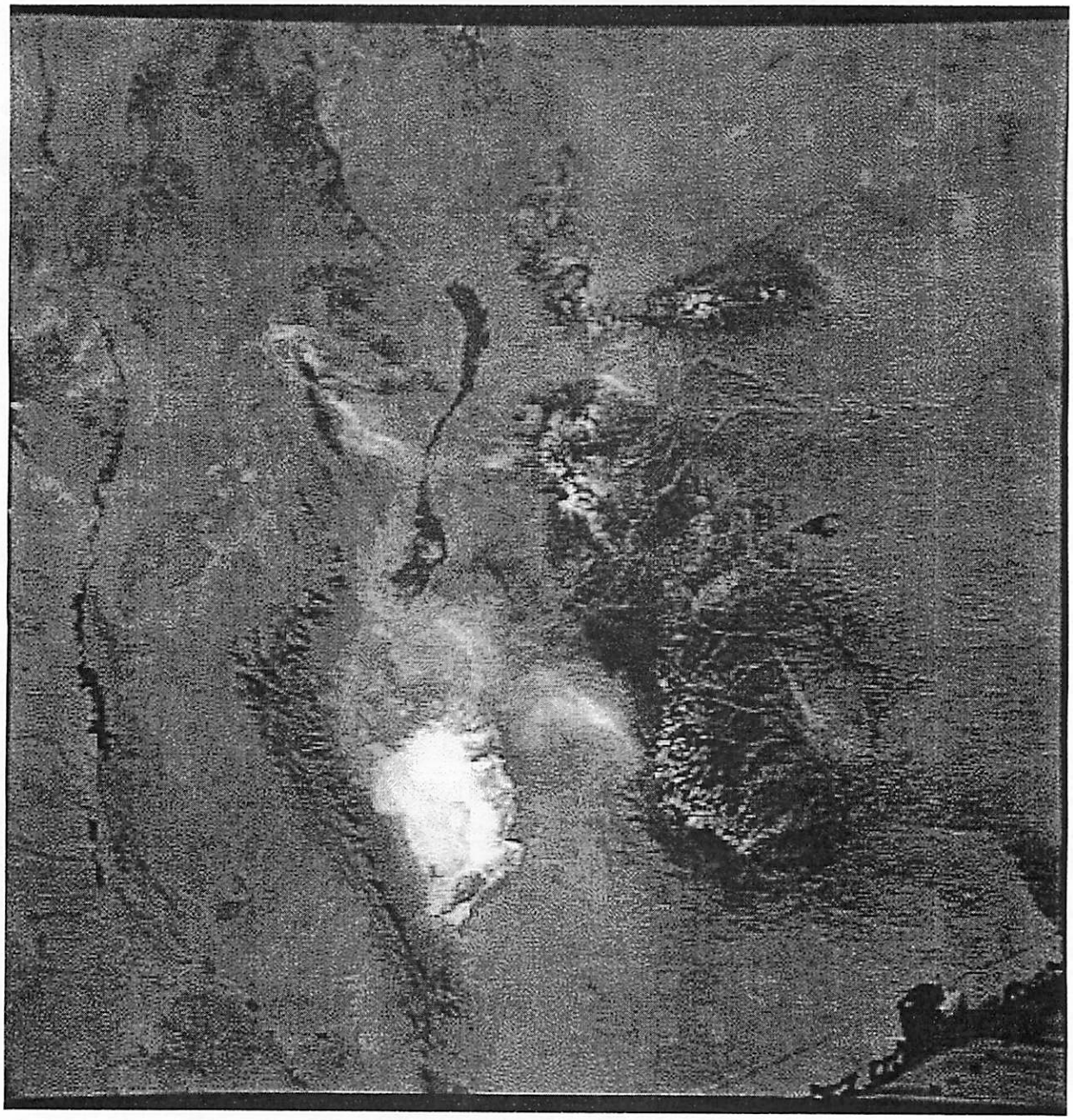

White Sands From the Space Shuttle

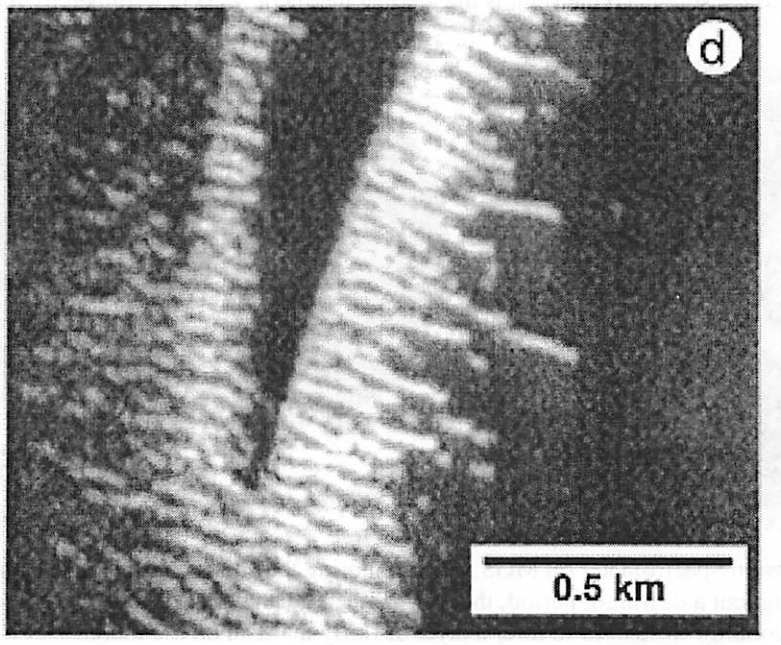

gypsum dunes on Mars?

Ralph's Bag of Pretend Spacecraft Instruments , with Assorted New Mexico Connections

Ralph D Lorenz

Thermal Inertia

As every cat stretched out on a road in an evening knows, some planetary surfaces hold their heat better than others. This heat retention depends on the density ρ, heat capacity c_p and thermal conductivity k of the material. The influence of the first two is obvious in determining the heat held by a given volume of material. The influence of conductivity is in determining the relevant volume of material affected over a given period of time (e.g. one day). These parameters are often lumped together in 'thermal inertia' or $(\rho c_p k)^{0.5}$.

Porous materials have low densities and conductivities, and hence low thermal inertia.

Carrizozo lave flow, being a more-or-less solid lump of rock, has a high thermal inertia. It appears white in this image derived from NASA's Heat Capacity Mapping Mission. It contrasts dramatically with the low-inertia sediments to the south. To the right is the thermal inertia of Mars determined by measurements from

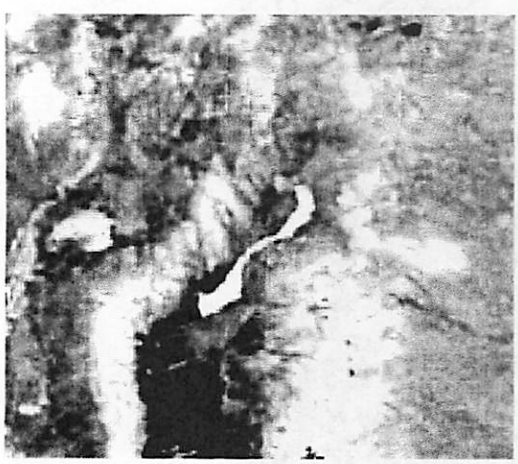

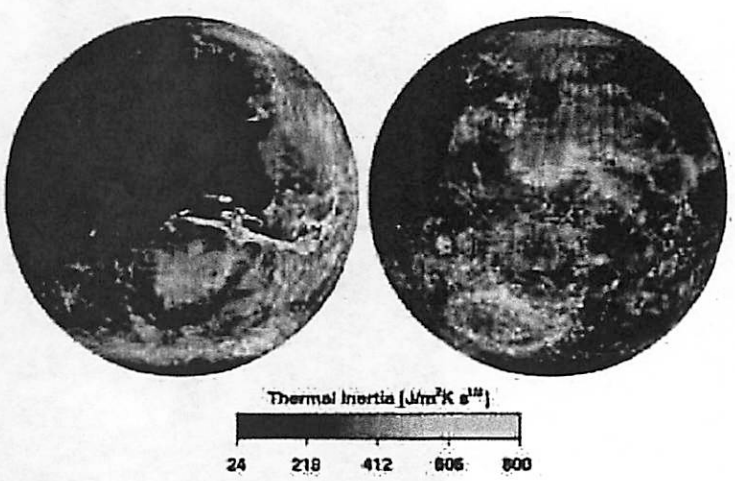

the Thermal Emission Spectrometer on MGS. By monitoring the emission (and hence surface temperature) of a surface throughout a day/night period, the thermal inertia can be estimated. Early measurements of this sort (eclipse cooling) were used to infer a layer of fluffy material on the moon.

I will attempt a demonstration of thermal inertia using an IR thermometer. The timescale will be rather shorter (and hence the probed depth much shallower) but there should be a detectable difference between dense and underdense materials.

Magnetic Field.

The Earth's magnetic field is instrumental in protecting the atmosphere from solar wind bombardment. It is also useful for navigation, where the field lines have significant horizontal projection on the surface. The vertical component has its uses too (e.g. for magnetotactic bacteria.) Magnetic field sensing is a powerful geophysical tool, being used to investigate iron deposits (duh) and impact craters on Earth.

In recent years, Mars has been found to have remarkable magnetic field anomalies, whose origin has not yet been established (next page). Cooling magma can 'freeze in' an ambient field (cv the magnetic stripes around mid-ocean ridges.)
I will bring a small fluxgate magnetometer. I have no idea what we can learn from it. (Laz says they are used in Hawaii to find cavities, like lava tubes.

50

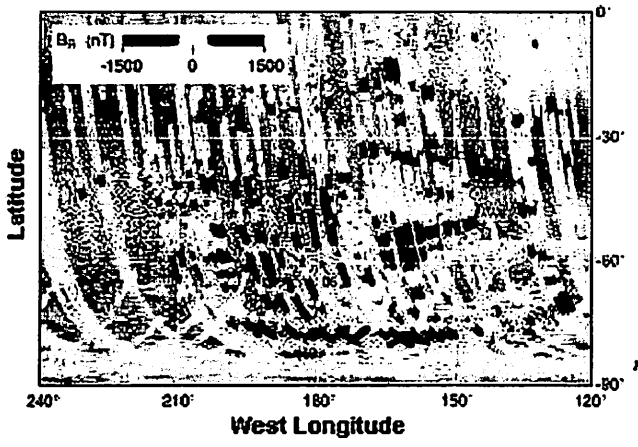

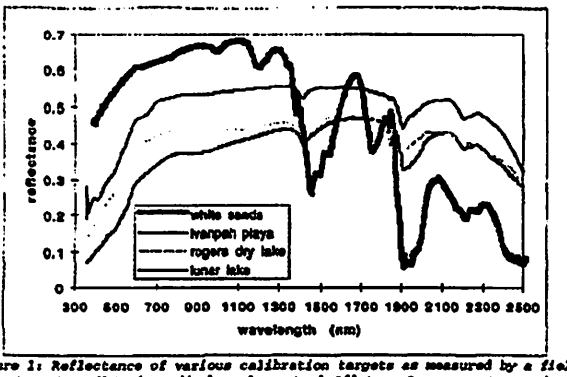

Figure 1: Reflectance of various calibration targets as measured by a field spectrometer. Note how albedo and spectral "flatness" compare to another popular remote sensing target, White Sands National Monument.

Identifying Minerals by Spectroscopy

White Sands National Monument is not quite as white at longer wavelengths, and differs noticeably from other playa or dune deposits. This method of composition classification has not done terribly well on Mars where everything is covered in the same damn dust.

Thermal and Evolved Gas Analysis

One approach to beating this problem is land, dig and analyze in-situ the material. This was planned on the Mars Polar Lander, to seek not only water ice beneath the surface, but also water of crystallization in minerals, and carbon dioxide released from the elusive but long-sought carbonate rocks. Diagnostic information in this kind of analysis includes evolved gases as a function of temperature, and the heat flow required as a function of temperature (since the decomposition reactions may be endo- or exothermic)

Data below show Heat Flow and Evolved Gas profiles for Gypsum in an experiment supporting the Thermal and Evolved Gas Analyzer (TEGA) experiment on MPL. The broad endothermic dehydration peak, accompanied by H2O release is evident. The spike in the heat flow is an indium pellet for calibration.

I will attempt a crude demonstration of water evolution at White Sands.

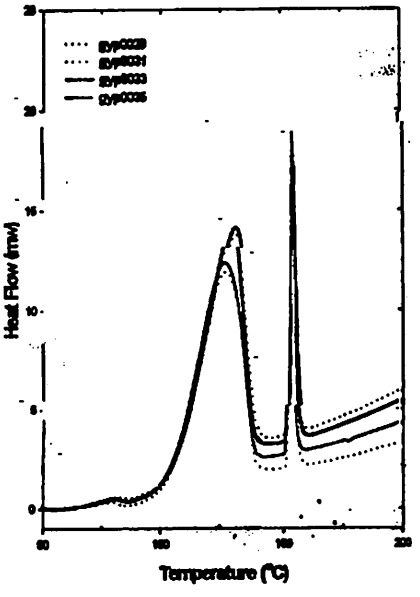

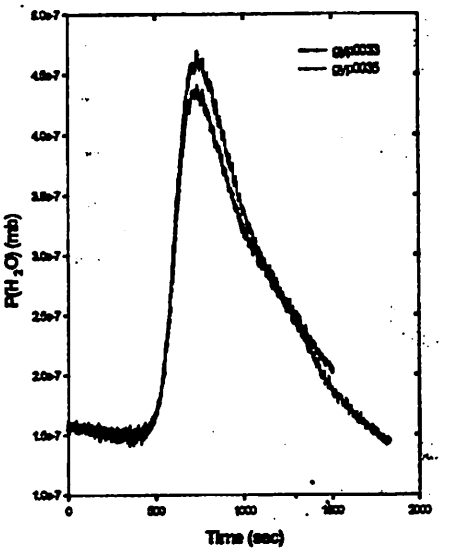

The Carrizozo Malpais

Windy Jaeger and Laszlo Keszthelyi

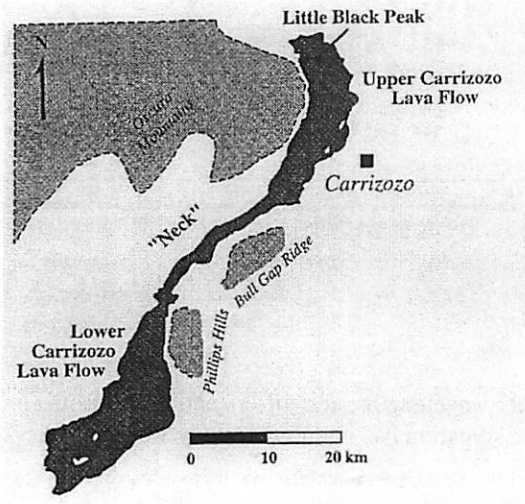

Fig. 2. Main physiographic sections of the Carrizozo flow field. The flow field is topographically constrained only along the northern half of the western side of the Upper Carrizozo Lava Flow and the southeastern side of the "neck" region.

from Keszthelyi and Pieri (1993)

The Carrizozo flow field is located in south-central New Mexico. It is the largest well-preserved lava flow in North America and arguably (depending on the definition of "well-preserved") the largest on Earth. It is 75 km long, covers 330 km^2, and has an estimated volume of 4.3 km^3 (Allen, 1952). The age of the flow is a point of contention. Based on vegetation and flow top morphology researchers have estimated it to be between 1 and 2 Ka (e.g. Weber, 1964). This is consistent with paleomagnetic data reported in the Albuquerque Journal which points to an age of ~1.7 – 1.8 Ka. However, ^{36}Cl cosmogenic dating suggests that the flow may be as old as 5.6±0.9 Ka (Dunbar, 1999). The lava was confined to the Tularosa Basin, and traveled down a shallow gradient of 0.2 – 0.4°. The only identified source for the lavas is the 27-m-tall Little Black Peak cinder cone. This cone sits on a shallow shield that is 2-5 km in diameter and 30-40 m tall.

In 1988 Dave Pieri at JPL organized a remote-sensing campaign over the Carrizozo flow field because of its obvious utility as a Mars analog. The primary objective of the campaign was to collect the kinds of data we would soon be getting from *Mars Observer*. This included high-resolution visible images and somewhat lower resolution thermal infrared spectra. Of particular interest was the recently developed method of mapping lava flows of different ages using thermal IR spectra (Khale et al., 1988). Preliminary geochemical surveys had suggested that the Carrizozo flow field consisted of 2 separate flows, the Upper and Lower Carrizozo flows. The Lower Carrizozo flow was, by the principle of superposition, older than the Upper Carrizozo flow and it also extended further to the south. The second objective was to test various techniques for quantitatively estimating eruption and lava parameters from remote sensing data.

The first objective yielded unexpected results. The 6-channel thermal IR spectra were able to cleanly separate limestone, quartz-rich sandstone, clay-rich shale and basalt. However, within the basaltic lava there was no discernable structure. The idea of distinct Upper and Lower Carrizozo flows was seriously challenged. After a review of the chemical data, it was found that the difference between the two "flows" was less than the 1σ error bars.

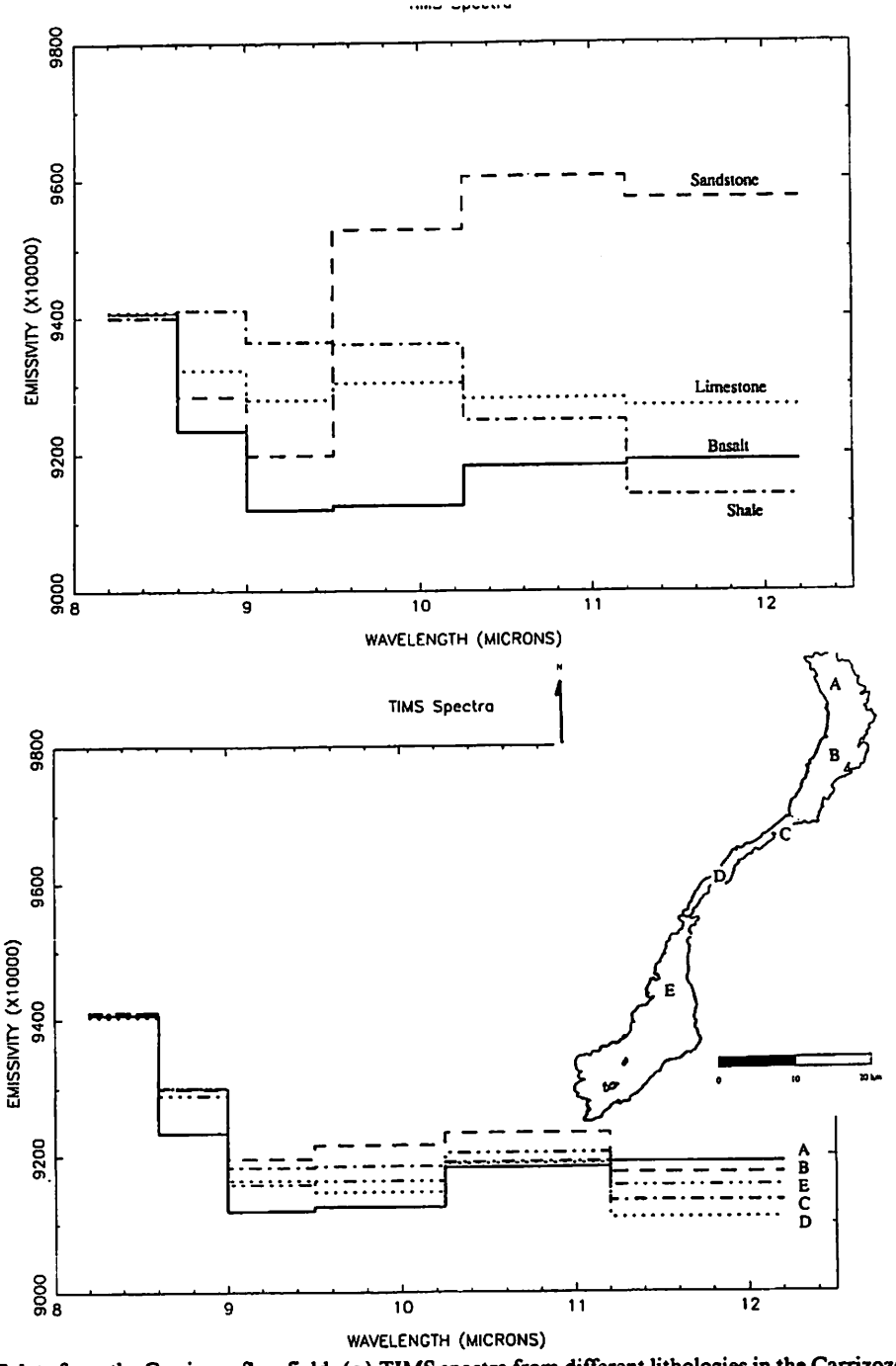

Fig. 5. TIMS data from the Carrizozo flow field. (a) TIMS spectra from different lithologies in the Carrizozo area. These spectra show that TIMS very clearly distinguishes the major lithologies. (b) Examples of TIMS spectra from parts of the Carrizozo flow field and location map for the spectra. The spectra show no systematic variation with distance from the vent or between the Upper and Lower Carrizozo flows. These data are consistent with a patchwork of lavas of slightly different composition and age. However, the scattered vegetation and eolian cover also contribute to the variations in the spectra.

from Keszthelyi and Pieri (1993)

For the second objective, Bingham models were applied to the flow to estimate its rheology. This technique was championed by Hulme (1974) as the way to remotely determine the rheology (and composition) of lava flows knowing only the flow width and thickness or flow thickness and basal gradient. Then using the estimated lava rheology, flow thickness, and gradient, the flow velocity and effusion rates were calculated. The result ranged from 0-100 m/s with effusion rates of 0-8x10^6 m^3/s. The preferred value was 10^5 m^3/s. At this rate, the entire volume of the Carrizozo flow field would be erupted in less than 12 hours (Keszthelyi and Pieri, 1989).

These findings were later retracted when the authors observed active Hawaiian volcanism and found one of their underlying assumptions to be wrong. Keszthelyi and Pieri (1989), like many other researchers, had assumed that the final flow thickness is equivalent to the active flow thickness. However, the Carrizozo Malpais is an inflated pahoehoe flow field. The term "pahoehoe" indicates that the surface is piece-wise continuous and the term "flow field" describes a complex of numerous smaller flows. "Inflation" refers to the process by which the lava is moving. It is behaving in a fluid/plasitic manner, stretching like a water balloon that is being filled. Once the top has solidified, the flow continues to thicken as lava is injected underneath the crust (Hon et al., 1994). The result is that the final thickness of the flow has no relation to the thickness of the lava when it was advancing. In fact, pahoehoe lobes are typically 20-50 cm thick, and in Hawaii they form only at effusion rates less than 10 m^3/s. In light of these findings, Keszthelyi and Pieri (1993) reworked the Carrizozo problem. Their new estimate of the effusion rate is 5 m^3/s and they hypothesize that the eruption duration was "nearly three decades". And the moral of the story... the key to producing long lava flows at such low effusion rates is the insulation provided by lava tubes.

REFERENCES

Allen, JE (1952) The Carrizozo Malpais. *Roswell Geologic Society Guidebook, 5th Field Conference*, pp. 9-11.

Dunbar, N (1999) Cosmogenic 36Cl-determined age of the Carrizozo lava flows, south-central New Mexico, New Mexico Geology, 21: 25-29.

Hon, K, J Kauahikaua, R Denlinger, and K Mackay (1994) Emplacement and inflation of pahoehoe sheet flows: Observatons and measurements of active lava flows on Kilauea Volcano, Hawaii, *Geol. Soc. Am. Bull.*, 106, 351-370.

Hulme, G (1974) The interpretation of lava flow morphology. *Geophys. J. R. Astron. Soc.*, 39: 361-383.

Kahle, AB and 6 others (1988) Relative dating of Hawaiian lava flows using multi-spectral thermal infrared images. *J. Geophys. Res.*, 93: 15239-15251.

Keszthelyi LP and DC Pieri (1989) Why is the Carrizozo flow field 75-km-long? *Lun. Planet. Sci. Conf.*

Keszthelyi, LP and DC Pieri (1993) The emplacement of the 75-km-long Carrizozo Flow Field, south-central New Mexico. *J. Volcanol. Geotherm. Res.*, 59: 59-75.

Weber, RH (1964) Geology of the Carrizozo quadrangle, New Mexico, New Mexico Geological Society Guidebook, 15: 100-109.

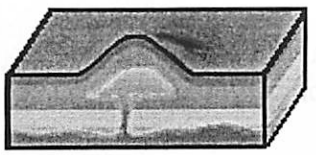

The White Oaks Laccoliths

James Richardson
Spring 2001 PTYS Field Trip

Introduction

About 12 *miles* to the northeast of Carrizozo lies the "ghost town" of White Oaks. This once thriving mining community rests in a small valley surrounded by three wrinkled and rounded mountain peaks: the remains of a ancient cluster of laccoliths (see attached *Figure 1*). To the northwest lies Lone Mountain with its associated peak, Baxter Mountain, while to the southeast lies Patos Mountain and the largest structure, Carrizo Mountain (elevation 9650 *feet*). It is to these structures that White Oaks owed its brief existence, not just for the beautiful setting for what was once called "the liveliest town in the territory," but more importantly, for the gold and silver commodities which fueled the towns' economy. To understand this, one must dig a little deeper underground.

Laccolith Formation and Evolution

Figure 2, below, shows a diagram of the various forms of intrusive and extrusive magmatic structures. A laccolith is shown at the *left* in this diagram, and consists of a intrusive layer of magma which is injected between the seams or layers of the surrounding country rock, similar to a sill, but such that the overlying country rock is pushed upward to form a bulge, or dome-like structure visible on the surface.

IGNEOUS ACTIVITY

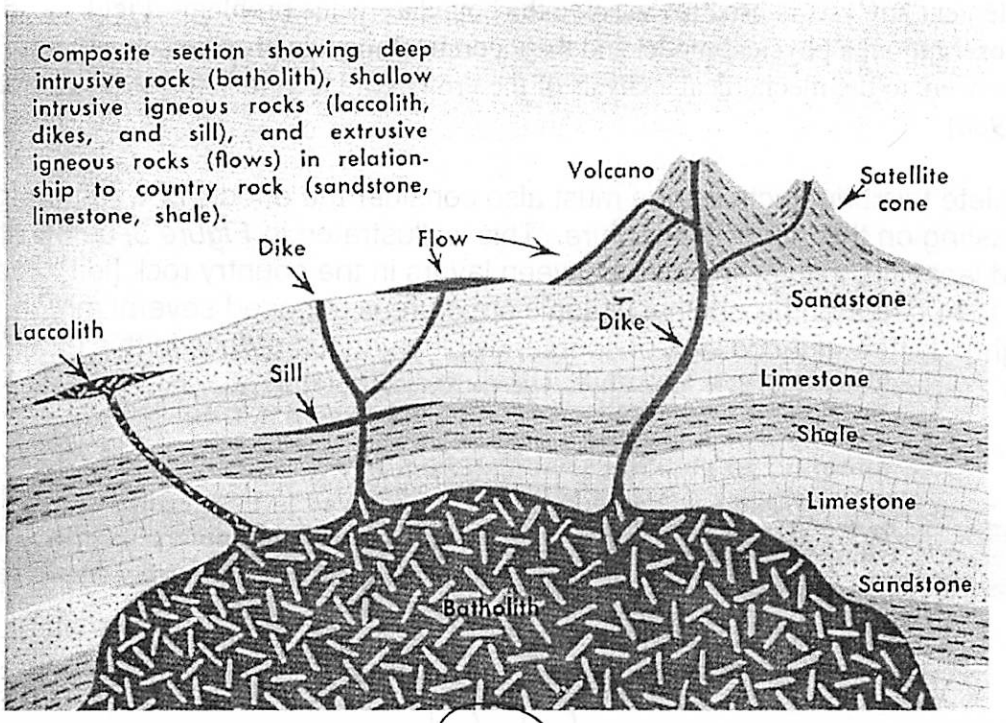

Once emplaced, the cooling magma in the laccolith can then spawn hydrothermal activity, which, in turn, can generate the ores and vein deposits once valued by the miners – but that is someone else's talk.

Laccoliths form a continuum of structure types, as described in the following excerpt:

> Gilbert (1877) proposed that the level of emplacement of laccoliths is controlled by the density contrast between rising magma and the weighted mean density of the overburden. For felsic laccoliths, his hypothesis is strongly supported by gravity surveys of a number of laccolith groups. Epizonal felsic laccoliths are consistently found to have zero density contrast with the host rocks. Constraining the emplacement level provides a basis for analysis of the growth of laccoliths.
>
> Mechanical analysis suggests that the diverse shapes of laccolithic intrusions observed in the field can be represented by a continuous series of intrusion modes between two distinct end members. The simplest end member is an epizonal intrusion formed by a single sill that acts mechanically as a vertical punch. Punched laccoliths are characterized by flat tops, peripheral faults, and steep or vertical sides.
>
> The other end member results from the intrusion of multiple sills stacked vertically in a fashion suggestive of a Christmas tree. The multiple-level loading results in plastic deformation of the country rock. Christmas-tree laccoliths lack peripheral faults and have a characteristic rounded dome appearance on the surface. The floor of these laccoliths may, or may not, sag. Gilbert's (1877) laccolith falls between these two end members.
>
> The end members of the laccolith growth series are treated as boundary value problems in continuum mechanics. Geometrically and materially nonlinear finite element analysis is used to the solve the boundary value problems. Field observation, a physical model and the theoretical models provide convergent answers to the mechanical analysis of the growth of laccoliths. [Charles E. Corry, 1988]

To complete this brief picture, one must also consider the effects of weathering and mass wasting on the laccolith structure. This is illustrated in *Figure 3*, below, in which a Punched laccolith, initially injected between layers in the country rock [left], is eroded away to the point that the original plutonic structure is exposed several million years later [right]. Different laccoliths, of course, display various stages in this erosion process.

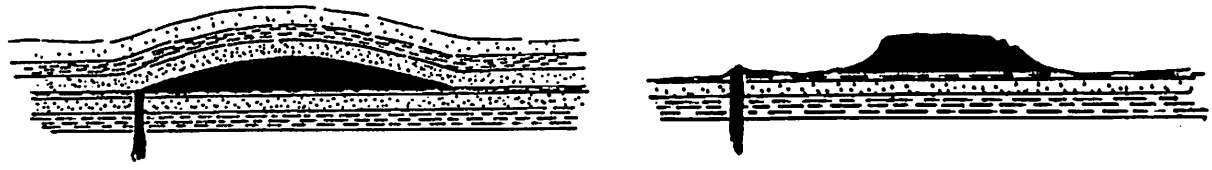

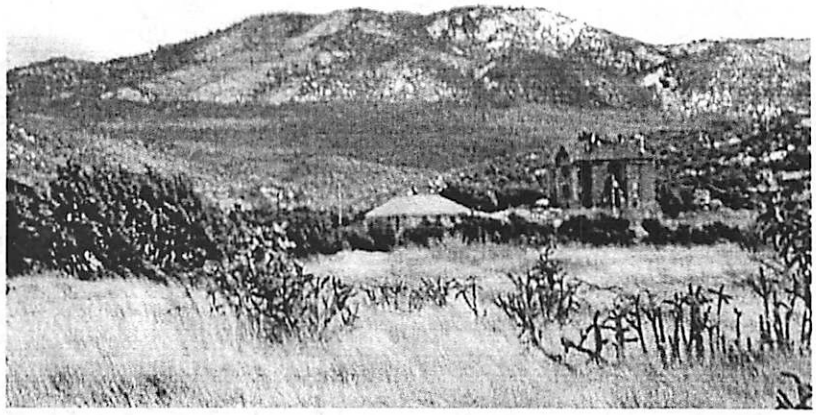

Figure 4: Illustrating the two end member types of laccoliths. [*above*] Crown Butte, Montana, represents a Punched laccolith, characterized by a flat top and steep sides. [*right*] The north side of Carrizo Mountain, New Mexico, represents a Christmas-tree laccolith, with a characteristic rounded-dome appearance (although quite eroded).

White Oaks Laccoliths: Carrizo Mountain

From highway No. 380, east of Carrizozo, the most prominently visible member of the White Oaks laccolith cluster is Carrizo Mountain (shown above in *Figure 4*). This is an eroded, dome-shaped, Christmas-tree laccolith, with a distinctive multi-ringed appearance created by the now exposed layers of upturned sedimentary rocks which once overlay the pluton. Direct information about this particular laccolith proved very difficult to come by, but if Carrizo Mountain is part of the same complex as Capitan Mountain, an elongated laccolith located just a few miles to the east, then the rock type for Carrizo Mountain would be granitic, having an age of around 28.8 Ma.

References

Chronic, H. (1987). *Roadside Geology of New Mexico*. Missoula: Mountain Press Pub.

Crown Butte Virtual Field Trip. Website: http://cbutte.freeyellow.com/

Corry, C.E. (1988). Laccoliths: Mechanics of Emplacement and Growth, *Geological Society of America,* Special Paper No. 220 [abstract].

Dunbar, N.W., Campbell, A.R., Candela, P.A. (1996). Physical, Chemical, and Mineralogical Evidence for Magmatic Fluid Migration Within the Capitan Pluton, Southeastern New Mexico, *Geological Society of America Bulletin*, 108; 3, pp. 318-333.

New Mexico Photos. Website: http://www.newmexicoet.com/nmet_town_photos_31.htm

Sorrel, C.A. (1973). *A Field Guide and Introduction to the Geology and Chemistry of Rocks and Minerals*. New York: Golden Books Pub.

White Oaks: Mining Town. Website: http://www.rozylowicz.com/retirement/whiteoaks/whiteoaks.html

FIGURE 1 : THE WHITE OAKS LACCOLITHS

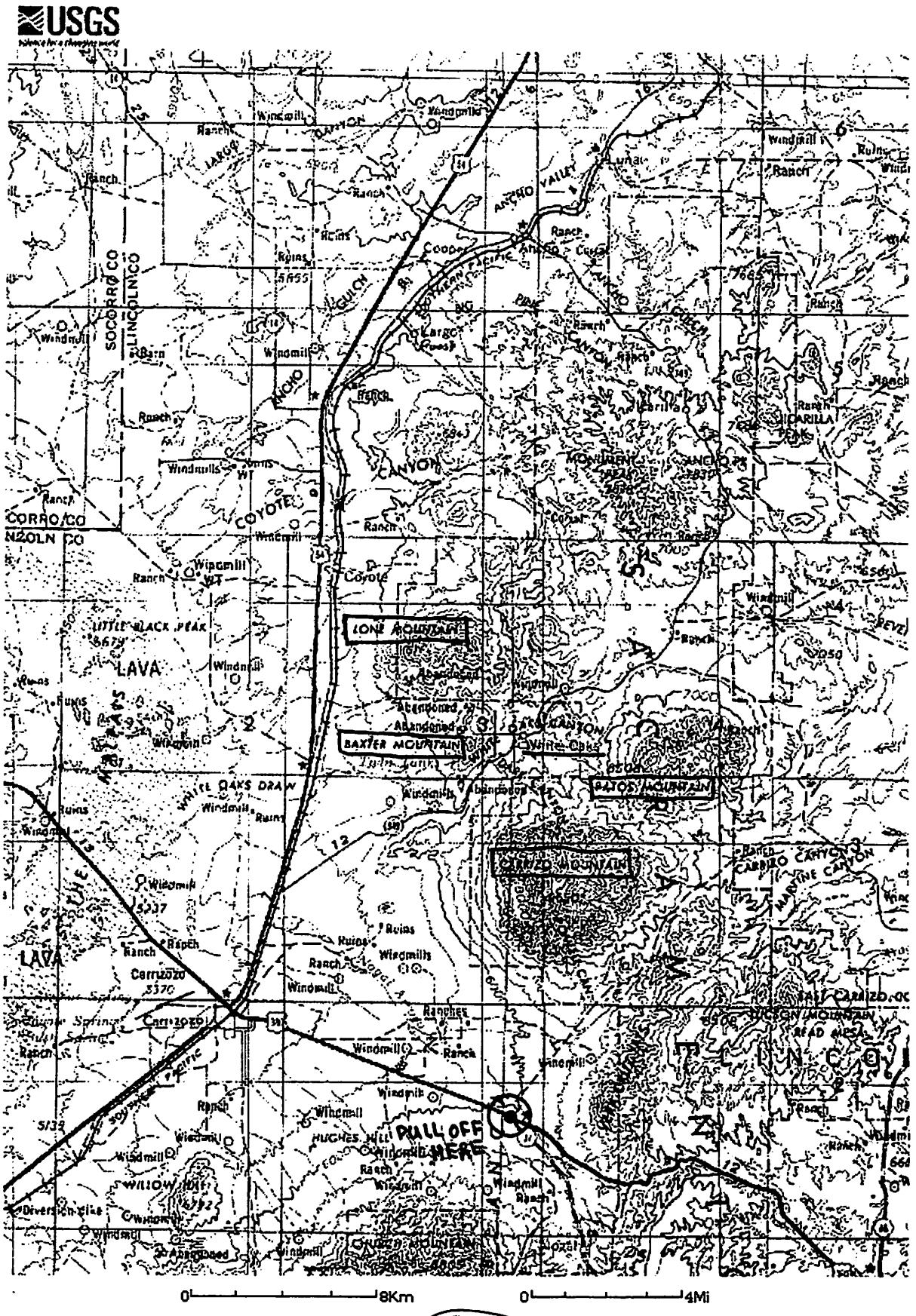

Socorro Magma Body

Joe Spitale

- Socorro seismic anomaly: [5]

  Most seismically active region in Rio Grande rift.

  Most events are relatively shallow, possibly caused by the sudden rupture of brittle crust triggered by injection of magma from below.

  SSA probably related to the presence of the deep zone of magma and possibly smaller intrusions.

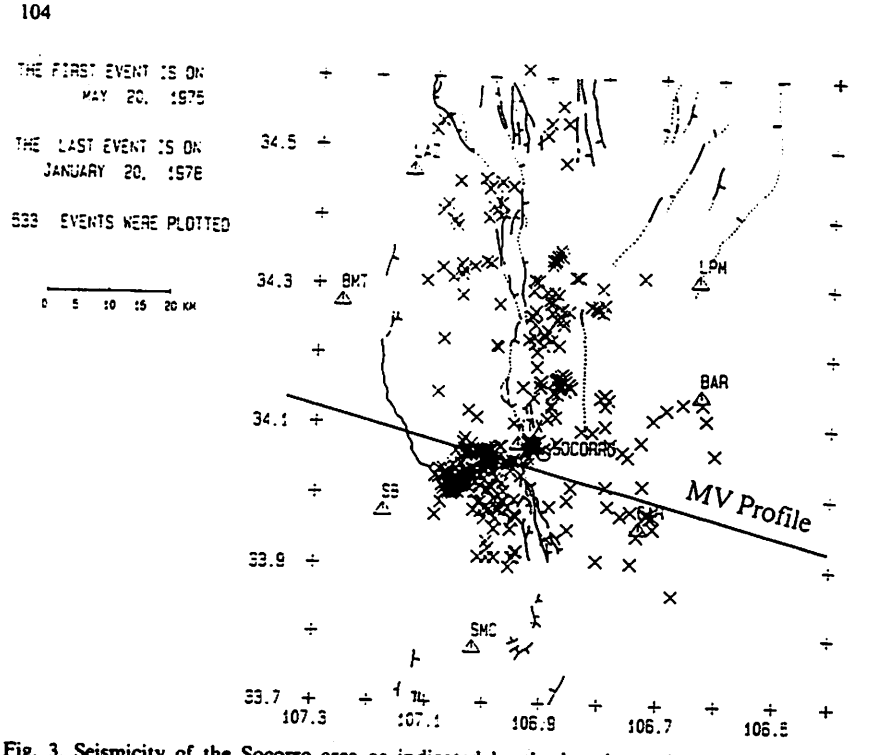

J.F. HERMANCE AND G.A. NEUMANN (1992)

Fig. 3. Seismicity of the Socorro area as indicated by the locations of 533 events (crosses) recorded during the period May 20, 1975–January 20, 1978. Faults shown are Pliocene or younger in age. The triangles mark the location of stations in the New Mexico Institute of Technology's permanent seismic network. After Sanford et al. (1983).

- Mid-crustal seismic reflector in the Rio Grande rift, southwest of Socorro, New Mexico.

- Unusual secondary phases first noticed in microearthquake seismograms in 1961. [6]

- Dimensions:
  area: > 3400 km^2 [2]
  thickness: < 500 m [4] [1]
  depth: 18 km – 19 km [4]

R. S. Balch, H. E. Hartse, A. R. Sanford, and K. Lin

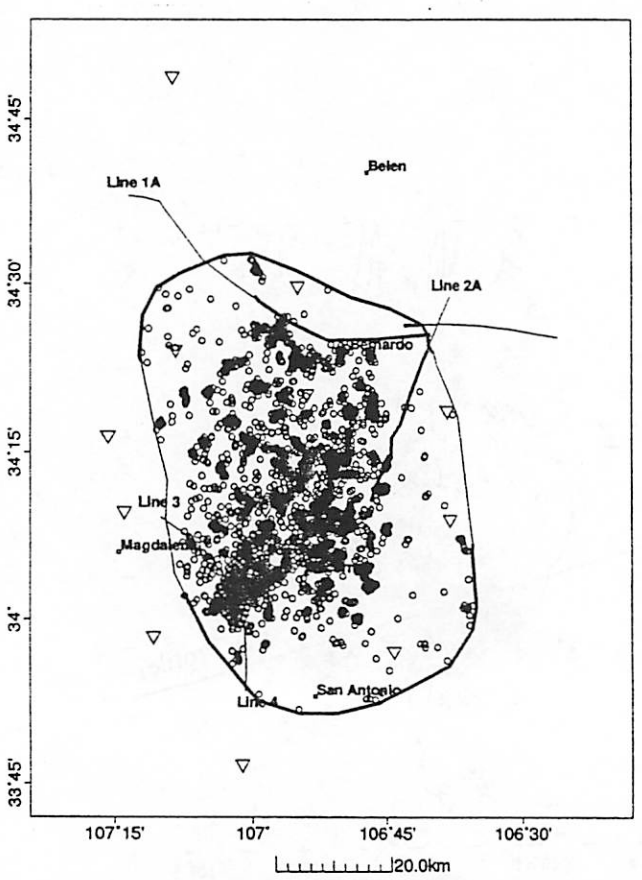

Figure 6. Reflection-point positions associated with the P_gP, S_gP, and S_gS phases and the new map of the outline of the Socorro magma body. Heavy solid lines indicate portions of the COCORP profiles that image the magma body clearly and boundary segments of the magma body constrained by this study.

Balch et al. (1994)

- Structure: [1]

  Poorly-correlated P-wave returns suggests scattering off multiple layers.

  Most shear-wave energy is reflected indicating that at least the top layer is nonrigid.

  Similarity of reflected shear waves suggests flat, planar upper surface.

  Preferred model:

  70 m full-melt basalt over 60 m crystalline "mush"

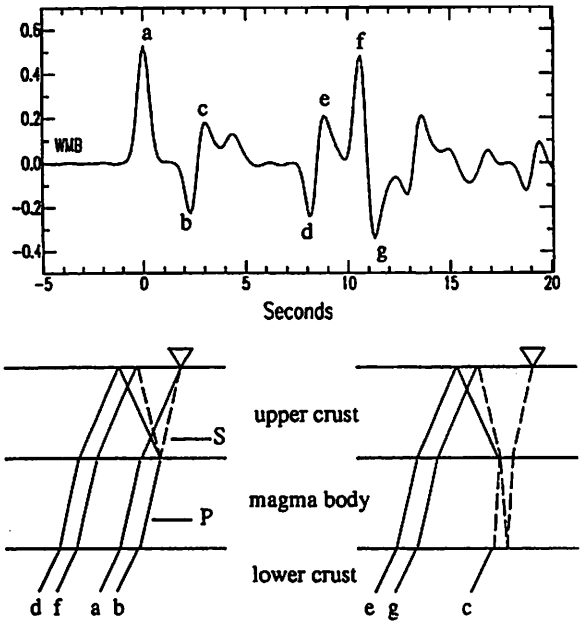

Fig. 5. (Top) Synthetic radial receiver function for model WMB. (Bottom) Schematic diagrams showing raypaths (p= 0.07 sec/deg) through the lower crust, magma body, and average upper crust of model WMB. The thickness of the magma body is exaggerated. Lowercase letters identify which rays are producing the arrivals associated with the magma body.

Sheriff et al. (1992)

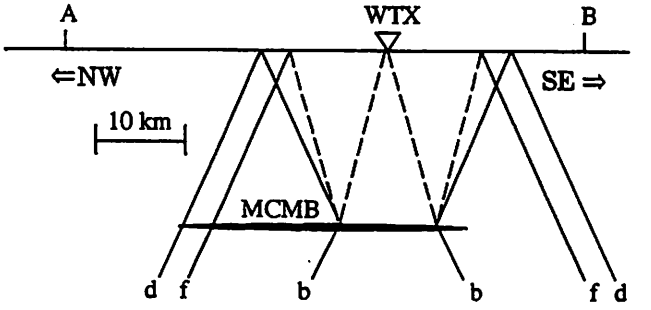

Fig. 7. Cross-section along line AB in Figure 6 to illustrate the location of the edges of the magma body with respect to WTX for teleseismic rays (p=0.07 sec/deg) arriving from the northwest and southeast. Raypath labels correspond to arrivals on the WMB receiver function in Figure 5.

References

[1] Ake J. P. and A. R. Sanford 1988. New evidence for the existence and internal structure of a thin layer of magma at mid-crustal depths near Socorro, New Mexico *Bull. Seism. Soc. Am.* **78;3**, 1335–1359.

[2] Balch R. S., H. E. Hartse, A. R. Sanford, and K. Lin 1997. A new map of the geographic extent of the Socorro mid-crustal magma body *Bull. Seism. Soc. Am.* **87;1**, 174–182.

[3] Balch R. S., and A. R. Sanford 1994. Focal mechanisms for two microearthquake swarms beneath the Socorro mountains, New Mexico, in May and July 1983 *Seismological Research Letters* **65;1**, 69.

[4] Hartse H. E., A. R. Sanford, and J. S. Knapp 1992. Incorporating Socorro magama body reflections into the earthquake location process *Bull. Seism. Soc. Am.* **82;6**, 2511–2532.

[5] Hermance, J. F. and G. A. Neumann 1992. The Rio Grande rift: new electromagnetic constraints on the Socorro magma body *Physics of the Earth and Planetary Interiors* **66**, 101–117.

[6] Sanford, A. R. and C. R. HOlmes 1961. Note on the July 1960 earthquakes in Central New Mexico *Bull. Seism. Soc. Am.* **51**, 311–314.

[7] Sheetz, K. E. and J. W. Schlue 1992. Inferences for the Socorro magma body from teleseismic receiver functions *GRL* **19;18**, 1867–1870.

The VLA and a wee bit of SETI

Jonathan Fortney
Spring 2001 Field Trip

VLA (Very Large Array)

History:
1972 August: approved by Congress
1973 April: construction started
1975 September 22: first antenna put in place
1976 February 18: first fringes
1980: formal dedication of the VLA
The total cost was $78,578,000 (in 1972 dollars), roughly $1 per taxpayer at the time; the project was completed nearly one year early, and within the allotted budget.

Size:
Each antenna: 25 m (82 ft) in diameter, 230 tons.
The array: There are four configurations: A array, with a maximum antenna separation of 36 km; B array -- 10 km; C array -- 3.6 km; and D array -- 1 km. The telescopes are switched between these configurations every four months or so.

Resolution: 0.04 arcseconds
The resolution of the VLA is set by the size of the array -- up to 36 km (22 miles) across. At our highest frequency (43 GHz) this gives a resolution of 0.04 arcseconds: sufficient to see a golf ball held by a friend 150 km (100 miles) away. Of course, very few golf balls contain high-power radio transmitters...

Frequency coverage: The VLA can observe at various bands between 74 and 50,000 MHz (400 to 0.7 cm): The data from the antennas is combined electronically to give the resolution of an antenna 36km (22 miles) across, with the sensitivity of a dish 130 meters (422 feet) in diameter.

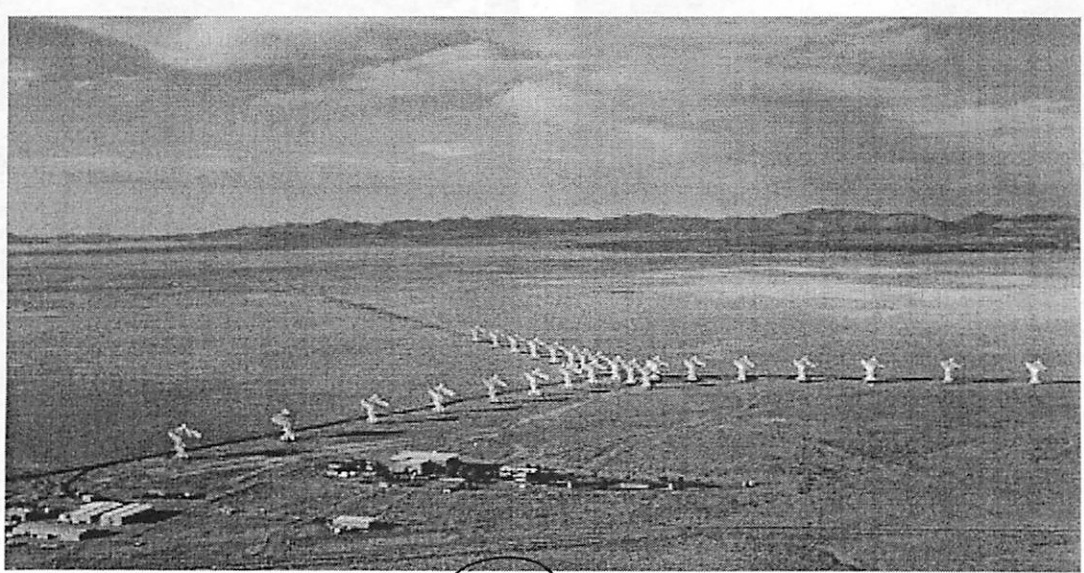

Figure 1

Figure 2

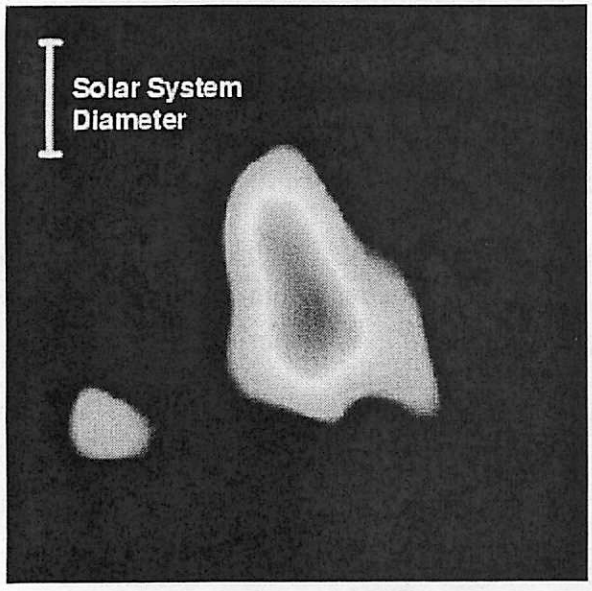

At right, the VLA image is shown as white contours laid over a model of the system which produces the observed radio-emission pattern. This model includes a disk of material being drawn into the young star, an outflow of material powered by the disk, and a previously unsuspected companion protostar.

CREDIT: D. Shepherd, M. Claussen, S. Kurtz, NRAO, AUI and NSF.

Available at: http://www.nrao.edu/pr/bigysodisk.html

VLA's Sharpened Vision Reveals Details of Still-Forming Massive Star

Using the Very Large Array radio telescope connected by a new fiber-optic link to an antenna of the Very Long Baseline Array (VLBA) at Pie Town, NM, astronomers made the image at **left** of a young star 6,000 light-years distant in the constellation Orion. The size of the young star and its surroundings is compared to our own Solar System.

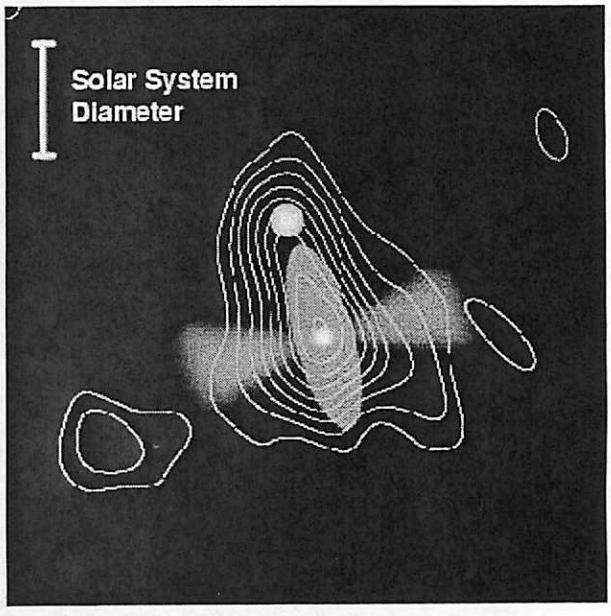

Uranium Mining in New Mexico

Abigail Wasserman

In 1950, a Navajo shepherd named Paddy Martinez in Grants, NM, discovered an odd yellow rock out in his field. Identified as uranium ore, a mining boom quickly followed, and New Mexico reveled in the boost to its economy. The Grants uranium region contains 50% of the uranium supply of the United States (Figure on right).

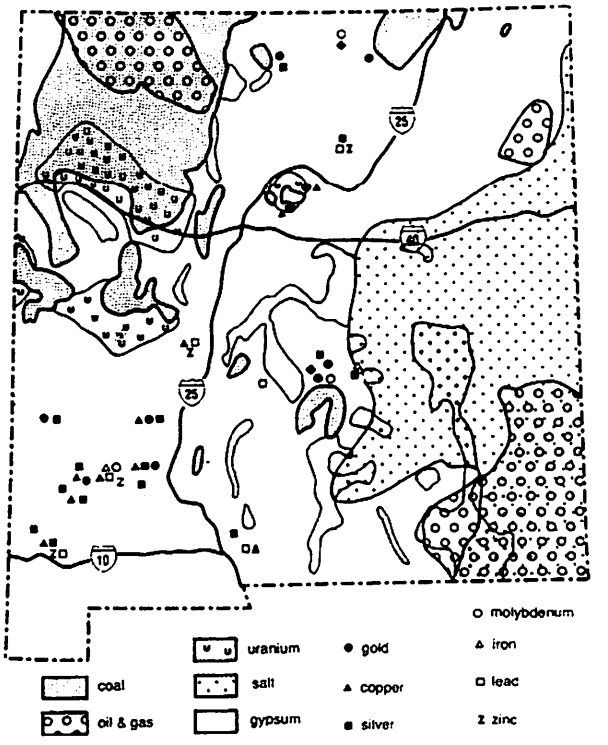

The majority of the ore is mined from deposits in fluvial sandstones of the Upper Jurassic Morrison Formation (Figure below). Water filtering through acidic volcanic rocks accumulates soluble uranium minerals, which are then deposited in areas with organic-rich material.

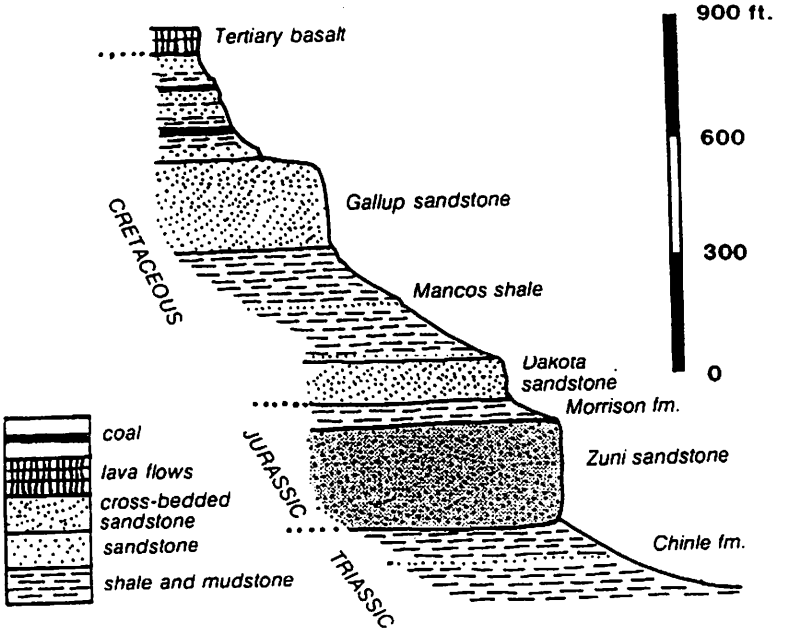

This stratigraphic diagram shows strata near I-40 between Arizona and Grants.

The Morrison formation consists of three large alluvial fans deposited along the southern border of the San Juan Basin. The uranium is highly concentrated in stream channels, now identified by thin lenses of orange sandstone enclosed in the predominantly gray sandstone of the Jackpile Sandstone and the Poison Canyon Sandstone members (Figure below). Near Grants, the Morrison formation visibly outcrops on the slopes of hills capped by Dakota sandstone, but further to the south, in Datil, it is covered by the more recently formed Datil-Mogollon volcanic field.

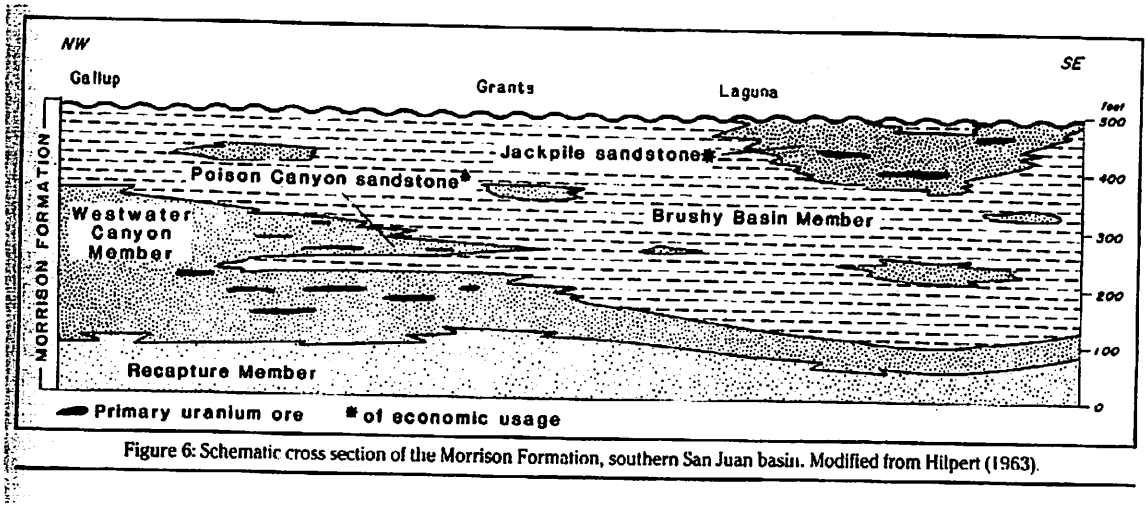

Figure 6: Schematic cross section of the Morrison Formation, southern San Juan basin. Modified from Hilpert (1963).

The chief uranium ore is uraninite - UO_2 - and its massive variety, pitchblende (usually U_3O_8). It is a dense black mineral with brown flecks. Secondary, but still important as an ore, is carnotite - $K_2(UO_2)_2(VO_4)_2 \square nH_2O$. Carnotite appears bright yellow, very soft, and can be processed for vanadium as well as uranium. The ore beds may also contain coffinite - $U(SiO_4)_{0.9}(OH)_{0.4}$. Each ore lens can be from 10-1000m long, 5-200m wide, and 5cm to 5m thick. The Morrison formation is on average 180m thick.

Tailings piles and ponds of water pumped out of mine shafts are a definite health hazard. July 16, 1976, in Church Rock, NM, a containment dam burst, sending eleven hundred tons of radioactive mill wastes and ninety million gallons of contaminated liquid pouring toward Arizona. It sent toxic metals at least 70 miles downstream in the Rio Puerco, and distributed residues of radioactive uranium, thorium, radium, and

polonium throughout the area. Ironically, it occurred 34 years to the day after the first atomic bomb test at Trinity.

Since the 1980's the demand for uranium has greatly decreased, and many of the Grants area mines were shut down. The mining industry has also been under heavy protest, primarily from the Indian tribes living nearby. Once, the mines were welcomed as "get rich quick" opportunities, but now that the environmental effects are better understood, most local residents want to shut down old mines and prevent the opening of new ones. Tailings piles and acid leaching pits are especially dangerous. Groundwater seepage and blowing dust carrying uranium and arsenic, as well as radon exhalation from the pile are major health hazards. Some mines in the area are still operational, some could be quickly reopened, and many potential mining sites have been identified. Whether the mines stay open, grow, or shut down altogether depends on the global political climate influencing demands for uranium in the United States.

References:

Chronic, H., 1987, *Roadside Geology of New Mexico*, Mountain Press Publishing Co., Missoula, 255 p.

Dahlkamp, F. J., 1993, *Uranium Ore Deposits*, Springer-Verlag, New York, 460 p.

Quartaroli, M.L., May 9, 2001, Uranium Mining on the Colorado Plateau, http://www.cpluhna.nau.edu/Change/uranium.htm.

Turner-Peterson, C., Santos, E., and Fishman, N. (ed), 1986, *A Basin Analysis Case Study: The Morrison Formation Grants Uranium Region New Mexico*, American Assoc. of Petroleum Geologists, Tulsa, 391 p.

WISE Uranium Project, May 9, 2001, Uranium Mining and Milling Wastes: An Introduction, http://www.antenna.nl/wise/uranium/uwai.html.

A final word of caution - Just like you don't eat yellow snow, don't play with yellow rocks.

HYDROTHERMAL ORE DEPOSITS NEAR SAFFORD, ARIZONA

Ingrid Daubar

HYDROTHERMAL ORES – GENERAL

Hydrothermal ore deposits have been thoroughly studied due to their importance as sources of economically significant ores such as gold, silver, lead, copper, zinc, and tungsten. Ores are deposited in several ways, but hydrothermal deposition is perhaps the most important method. Although signs of many (usually extinct) hydrothermal systems have been found all over the world, hydrothermal ore deposits are rare. Therefore the conditions necessary to produce ore deposits from hydrothermal systems must be exceptional. The systems depend on many variables — host rock chemistry, fluid composition, physical characteristics, etc. Although specific circumstances at certain deposits have been studied, completely general conditions are not well-known.

GENERAL NECESSITIES FOR HYDROTHERMAL ORE DEPOSITION:

- Solution capable of dissolving minerals and transporting them.
- Permeable rocks, to allow fluids to flow through.
- Sites for deposition of minerals.
- Conditions which promote deposition of minerals.
- Minerals in high enough concentrations to make an economically "worthwhile" deposit.

WHERE DO ORE-FORMING ELEMENTS COME FROM?

Siderophile elements, although depleted in the crust and mantle relative to the bulk Earth, are still present in the upper mantle in the form of Fe-Ni sulfides. Ore minerals, most especially metals, can be concentrated into magmas via partial melting of the mantle or crust, or transfer of mass from subducting slabs [Hedenquist & Lowenstern 1994]. The metals are then dissolved into hydrothermal fluids, which exsolve out of magmas as they rise to lower pressures.

As hydrothermal fluids rise and flow through rocks, changes in temperature, pressure, or pH can change the solubility of minerals in the water. Drops in temperature and pressure result in lowered solubility for most minerals, and so they precipitate out. Reactions between the fluids and the surrounding rocks can also change the chemistry of the fluids, causing precipitation of minerals.

General properties of hydrothermal fluids are in the table at the right. The source of these fluids, and thus the metals dissolved in them, is not clear. Meteoritic water is the most likely source, however, magmas are saturated with fluids (usually water) at depth; the release of these with lower pressures could provide the primary fluids in hydrothermal systems. Stable isotope studies show a predominantly meteoritic source for the fluids

Primary fluid	H_2O
Temperature	50 – 650 °C
Salinity	high, > seawater
pH	neutral to low

[Hedenquist & Lowenstern 1994], however a high flux of meteoritic water could erase the signatures of earlier, primary magmatic fluids.

...AND WHERE DO THEY GO?

Examples of places minerals are deposited:

- pore spaces
- crystal boundaries
- vesicles
- cooling cracks
- breccia cavities
- fissures
- cavities produced by tectonic activity

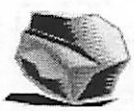

There are two types of mineral deposition: replacement mineralization, and cavity filling. Petrified wood is an example of **replacement mineralization**; in this case wood is replaced by silica. Minerals do similar things, often taking the same form and volume as the old mineral (pseudomorphism). Hydrothermal fluids bring in the new minerals, dissolve and carry away the old ones. Replacement is the dominant process at high temperatures and pressures. Replacement minerals form in **massive deposits**, where large volumes of rock are replaced; **veins**; or **disseminated deposits**, where the ore minerals are only present in specks or blobs. Disseminated deposits, such as porphyry copper deposits, are often spread out over large areas, and suitable for pit mining techniques.

Cavity filling is when minerals fill existing spaces in the rock. This process dominates at lower pressures and temperatures, often farther away form the heat source. In this case, minerals first precipitate on the walls of the cavity and form successive layers of more-soluble minerals. The last minerals to form are the most soluble, and form in the last unfilled spaces, or vugs. This is the source of many beautiful geodes. **Fissure vein** filling is the most common type of cavity filling. Fissures can be formed by tension or compression, resulting in veins with two dimensions much larger than the third. Precipitation of minerals can be responsible for opening these fissures or for widening them further.

Further Reading:

Bateman, A.M. (1951) The Formation of Mineral Deposits. John Wiley & Sons, New York.

Browne, P.R.L. (1978) Hydrothermal alteration in active geothermal fields. Ann. Rev. EPS 6, 229-250.

Evans, A.M. (1980) An Introduction to Ore Geology. Elsevier, New York.

Hedenquist, J.W. and J.B. Lowenstern (1994) The role of magmas in the formation of hydrothermal ore deposits. Nature 370, 519-527.

HYDROTHERMAL ORES NEAR SAFFORD, ARIZONA

RELEVANT GEOLOGY OF THE AREA.

The mountains to the north are a mixture of tertiary and quaternary volcanics, with older precambrian rocks sometimes exposed on the south sides. There are also small areas where paleozoic rocks are exposed by faulting; these contain most of the mineralization valuable for mining [1]. The Sonoran Desert contains many large copper-bearing plutonic bodies which intruded during the Laramide Orogeny ~80-35 Ma [2]. Mining of these deposits has made Arizona the leading producer of copper in the country [2].

MINES OF THE AREA.

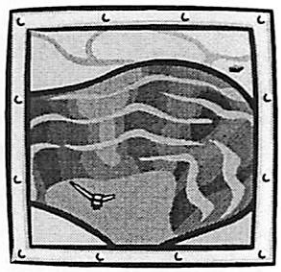

The **Clifton-Morenci** deposits were discovered by a prospecting party from Silver City, NM in 1872. This mine alone produces ~18% of the total copper in the country [3]. Several mining companies have operated the mine, including the Detroit Copper Co., the Arizona Copper Co, and (currently) Phelps Dodge. The deposits are disseminated chalcocite in granitic rocks. The copper ore is low-grade, so open pit mining has been used to extract it. Silver is a minor constituent. It was first produced from replacement deposits in limestone, and fissure veins with quartz-sulfide ores. Later, silver and gold were obtained from the disseminated copper deposits. Iron is also produced from pyrite deposits.

Volcanic rocks in the **Lone Star** mining district contain a huge low-grade disseminated copper deposit which has not yet been mined. There is also a hydrothermal gold-quartz vein.

Ash Peak has fissure veins in the Tertiary tuffs and rhyolitic to andesitic volcanic rocks. The veins are 3 to 18 feet thick, and contain quartz, argenite, pyrite, calcite, and rhodochrosite. Silver and Gold have also been found. The gold is in a fissure vein containing metallic sulfides.

The **Aravaipa** mining area is primarily a source of silver. Several mines are located here, including the Head Center, Grand Reef, Grand Central, Iron Cap, and Arizona mines. Veins of quartz and lead sulfides are found in rocks with limestone along the walls. There are also quartz-specularite-flourite sulfide deposits along breccia reefs, and quartz sulfide fissure veins which fill faults and brecciated zones.

[1] Roadside Geology

[2] Arizona Roadside Environments – REGIONAL GEOLOGY, http://dana.ucc.nau.edu/~are-p/road_map/eco/geology.html

[3] BLM Arizona Safford Field Office What We Do, http://www.az.blm.gov/sfo/whatwedo.html

remainder:

Mineral and Water Resources of Arizona (1969), Arizona Bureau of Mines Bulletin 180, University of Arizona, Tucson.

PLANETARY CONNECTION…

Finding ore deposits on other planets and the moon!

HYDROTHERMAL ORE DEPOSITS NEAR SAFFORD, ARIZONA

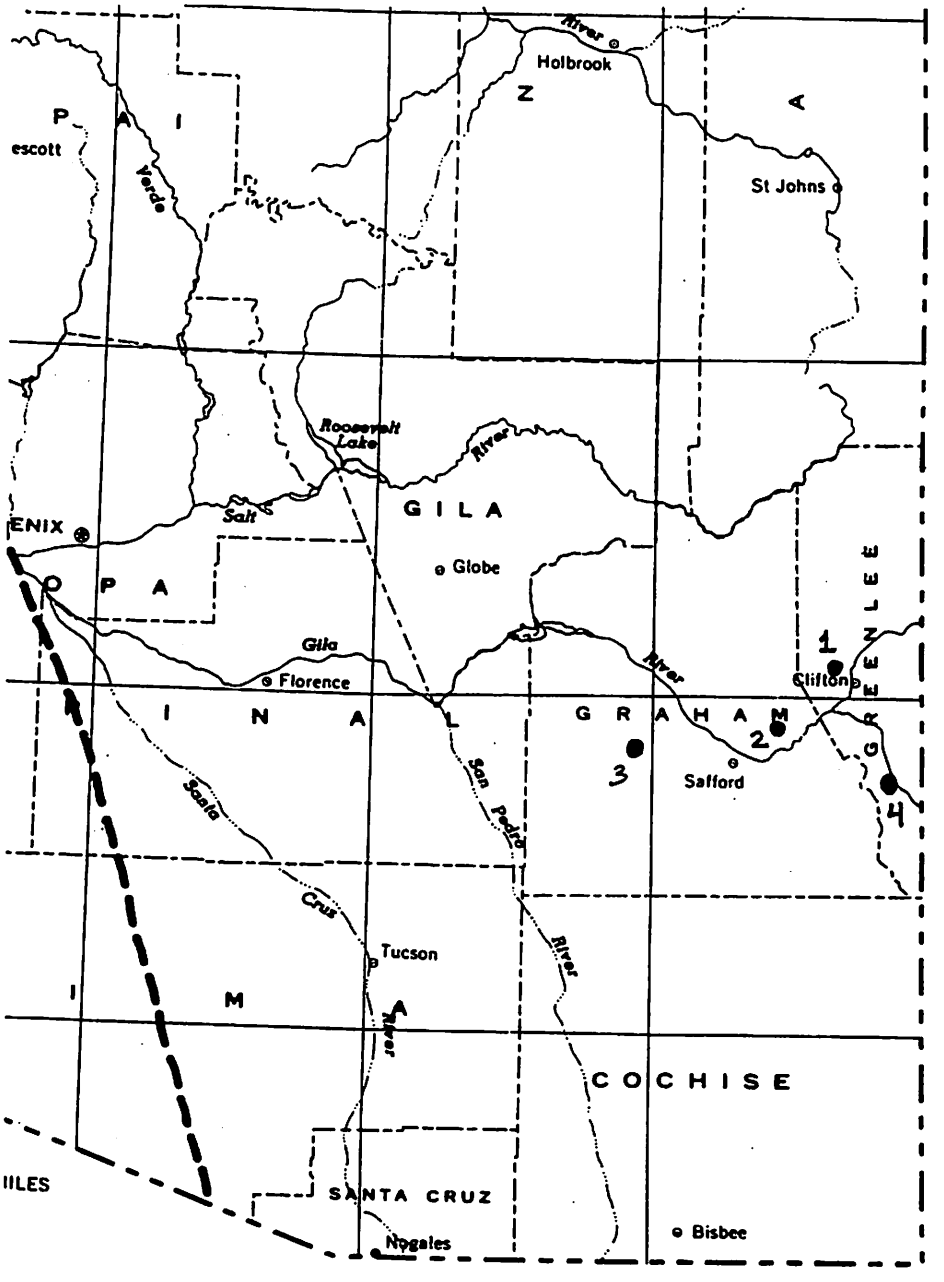

1 – MORENCI - CLIFTON
2 – LONE STAR
3 – ARAVAIPA
4 – ASH PEAK

72

from Mineral & Water Resources of Arizona (1969).

Porphyry Copper Deposits: Formation and Mining

Dave O'Brien

1 Introduction

The term 'porphyry copper' generally refers to large, low grade (around 0.5% Cu by weight) ore bodies. They are formed when a large sub-surface intrusion of porphyritic (large grains in a fine grained matrix) rock induces hydrothermal activity and subsequent enrichment of ore within the intrusion and/or within the surrounding rock. Copper is the primary metal enriched, but molybdenum, silver, gold, and other metals may also be enriched. Subsequent alteration and enrichment in certian zones of the ore body may occur due to the action of groundwater.

Arizona is the largest producer of copper in the U. S. (2.4 billion pounds in 1999), accounting for 65% of the total U. S. mine production, most of which is porphyry copper (as opposed to high-grade ores). Only Chile produces more copper. The production of this much copper requires the removal and processing of an enormous amount of ore. This is generally done by open-pit mining with high-volume extraction and refining processes. The Morenci mine which we'll be seeing is the largest open pit mine in the U.S.

2 How is the Deposit Formed?

A porphyry copper deposit generally begins forming when a large mass of porphyritic rock, such as granite, quartz monzonite, or granodiorite, is emplaced in surface rocks as a pluton, possibly with associated dike swarms. As the intrusion cools, it cracks, allowing for the free movement of groundwater and leading to a hydrothermal system. Hydrothermal activity concentrates copper, and possibly molybdenum and other metals. Concentration can occur in the intrusive rock, in the host rock, or both. This depends in a large part on the extent of fracturing. Occasionaly, a copper skarn deposit forms at the intrusion-host contact, especially if there are carbonates in the host rock. I don't know exactly what this means, but it's basically some kind of mineral deposit. This is the case at Morenci. In all cases the primary copper bearing mineral is chalcopyrite ($CuFeS_2$), but this may change due to subsequent alteration.

Further action of groundwater can lead to a concentration of copper bearing minerals. Pyrite (FeS_2) and chalcopyrite can be oxidized in the presence of water to form copper sulfate, iron sulfate, and sulfuric acid. This soultion percolates downward until the acid is neutralized, and in the absence of oxygen the copper sulfate reacts with pyrite and chalcopyrite to form a mineral such as chalcocite (Cu_2S). If oxygen is present, copper oxides such as cuprite (Cu_2O) form instead. In this way, a 'leached capping' above the ore body is formed, which is depleted in copper, while the upper part of the remaining ore body is enriched in copper.

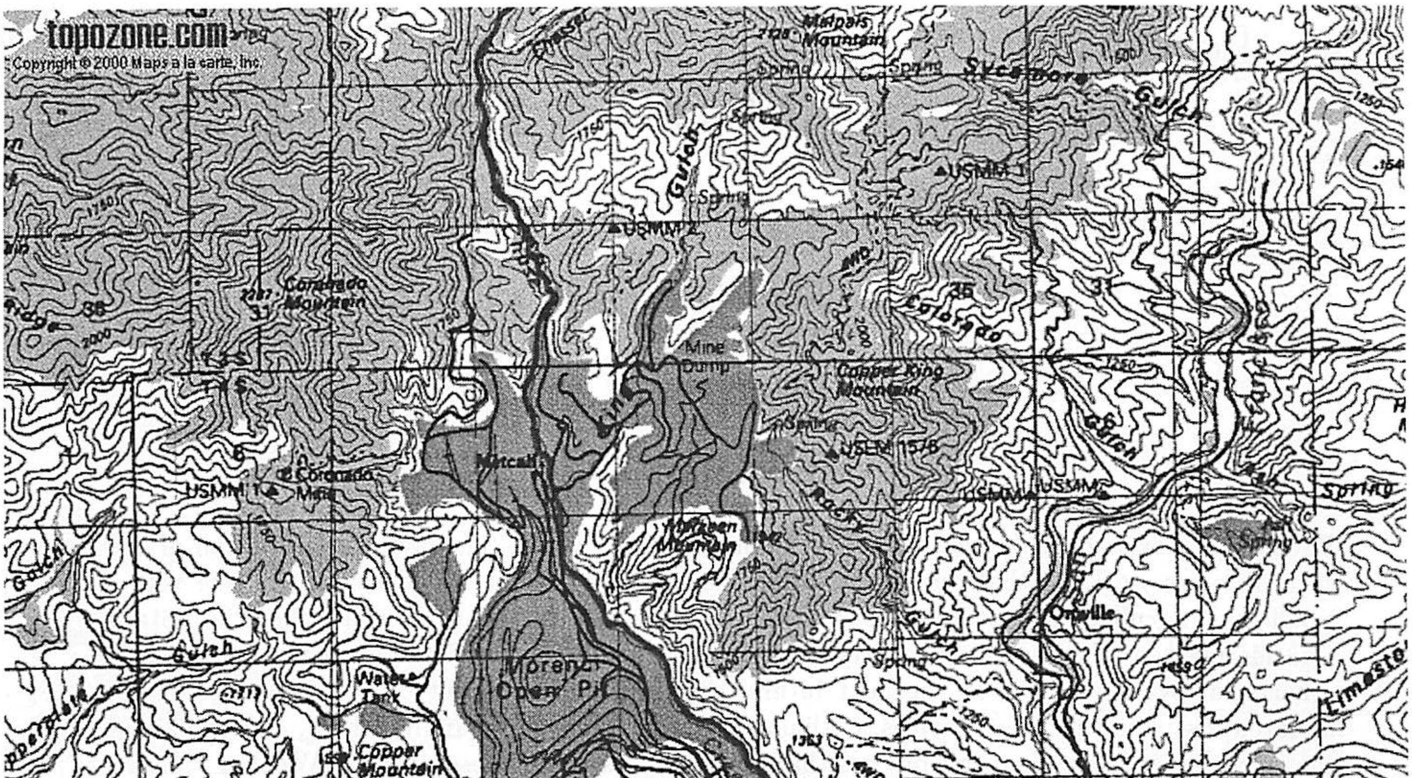
topozone.com
Copyright © 2000 Maps a la carte, Inc.
Malpais Mountain
Sycamore Gulch
Spring
USMM 1
USMM 2
Gulch
Coronado Mountain
Colorado
Mine Dump
Copper King Mountain
USLM 1576
Metcalf
Coronado Mine
Rock
Spring
Gulch
Ondville
Water Tank
Morenci Open Pit
Copper Mountain
Morenci
Stargo
USMM
Timestone
Water Tank
Clifton Peak
Water Tank
Silver Basin
Gold Gulch
Clifton
Gaging Sta
Ward Canyon
Mine Dump
TAILINGS POND
Tailings Pond
Water Tank
Cave
meters
0
2000
4000
6000
8000
miles
0
2.0
4.0

Potato Guns: Chemistry, Physics and Planetary Applications

Jason W. Barnes, Fred J. Ciesla, Terry A. Hurford, and David P. O'Brien

May 10, 2001

Abstract

Potato guns, or so called *spudzookas* have been around for years. The layman description of how such a device works is that one starts an explosion in an almost sealed container: one with a small opening plugged by a potato. The energy from the explosion then launches the potato. Considering the advances in chemistry, physics and engineering, and the expect colonization of other solar system bodies in the near future, this explanation is out of date. We present an updated discussion of these devices, outlining the legal issues surrounding them, and explaining the chemistry, engineering and physics that goes into designing these devices. We then consider the planetary implications for potato guns.

1 Legal Issues

Some may be wondering if potato cannons are in fact "legal." To fully understand the issue, here are the relevant United States legal codes:

U.S.C. Title 18, Chapter 44, S 921 (a) (3): The term "firearm" means (A) any weapon (including a starter gun) which will or is designed to or may readily be converted to expel a projectile by the action of an explosive; (B) the frame or receiver of any such weapon; (C) any firearm muffler or firearm silencer; or (D) any destructive device. Such term does not include an antique firearm.

U.S.C. Title 26, Chapter 53, S 5845: For the purpose of this chapter -

(a) Firearm The term "firearm" means (1) a shotgun having a barrel or barrels of less than 18 inches in length; (2) a weapon made from a shotgun if such weapon as modified has an overall length of less than 26 inches or a barrel or barrels of less than 18 inches in length; (3) a rifle having a barrel or barrels of less than 16 inches in length; (4) a weapon made from a rifle if such weapon as modified has an overall length of less than 26 inches or a barrel or barrels of less than 16 inches in length; (5) any other weapon, as defined in subsection (e); (6) a machinegun; (7) any

silencer (as defined in section 921 of title 18, United States Code); and (8) a destructive device. The term "firearm" shall not include an antique firearm or any device (other than a machinegun or destructive device) which, although designed as a weapon, the Secretary finds by reason of the date of its manufacture, value, design, and other characteristics is primarily a collector's item and is not likely to be used as a weapon.

(b) Machinegun The term "machinegun" means any weapon which shoots, is designed to shoot, or can be readily restored to shoot, automatically more than one shot, without manual reloading, by a single function of the trigger. The term shall also include the frame or receiver of any such weapon, any part designed and intended solely and exclusively, or combination of parts designed and intended, for use in converting a weapon into a machinegun, and any combination of parts from which a machinegun can be assembled if such parts are in the possession or under the control of a person.

(c) Rifle The term "rifle" means a weapon designed or redesigned, made or remade, and intended to be fired from the shoulder and designed or redesigned and made or remade to use the energy of the explosive in a fixed cartridge to fire only a single projectile through a rifled bore for each single pull of the trigger, and shall include any such weapon which may be readily restored to fire a fixed cartridge.

(d) Shotgun The term "shotgun" means a weapon designed or redesigned, made or remade, and intended to be fired from the shoulder and designed or redesigned and made or remade to use the energy of the explosive in a fixed shotgun shell to fire through a smooth bore either a number of projectiles (ball shot) or a single projectile for each pull of the trigger, and shall include any such weapon which may be readily restored to fire a fixed shotgun shell.

(e) Any other weapon The term "any other weapon" means any weapon or device capable of being concealed on the person from which a shot can be discharged through the energy of an explosive, a pistol or revolver having a barrel with a smooth bore designed or redesigned to fire a fixed shotgun shell, weapons with combination shotgun and rifle barrels 12 inches or more, less than 18 inches in length, from which only a single discharge can be made from either barrel without manual reloading, and shall include any such weapon which may be readily restored to fire. Such term shall not include a pistol or a revolver having a rifled bore, or rifled bores, or weapons designed, made, or intended to be fired from the shoulder and not capable of firing fixed ammunition.

(f) Destructive device The term "destructive device" means (1) any explosive, incendiary, or poison gas (A) bomb, (B) grenade, (C) rocket having a propellent charge of more than four ounces, (D) missile having an explosive or incendiary charge of more than one-quarter ounce, (E) mine, or (F) similar device; (2) any type of weapon by whatever name known which will, or which may be readily converted to, expel a projectile by the action of an explosive or other propellant, the barrel or barrels of which have a bore of more than one-half inch in diameter, except a shotgun or shotgun shell which the Secretary finds is generally recognized as particularly suitable for sporting purposes; and (3) any combination of parts either designed or intended for use in converting any device into a destructive device as defined in subparagraphs (1) and (2) and from which a destructive device may be readily assembled. The term "destructive device" shall not include any device which is neither designed nor redesigned for use as a weapon; any device, although originally designed for use as a weapon, which is redesigned for use as a signaling, pyrotechnic, line throwing, safety, or similar device; surplus ordnance sold, loaned, or given by

77

the Secretary of the Army pursuant to the provisions of section 4684(2), 4685, or 4686 of title 10 of the United States Code; or any other device which the Secretary finds is not likely to be used as a weapon, or is an antique or is a rifle which the owner intends to use solely for sporting purposes.

(g) Antique firearm The term "antique firearm" means any firearm not designed or redesigned for using rim fire or conventional center fire ignition with fixed ammunition and manufactured in or before 1898 (including any matchlock, flintlock, percussion cap, or similar type of ignition system or replica thereof, whether actually manufactured before or after the year 1898) and also any firearm using fixed ammunition manufactured in or before 1898, for which ammunition is no longer manufactured in the United States and is not readily available in the ordinary channels of commercial trade.

(h) Unserviceable firearm The term "unserviceable firearm" means a firearm which is incapable of discharging a shot by means of an explosive and incapable of being readily restored to a firing condition.

(i) Make The term "make", and the various derivatives of such word, shall include manufacturing (other than by one qualified to engage in such business under this chapter), putting together, altering, any combination of these, or otherwise producing a firearm.

(j) Transfer The term "transfer" and the various derivatives of such word, shall include selling, assigning, pledging, leasing, loaning, giving away, or otherwise disposing of.

(k) Dealer The term "dealer" means any person, not a manufacturer or importer, engaged in the business of selling, renting, leasing, or loaning firearms and shall include pawnbrokers who accept firearms as collateral for loans.

(l) Importer The term "importer" means any person who is engaged in the business of importing or bringing firearms into the United States.

(m) Manufacturer The term "manufacturer" means any person who is engaged in the business of manufacturing firearms.

For those, who still have doubts, here is a letter from the ATF responding to an inquiry on the legality of such devices:

DEPARTMENT OF THE TREASURY
Bureau of Alcohol, Tobacco and Firearms
Washington, DC 20226
E:CE:F:TE:RAT
Sep 12 1995 3311.4
Mr. XXXXXXXXX
address...
City, State Zip

Dear Mr. XXXXXXXXX

This refers to your letter of August 18, 1995, in which you ask about the legality of a device known as the "Spud Gun."

78

These subject devices are generally constructed from PVC tubing and fittings and are designed to launch a muzzle loaded potato using aerosol hair spray or other type of propellant. Ignition is by means of some type of "spark" igniter.

The Bureau has previously examined devices known as "Spud Guns, Potato Guns, or Spudzookas" and have determined that such devices, in and of themselves, are not firearms as defined in Title 18 United States Code (U.S.C.), Chapter 44, S 921(a)(3) or 26 U.S.C., Chapter 53, S 5845.

However, any similar devices which can be determined to be weapons by reason of their design construction, intended use, actual use, ammunition or other factors may meet the definition of a firearm under Title 18 or 26 U.S.C.

We suggest that you contact your State and local law enforcement authorities concerning possession of such devices.

We trust that the foregoing has been responsive to your inquiry. If we may be of further assistance please contact us.

Sincerely yours,
Edward M. Owen, Jr.
Chief, Firearms Technology Branch

2 Chemistry

The propulsive energy of a vegetative impeller device comes from the expanding hot gases resulting from the chemical reactions in the combustion chamber. Although there are many different types of reaction that might serve this purpose, we analyze that which is most often used in Earth-bound potato cannons: the combustion of hydrocarbon aerosols. In such a reaction, fuel reacts exothermically with oxygen to form carbon dioxide, water, and heat. For methane:

$$CH_4 + 2O_2 \rightarrow CO_2 + 2OH_2 \quad (1)$$

Thus for methane, combustion of the maximum number of molecules occurs when the partial pressure of methane in the combustion chamber is equal to $^1/_2$ the partial pressure of oxygen. Since on Earth

$$P_{methane} + P_{oxygen} + P_{nitrogen} = 1 \text{ bar} \quad (2)$$

$$P_{methane}/P_{oxygen} = .79/.21 = 3.76 \quad (3)$$

the greatest combustion is achieved under a fuel partial pressure (P_f)of .950 bars for methane. Achieving this precise mixture is one of the hardest aspects of melon mortar operation. Proper partial pressures for other fuels are located in table 1. This pressure can be calculated for any given fuel by using the stoichiometric ratio between fuel and oxygen in the combustion reaction. If the fuel:oxygen ratio is m ($= P_f/P_{O_2}$), then the optimal pressure is given by:

$$P_{fuel} = \frac{.42\,m}{2 + .42\,m} \tag{4}$$

$Fuel$	$ChemicalFormula$	$P_f(bar)$
Methane	CH_4	.0950
Butane	C_4H_{10}	.0313
Propane	C_3H_8	.0206
Ether	$(C_2H_5)_2O$	.0338
Alcohol	C_2H_5OH	.0654

Table 1: *Optimal partial pressures of various propellants inside the combustion chamber.*

Given that the optimal mixture of fuel and oxygen exists in the combustion chamber, we now determine the amount of energy provided by combustion that is available for accelerating plant particles. In doing so, we will assume that combustion is complete, and that the situation can be approximated as an isobaric expansion of the combusted gases such that the net enthalpy change is equal to the difference of the enthalpies of formation (ΔH_f°) between the products and the reactants.

$$\Delta H = \Delta H_{reactants} - \Delta H_{products} \tag{5}$$

For methane, the specific ΔH_s of the reaction is -8.01×10^5 J/mol. From setting the total enthalpy change for the total reaction, $\Delta H_s * n * \frac{P_f + P_{O_2}}{1\text{ atm}}$ (n is the total number of moles of gas inside the combustion chamber prior to ignition), equal to the enthalpy change of the whole gas, $\Delta E + P\Delta V$, we can solve for the temperature difference between before and after combustion.

$$\Delta T = \frac{\Delta H_s}{29.1 \frac{\text{J}}{\text{mol K}}} \cdot \frac{P_f + P_{O_2}}{1\text{ atm}} \tag{6}$$

From this the total work done by the expansion of the hot post-combustion gases can be calculated and compared to empirical measurements of kinetic energy of the projectile. The work done by the expanding gases is equal to

$$W = P\Delta V = nR\Delta T \tag{7}$$

$$W = n \cdot 8.31 \frac{\text{J}}{\text{mol K}} \cdot \Delta T \tag{8}$$

80

Also, based upon the ratio of the gas volumes before and after combustion it should be possible to calculate the optimal barrel length given fuel composition and cannon geometry. This has also been studied empirically by *Barnes A. B., 1998*. The ratio of volumes is

$$\frac{\Delta V}{V} = \frac{P_f + P_{O_2}}{1 \text{ atm}} \cdot \Delta H_s \cdot 1.26 \times 10^{-7} \ \frac{\text{mmols}^2}{\text{kg}} \tag{9}$$

3 Engineering

In this section some aspects of building potato cannons will be discussed.

3.1 Barrel

The barrel of the potato gun is made from one long piece of pvc. It is important to use a long barrel so that the expansion of the gas in the combustion chamber provides acceleration all the way along the pipe until the potato is ejected. Since the expansion of the gas provides the acceleration it is possible to make your barrel too long. The optimal barrel length has been studies by *Barnes A. B., 1998* and is discussed in §2 Chemistry.

One end of the barrel should be fitted with a male pipe attachment, enabling the barrel to be removed from the combustion chamber. This can also aid in the loading of the barrel with various projectiles. From this end you can breech load projectile or you can ensure that projectile loaded from the other end with a ramming rod are not jammed into the combustion chamber. To aid in muzzle loading procedures the end of the barrel without the male attachment can be sharpen. This aids in slicing through potatoes while loading.

3.2 Combustion chamber

The rear section of the potato cannon is the combustion chamber. This short piece of pipe should be wider then the barrel that attaches to it. The end which attaches to the barrel is fitted with a reducing female connector, allowing the barrel to be screwed on or off. The other end is fitted with a removable drainage plug.

A combustion chamber with both ends able to be removed allows for better ventilation between firings. After a projectile is launched the barrel can be removed and reloaded. The other end can be opened to allow fresh air to easily flow into the chamber. This is important for getting the right fuel to oxygen ratio (§2 Chemistry).

Once the barrel is attached to the cannon. Fuel can be added from the rear through the drainage opening.

3.3 Ignition system

With the cannon built, the ignition system needs to be installed. This simple circuit consists of a piezoelectric ceramic attached to two screws by wires. The screws are set into the combustion chamber so that their tips almost touch. They behave like a capacitor, storing charge that is

81

released by the piezoelectric ceramic. When the charge is great enough there is a discharge of energy from one screw to the other, producing a spark, igniting the fuel in the chamber (See §3).

4 Ignition systems

Two of the three combustion chambers built have been designed to use a piezoelectric ignition systems. Only the large cabbage cannon uses a model rocket igniter. In this section the *physics* behind the piezoelectric ignition system will be discussed.

4.1 Piezoelectric ceramics

When a piezoelectric material experiences compression along one of its axis, a voltage appears appears along one of the other axis. These materials directly convert mechanical energy into electrical energy. These materials are good insulators with long molecular chains that have charge imbalances at their ends.

A piezoelectric material is polarized. The unbalanced charges at the end of the molecular chains will provide one surface with excess of electrons while the other will be deficient. This imbalance produces an net electrical field but since the material is a good insulator the elect-ons can not rearrange themselves to balance the charges.

Placing a conductive material at the surfaces of the piezoelectric can make it a current generator. Applying a stress to the material squeezes the molecular chains together while elongating them in the perpendicular direction. This increases the distance between the free electrons and the bipolar molecules which reduces the force of attraction. At the same time the end having the free electrons is being compressed which leads to a stronger repulsive force between the electrons. As a result some electrons will be releases and flow into the conductor. Similarly on the other side of the material electron can flow from the conductor onto the piezoelectric material.

4.2 The ignition circuit

Below is an illustration of the simple circuit for the ignition system. As the piezoelectric ceramic is compressed current flows charging the capacitor. Once the charge on the capacitor is high enough the air between the plates becomes conductive, allowing an arc to jump from one plate to the other. This spark ignites the propellant in the combustion chamber.

The dielectric strength of air is $3\frac{\text{kV}}{\text{mm}}$. Stronger electric fields cannot be maintained. For a capacitor with plates separated by a few mm the voltage produced by this breakdown is $\sim$ 5000kV.

5 Physics of Projectiles

As an object travels through the Earth's atmosphere, it is acted upon by two main forces: *gravity*, which pulls the object back towards the surface of the Earth, and *gas drag*, which works opposite the direction of motion of the object. While the effect of gravity can be either to increase or decrease the absolute *speed* of the object, gas drag will always tend to force the object to asymptotically approach a speed of zero. We will examine both of these forces in more detail.

82

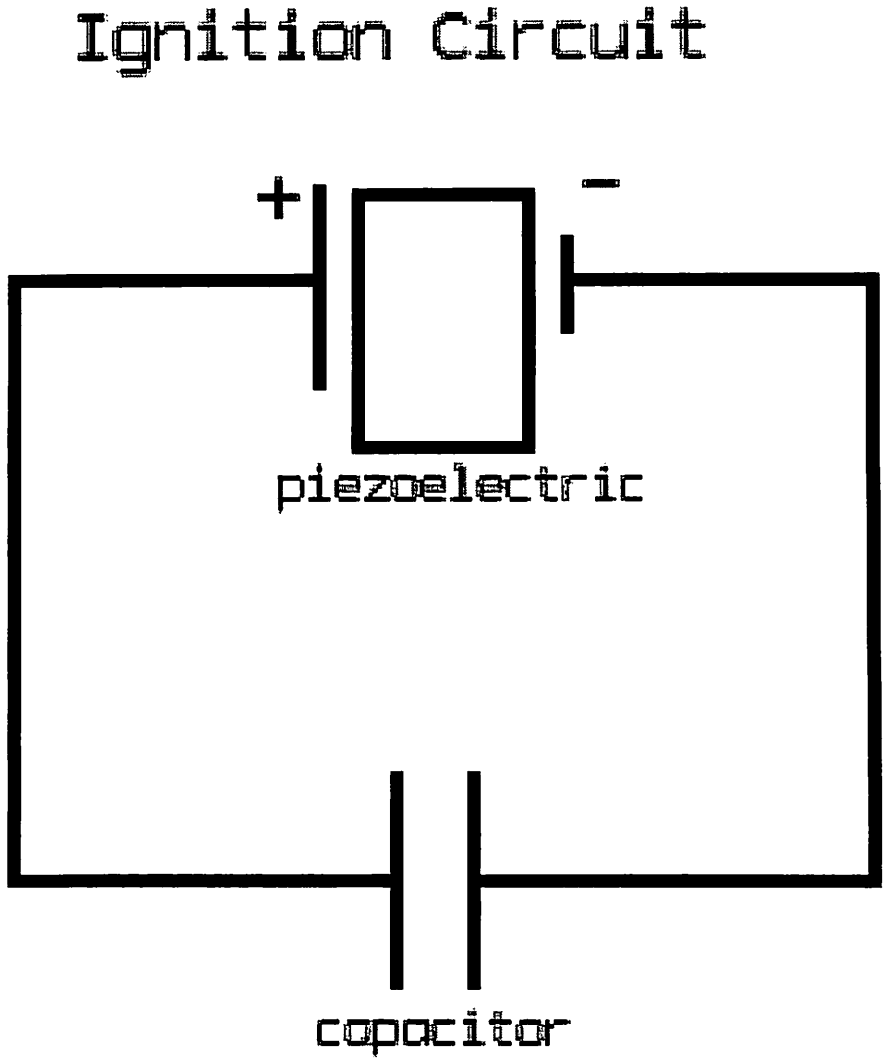

Figure 1: A schematic of the ignition circuit.

83

5.1 Gravity

Any object that has mass will exert a gravitational tug on another object with mass: from the most massive black holes to the longest wavelengths of light. It was Sir Isaac Newton (1687) who first learned that the force that one mass exerts on another is proportional to the product of the two masses and inversely proportional to the square of the separation of the masses. That is:

$$F_g = G\frac{m_1 m_2}{r^2} \tag{10}$$

Here G is the constant of proportionality, which has become known as the Gravitational constant and has a value of 6.67×10^{-11} kg^{-1} m^3 s^{-2}.

In discussing the path of a projectile above the surface of the Earth, r would represent the distance between the object and the center of mass of a (spherical) planet. It is generally assumed the the force of gravity is constant which requires that the planet is approximately spherical, and that the projectile never reaches a distance above the surface that is comparable to the radius of the planet ($h \ll r$).

5.2 Gas Drag

The force on an object due to gas drag is more complicated than that of gravity, and therefore requires more detailed discussion. The existence of this force is evident if you have stuck your hand out the window of a moving car, or watched objects blow in the wind. It exists as long as there is a relative motion of an object with respect to the gas it is moving through. Therefore it becomes important in evaluating the path of an object through Earth's atmosphere.

The equation for the force exerted on a spherical object due to gas drag is given by:

$$F_d = \pi a^2 \frac{C_D}{2} \rho_g \mid \vec{V} \mid \vec{V} \tag{11}$$

where a is the radius of the object, ρ_g is the mass density of the gas, and V is the relative velocity of the object with respect to the gas. The term C_D is called the drag coefficient. This is not an easily derived parameter, but rather something that must be measured for an object. Based on such measurements, the drag coefficient can be fitted by the analytic expression:

$$C_D = 0.48 + 28Re^{-0.85} \tag{12}$$

Here Re is the Reynolds number:

$$Re = \frac{aV}{\nu_g} \tag{13}$$

where the molecular viscosity $\nu_g \sim cl/2$. Here c is the speed of sound in the gas and l is the mean free path of a gas molecule. These are found as:

$$c = \left(\frac{\gamma k T_g}{m_g}\right)^{\frac{1}{2}} \tag{14}$$

$$l = \frac{m_g}{\sigma \rho_g} \tag{15}$$

84

Typical values for γ, the ratio of specific heats of the gas, and σ, the collisional cross-section of a gas molecule, are 1.4 and 6×10^{-20} m^2 respectively. T_g and m_g are the atmospheric temperature and mass of a single gas molecule respectively.

5.3 Theoretical Modeling of a Projectile's Path

Having identified the forces that act upon the projectile, we can now solve the equations which describe the motion of the particle. If we choose a simple two dimensional cartesian coordinate system such that x represents the horizontal direction of motion and y the vertical, we have:

$$m\frac{dv_x}{dt} = -F_{dx} \tag{16}$$

$$m\frac{dv_y}{dt} = -F_g - F_{dy} \tag{17}$$

These equations become:

$$m\frac{dv_x}{dt} = -\pi a^2 \frac{C_D}{2}\rho_g v_x^2 \tag{18}$$

$$m\frac{dv_y}{dt} = -G\frac{M_\oplus m}{R_\oplus^2} - \pi a^2 \frac{C_D}{2}\rho_g \mid v_y \mid v_y \tag{19}$$

for looking at the projectile's passage through Earth's atmosphere. This alone just gives us the velocity profile. To get the position as a function of time, we must integrate the velocities. That is:

$$x(t) = \int_0^t v_x(t')dt' \tag{20}$$

$$y(t) = \int_0^t v_y(t')dt' \tag{21}$$

Note that the expression above for the Reynolds number, Re, which is needed to calculate the drag coefficient, C_D, is dependent on the velocity of the projectile. Because of this dependence, the differential equations described above have no analytic solution. They must be solved numerically.

5.4 Model Results for Different Planetary Bodies

We have applied our model to investigate how a potato fired from one of our pyrotechnic produce propellers would propagate on different solar system bodies. For all of our simulations, we examined a potato launched from the origin of our coordinate system at a muzzle velocity of 60 m/s, at an angle of $\frac{\pi}{4}$ to the horizontal. We assumed that the height of the potato was never comparable to the radius of the body that we launched from, and therefore gravity was constant, and the properties of the atmosphere were constant over the traveled paths. We also assumed a perfectly flat surface for the planet, ignoring possible topographies and gravity anomalies. We tracked the potato until it re-impacted upon the surface. The potato itself was assumed to have a radius of 5 cm and a mass of 1 kg. The specifics of the combustion on other planets are ignored,

85

we only assume that we are able to fire somehow. The results for our model runs can be seen in Figures 1 and 2

The inputs and results from our model are summarized in the table below. We have left out the exact values for y_{max} and x_{max} for the Moon. The Moon essentially has no atmosphere, and therefore there would be no drag force on the potato. This allows for an analytic solution for the equations of motion which we leave to the reader.

	Moon	Mars	Titan	Earth	Venus
$g\,(m/s^2)$	1.6	3.7	1.4	9.8	8.9
$\rho_g\,(kg/m^3)$	0	0.0155	5.55	1.23	64.8
$T_g\,(K)$	0	214	94	288	735
$\mu\,(m_{proton})$	0	44.0	28.0	28.84	44.0
$y_{max}\,(m)$		240	130	76	12
$x_{max}\,(m)$		950	255	250	25

5.5 Discussion

A potato, all things being equal, will travel farthest on the Moon than any of the other bodies considered. Mars would be second, followed by Earth, Titan and finally Venus. It is interesting that Mars, despite having a surface gravity over 2.5 times that of Titan, allows a potato to travel much further horizontally and reach greater heights. This helps to demonstrate how thick Titan's atmosphere is. We imagine Ralph will have some tidbits to say (possibly about helicopter/blimp exploration of either of these bodies?).

The thickness of the Venusian atmosphere is also demonstrated in our model. Earth and Venus have similar surface gravities, but the path of the potato on Venus is so drastically different on the two planets because of thickness of Venus's atmosphere.

86

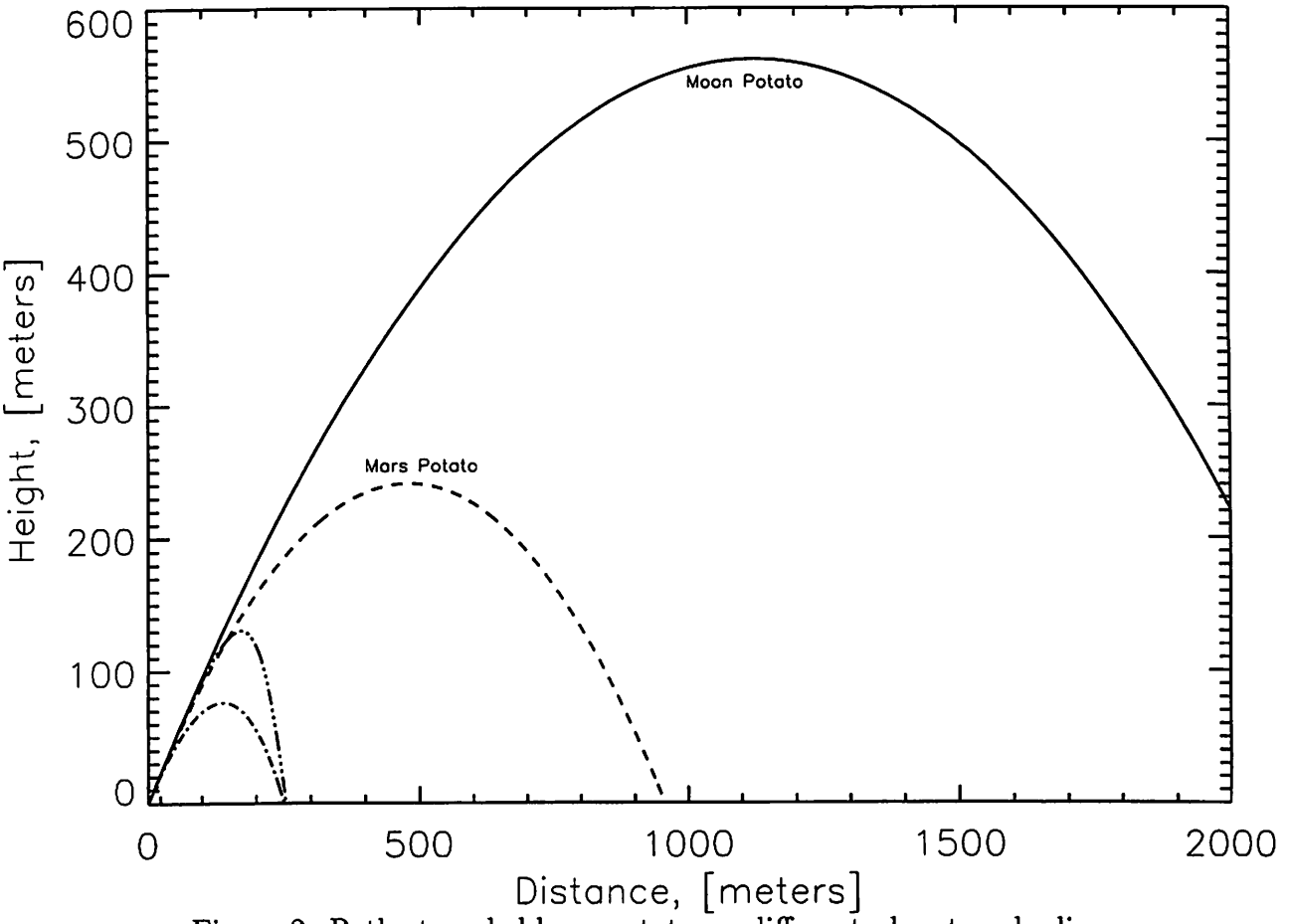

Figure 2: Paths traveled by a potato on different planetary bodies.

87

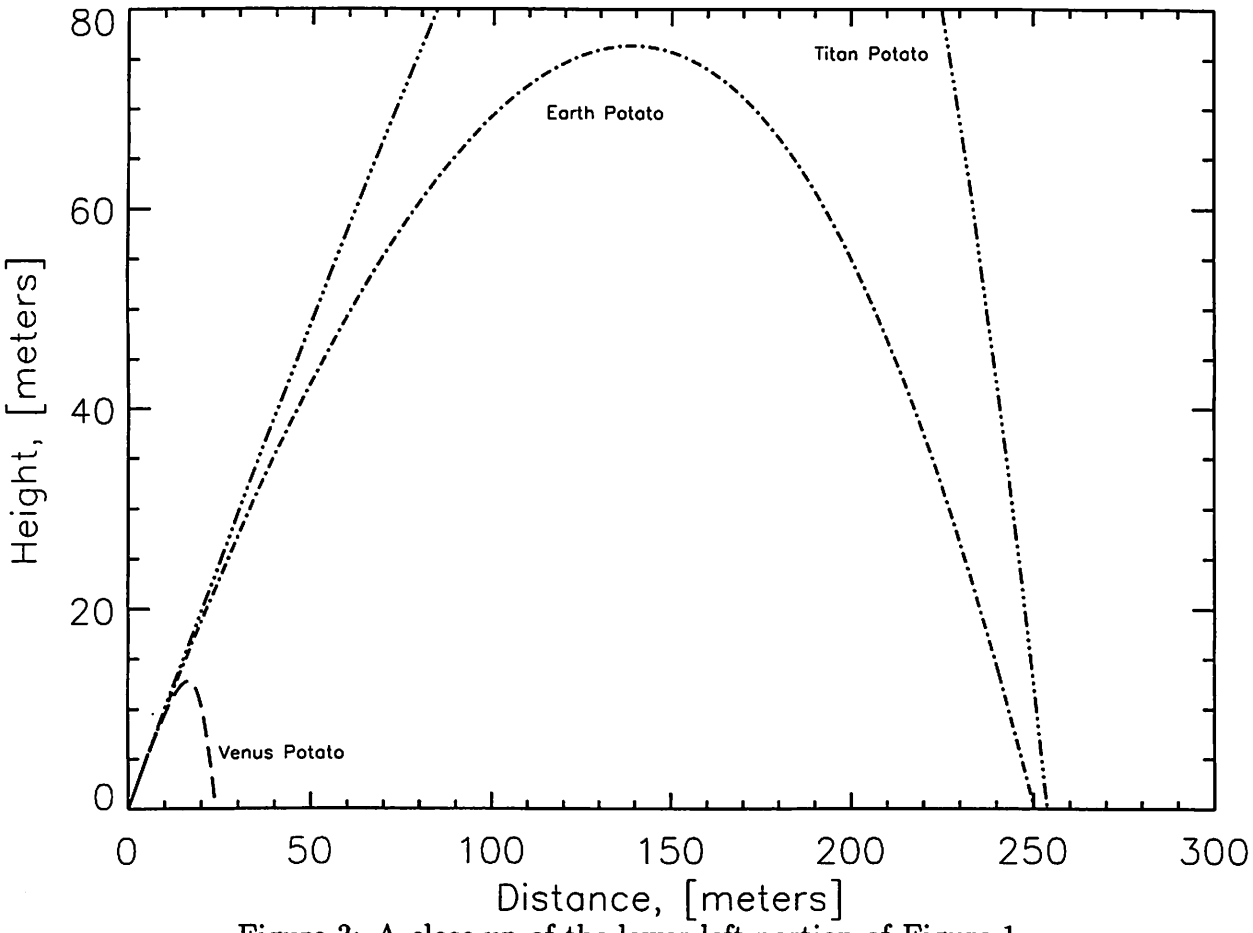

Figure 3: A close up of the lower left portion of Figure 1.

88